# 博　士　論　文

**DETECTION OF HUMAN BY THERMOPILE INFRARED SENSORS**

サーモパイル型赤外線センサによる人検出に関する研究

金沢大学大学院　自然科学研究科

システム創成科学専攻

機能創成システム講座

**学籍番号（Student ID Number）: 1223122006**

**氏名（Name）:張　西鵬**

**主任指導教員（Chief Adviser）：関　啓明**

**提出年月（Date）：2016 年 3 月 22 日**

# Contents

# CHAPTER 1. INTRODUCTION

## 1.1 Research background

In recent years, the detection of human-beings is very important in many different areas, such as human-robot interaction [1], [2], [3], work-cell safety [4], [5], people counting [6], monitoring and tracking [7], [8], [9], [10], [11], [12] etc (**Fig. 1.1**). Among these areas, many types of equipment, such as automatic doors, automatic switches, voice guidance devices, are automatically controlled by detecting human-beings. The types of sensors used are as diverse as the application equipment. For example, the motion sensors and voice guidance equipment are implemented on automatic doors.

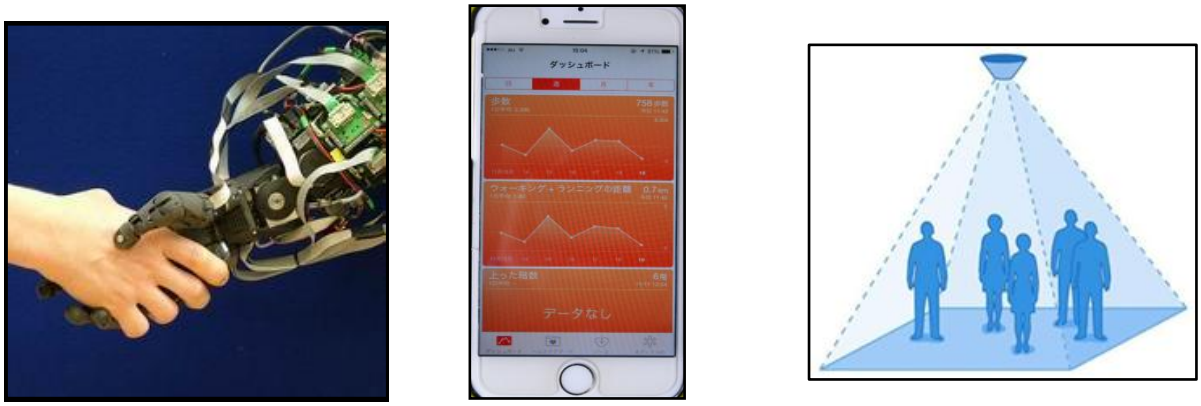


Human-robot interaction  Monitoring and tracking  People counting

Fig. 1.1 Purposes for human detection

However, these detectors have their respective problems in the detection process. For example, they work all the time, even when they are not necessary (**Fig. 1.2(a)**), such as when an automatic door opens for a person who is just standing near it and has no intention to go through it. Sensor systems that detect people's positions and movements, such as coming near, going away, stopping, and passing, are needed. Common cameras and thermography cameras [13] employed in buildings can produce real-time images and identify human situations well, but cost and privacy can be problems; people do not like to be photographed unless there is a good reason. Ultrasonic sensors (**Fig. 1.2(a)**) by [14], [15] are often used in location systems but they tend to be disturbed by sources of noise in the natural environment, and it is difficult to detect not only the presence but also the movement of people. Pyroelectric detectors [16], [17] (**Fig. 1.2(b)**) are widely used in motion detection applications for home security and automation systems (**Fig.**

**1.2(b)**), but their outputs are differential (**Fig. 1.3**), or proportional to the rate of change of incidental radiation. This leads to slightly lower detection: pyroelectric detectors can only detect people when they move.

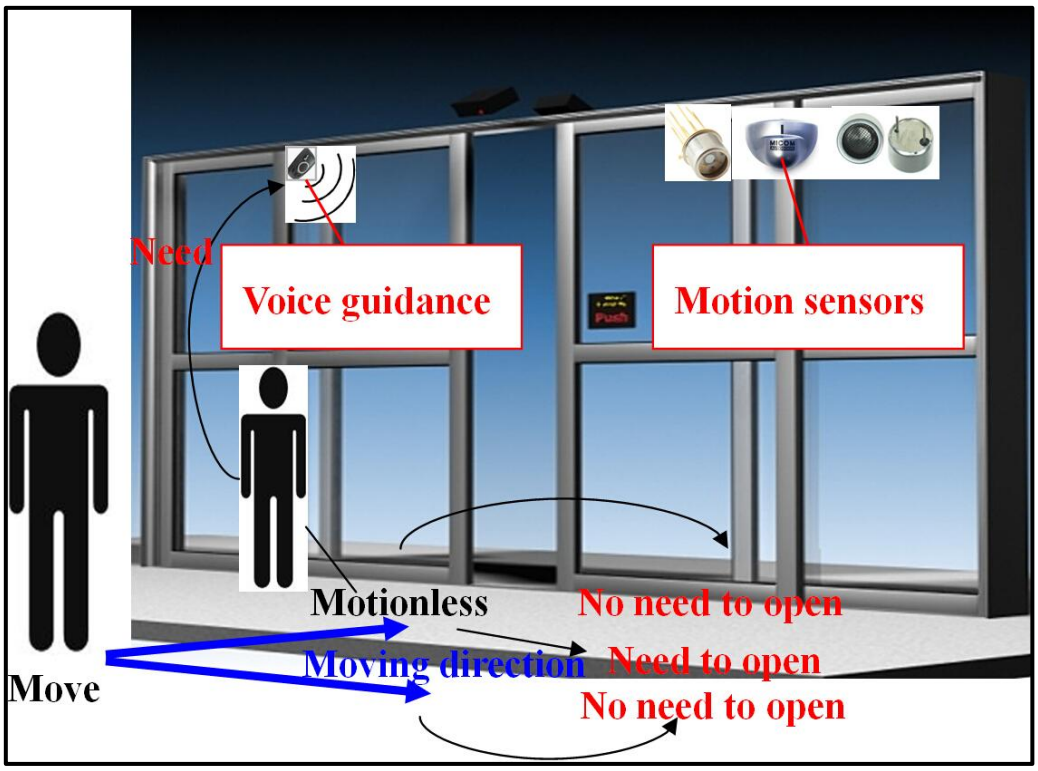


(a)

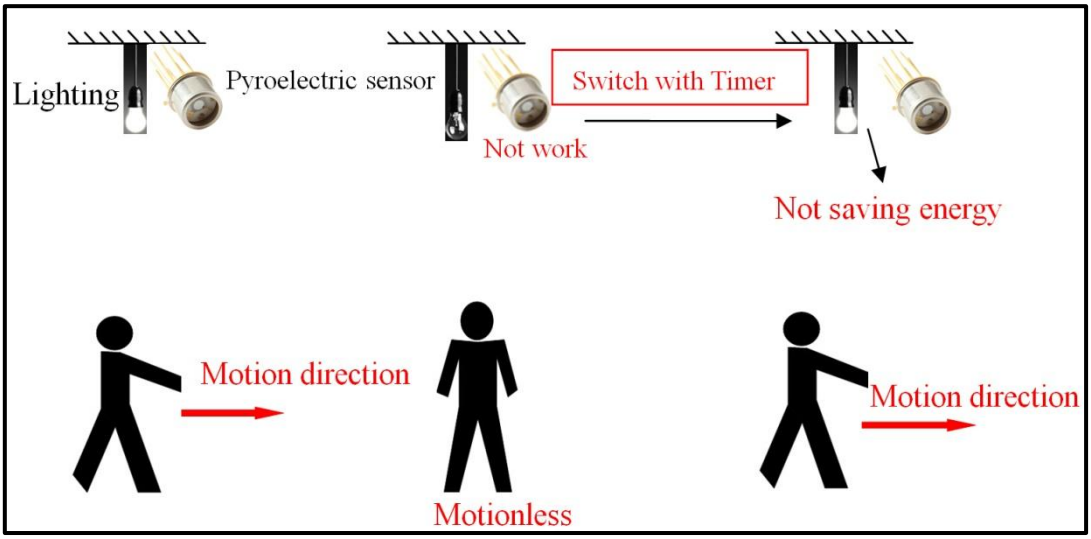


(b)

Fig. 1.2 Devices to detect human-beings

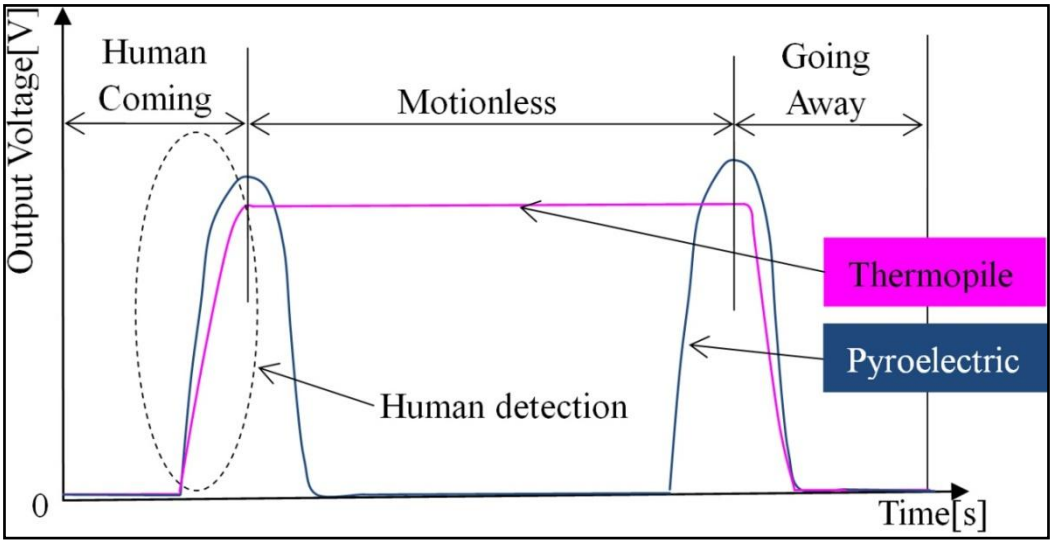


Fig. 1.3 Sensor outputs of pyroelectricity and thermopile

Thermopile infrared sensor is a thermoelectric device that consists of an array of thermocouples connected in series. It is widely used in non-contact temperature measurement applications, such as gas sensing and monitoring [18], ear thermometry [19], Intrusion alarms [20], pyrometry [21], etc.

## 1.2 Thermopile sensor

During 1810-1820, Thomas Johann Seebeck began to study the behavior of the junction of conductive materials. In 1821, he found a small current will overflow in a closed loop of two different metallic conductors, when their junctions are kept at different temperatures [22],[23],[24].

The discovery of Seebeck indirectly contributed to the revival of the thermal properties of the debate. Most physicists believed that radiant heat and light have different phenomena. But this incorrect belief was caused by the fact that it was not possible to measure small temperature differences with available measurements. Unfortunately, the small output voltage of Seebeck's thermocouples, some μV/K, mainly also prevents a very small temperature difference measurements. However, There are several Nobili bismuth copper thermocouples connected in series, to produce a higher output voltage and therefore measurable idea. This thermocouple output voltage linearly increases the number of connected structures thermocouples. Higher sensitivity of this device allows for a more accurate temperature measurement. After 1850, it resulted in which light and heat radiation differ only in their respective wavelength [25],[26].

Today thermopile can be used to measure temperature or radiation that found in various applications. For example, gas sensors, surface temperature sensors and vacuum sensors. Until now, the working principle of the thermocouple remains unchanged. But like all electronic devices, they experienced a common trend of miniaturization. Thus, new manufacturing methods have been developed. The result showed that semiconductors are beneficial materials not only due to positive experiences in integrated circuit production. For the explaination of thermopiles in the μ m scale, They provided a higher Seebeck coefficient and facilitated the use of micro-machining technology. In recent years different semiconducting material systems have been explored. For technical and economic reasons, the common industrial system is today's CMOS thermocouple, which consists of aluminum-silicon thermocouple [27],[28].

## 1.3 Research concerning human detection by thermopile infrared sensor

Let's take a look at some of the practical researches available on human detection by thermopile sensor.

(A) *Advances in Thermal Infrared Localization: Challenges and Solutions*

This research mainly introduced how to localization in indoor environments. It works by using low-resolution line and an array of thermopile sensors, they are placed at the edge of the room. More specifically, each edge with two thermopile arrays, each thermopile array having eight pixel resolution. Also, depending on each thermopile array of six degrees which leads to the total FOV 48 ° (FOV) fields. The easiest way to determine the position of the heat source is the use of cross-point, which is created by the pixel having the highest result of the direction. The positioning based on thermopile array can be reached by measuring the angle of arrival (AOA) under which an object is seen. If several sensors are placed at different locations, people can finally calculate the position through triangulation. An example of this is shown in **Fig. 1.4**.

Some methods based thermopile sensor array were introduced for human positioning. For example, determined by the direction of the pixel source location with the highest results, and building relationships between the target and the sensor, then calculated by a simple algorithm based positioning triangulation of the position [29], [30], [31], [32].

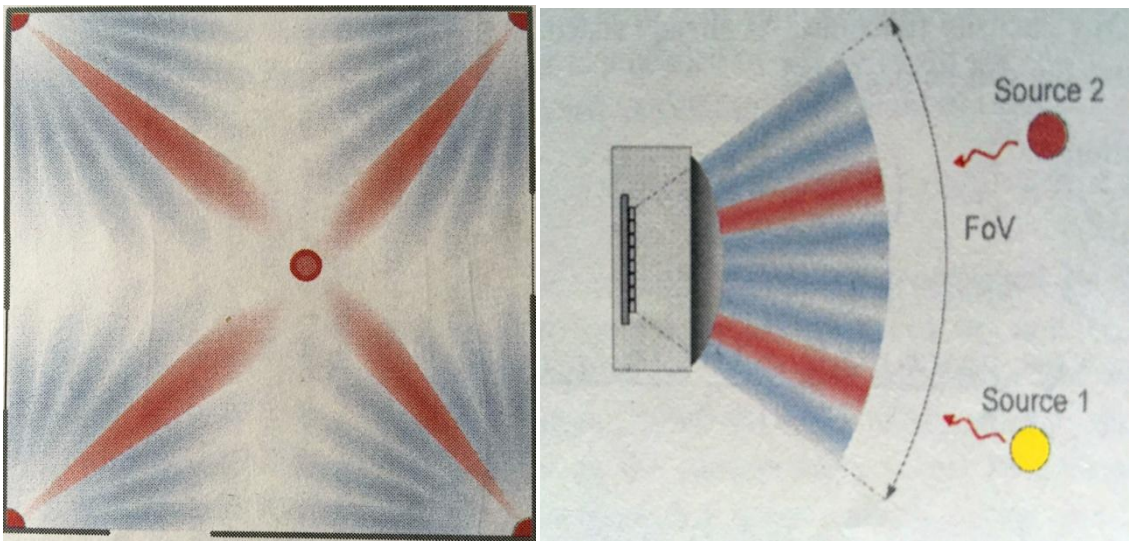


Fig. 1.4 Sample setup and Principle of AoA estimation

(B) *Human Detection Using Thermopiles*

This paper presents a simple approach to detect people using an 8×1 thermopile array sensor. To evaluate the performance of the sensor in the detection rate and false positives, which obtain people from the mobile robot's environment in doorways and pedestrian detection count in our actual life. (**Fig. 1.5**). Noted that each sensing element having a thermopile array field of view of 5.125 ° × 6 °.[33]


(a) (b)

Fig. 1.5 Human detection applications: (a) counting pedestrians in the campus entrance (b) detection of human for mobile robots

(C) *Using a thermopile matrix sensor to recognize energy-related activities in offices*

This study describes a novel generation of their study 2D matrix thermopile sensor, which is used to identify interactions from their heat occupant objects and object model, a total of 21 activities using the installation of a single sensor. Activities are selected according to their own devices energy correlation, and proposed the concept of a suitable matrix thermopile sensors to detect and track the object processed. Also, interactive test object is based on the object status and occupant classification. [34]


(a) Thermopile sensor used: GridEye. (b) For evaluation about office pantry area.

**Fig. 1.6** Illustrations thermopile sensor and location. The sensor was placed on the ceiling, capturing corner table, microwave, and faucet, refrigerator and coffee maker counter.

Research (A) as mentioned above, linear array thermopile sensors can only detect horizontal direction. Consequently, they must be placed at chest height due to their small limited vertical FOV, so they are not practical in real applications with some objects. And the drawback of research (B) is that when ambient temperature increases and becomes similar to that of the human body it becomes harder to distinguish people from the background. This fact limits the practical application of the sensor to air conditioned buildings or places where the weather does not exceed 30–32℃.

## 1.4 Our research goal

Therefore, we proposed to use mono-thermopile sensor without focus lens and with high-gain amplifier to detect human position, body orientation and motion. Although it has a high stability in the thermal environment, however, thermopile sensor has a common drawback. It detects the temperature of an object by absorbing the infrared radiation that emits from the object's surface, and the sensitivity of the sensor depends

on the ambient temperature, so it does not work well where the surveillance area is partially hot due to sunlight, heater or any heat sources.

Thermopiles detect the temperature of an object by absorbing the infrared radiation that emits from the object's surface, moreover, see also **Fig. 1.3**, it obviously can detect motionless human from its output, we thus focused on the thermopile sensor, which needed with a wide FOV in both the horizontal and vertical directions under any natural temperatures. Therefore, we proposed the use of mono-thermopile sensors without focus lenses and with high-gain amplifiers to detect the position, orientation and motion of human subjects.

Hence, the objectives of the research are defined as follows:

1. Detection of human position by two thermopile infrared sensors from wall.
2. Detection of human position and motion by two thermopile infrared sensors from ceiling.
3. Detection of human position and motion by two tilted thermopile infrared sensors from ceiling.

This theses is arranged where Chapter 2 is the basic physical principles and circuits of the thermopile sensor, and Chapter 3 explains measurement and approximation of sensor characteristic. The proposed method to detect human and accuracy and experimental results are respectively discussed in Chapter 4. Then Chapter 5 discusses about human detection from the ceiling by two sensors, which be attached in vertical direction, meanwhile some measurements and approximation about sensor also are introduced and proposed method also be discussed in this Chapter. Based on Chapter 5, Chapter 6 describes method about detection of human by tilted sensors. Last but not least, Chapter 7 contains the conclusions and future works of this research.

# CHAPTER 2. THERMOPILE INFRARED SENSOR AND CIRCUIT

## 2.1 Principle of Thermopile Infrared Sensor

Based on the thermoelectric effect, thermopile can be used as a thermal sensor for measuring thermal radiation. Thermocouples composed of polysilicon and aluminum, which connected in series. When temperature rises in each thermocouple junction, thermal electromotive force will be generated directly proportional to the differential temperature produced between the thermocouple, so the output can be got by their additive voltage. This effect is called a thermoelectric effect. The connection of many thermocouples in series produces higher voltage, known as the Seebeck Effect [35]. By using this characteristic of thermopile sensors, the transferring the heat radiation emitted from the objects into a voltage output, human-beings can be detected.

## 2.2 Characteristics of Thermopile sensor

There are many types of thermopile infrared sensor, the type we used is called MIR-1002 [36], which have a hermetically sealed and rugged construction are made by the SSC Company, and **Fig. 2.1** shows the external dimensions and picture which we used.

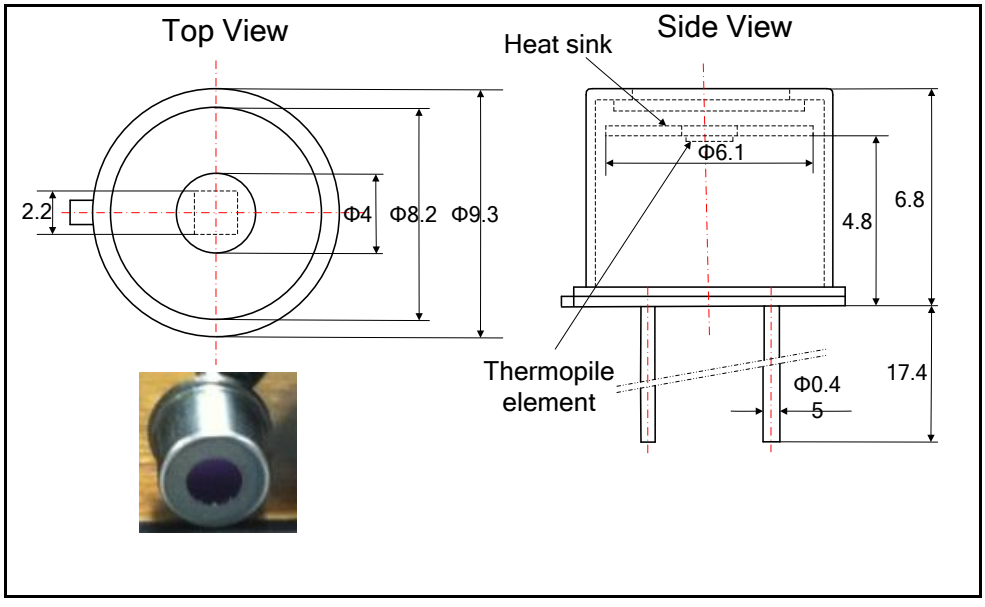


Fig. 2.1 External dimensions of thermopile sensor we used

It is with advantages of adequate sensitivity (11.5V/W) and flat spectral response, the filter's substrate is made of silicon and transmission is about 75%. Meanwhile they measure infrared radiation in the range of 6.4–14μm, thus almost can't affected by some factors, i.e., lighting. The specifications of sensors are shown in **Table 2.1** [37].

There are many types about thermopile sensor, why do we select this product? That is because it has built-in thermistor, which makes temperature compensation easy, while high stability in the thermal environment can ensure stability in the process of detection.

TABLE 2.1 CHARACTERISTICS WITHOUT WAVE FILTER
(AMBIENT TEMP.: 25°C)

| | Min | Typical | Max | Unit |
|---|---|---|---|---|
| Sensitivity | 20.1 | 25.0 | 30.9 | V/W (500K,DC) |
| Resistance | 8 | 11 | 14 | K-Ohm |
| Output Voltage | 750 | 950 | 1150 | μV(500K,DC) |
| Noise Voltage | 11.5 | 13.4 | 15.2 | nV/ root Hz. |
| NEP | 0.37 | 0.53 | 0.76 | nW/ root Hz. |
| Detectivtiy D* | 2.8 | 4.2 | 6.0 | 10cm root Hz. /W(500K,DC) |
| Thermal Time Constant | . | 120 | . | mSec |
| Field Area | . | 52 | . | Degree |
| Thermistor Resistance | 50K Ohm +/- 2% | | | Ambient temp.: 25℃ |
| Thermal Coefficient NTC | 3840K +/- 1% | | | B ntc |
| Operating Temp. | -20 to +50 | | | ℃ |
| Storage Temp. | -40 to +80 | | | ℃ |

The meaning of some parameters in detail will be introduced in the **Table 2.1** as follows:

Sensitivity:

To a thermopile sensor, the most important parameter is its sensitivity, named S, also be called responsivity, which connects the output voltage $V_{out}$ to the absorbed radiation source $S_{rad}$. It can be defined as:

$S = V_{out} / S_{rad}$

The result should be as high as possible. Normally the sensitivity of thermopiles are in the range of 10-100V/W, which rely on thermocouple type and number and absorber area.

Noise equivalent power (NEP):

Each circuit and an output signal of each sensor of distortion produced by electrical noise. The maximum noise source, which is apparatus considered here, is random (white) due to the ohmic resistance of the conductor charged internal fluctuation noise generated. The temperature makes the charge carriers moving back and forth. The average noise voltage ($V_{noise}$), which is in the output lead of the sensor is proportional to the square root of the resistance of the sensor ($R_{sens}$) and temperature T, which is given by:

$$V_{noise} = \sqrt{(4k_B T \cdot R_{sens} B)} \quad (2.1)$$

In 2.1, $k_B$ means the Boltzmann constant and B is the considered bandwidth which is usually decided by the measured facility. In order to become independent method by measuring, the noise voltage is normalized by B and therefore given in $V/Hz^{1/2}$. Below the noise value signal voltage cannot be resolved. The incident radiation has to provide an output voltage, which at least has noise value. The minimum resolvable radiated power referred noise equivalent power (NEP) and is given by

$$NEP = V_{noise} / S \quad (2.2)$$

The unit is recorded in $W/Hz^{1/2}$.

Thermopower:

Power generated by the temperature difference $\Delta T$ between the hot and cold end of the incident radiation, which caused the mentioned thermal voltage. The voltage relative to the size of the temperature difference is called the total thermal power, α, which can be wrote as follows:

$$\alpha = V_{out} / \Delta T \quad (2.3)$$

The unit is recorded in V/K. The typical value of a single thermocouple, which Si and Al is 250μV / K.

Detectivity:

NEP as a situation which does not exist as to the feature chart below, but the reciprocal value 1 / NEP, which is called detectivity D, and the unit is recorded in $Hz^{1/2}/W$.

Specific detectivity:

NEP parameters and thus the detection area depending on the detector $A_D$. There is usually a square root dependence of the detector area. In order to compare different

sensor types, the detectivity is normalized by $A_D$ $^{1/2}$ defining a specific detectivity D*, expressed like:

$$D* = \frac{AD^{\frac{1}{2}}}{NEP} = S(A_D B)^{1/2}/V_{noise} \quad (2.4)$$

The unit is recorded in cm・$Hz^{1/2}$ /W.

## 2.3 Application of Thermopile Sensor for Human Detection

The most important characteristic of the sensor is that it has no focus lenses. In a thermopile array, which is composed of a number of small sensors, each sensor has a field of view (FOV) of a few degrees, which leads to a larger total FOV. The detection area can be specified and accuracy improved by using focus lenses. However, the sensor we used is different from those in thermopile arrays as only one sensor is used, and the lack of a focus lenses does not decrease its FOV. Meanwhile, there are one limitation that we must keep FOV larger than object, show as **Fig. 2.2**.

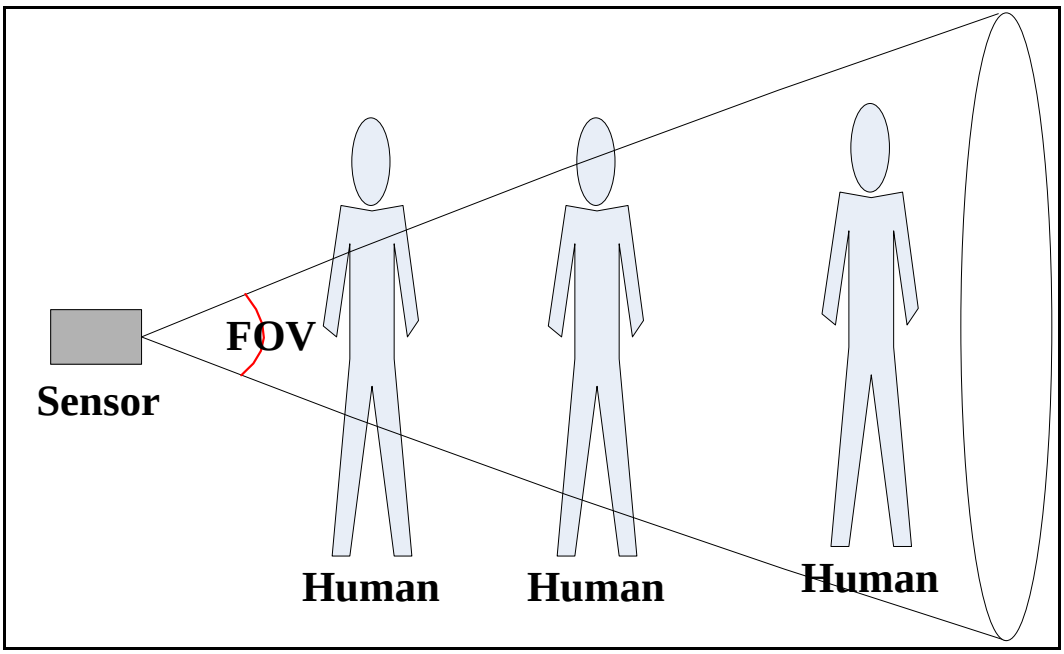


Fig.2.2 Relationship between FOV and human

Although they have a high levels of thermal stability, thermopile sensor has a common drawback. They detect the temperature of objects by absorbing the infrared radiation emitted from the objects' surface, but the sensitivity of the sensor depends on the ambient temperature. Therefore, they do not work well when the surveillance area is partially heated by sunlight, heaters or any heat sources. Still, the reference portion of

the detector is constantly absorbing heat and this brings some drifts, that we should consider when we use this sensor. A rubber cover show as **Fig. 2.3** is used to fix the sensor and to decrease sensor drift caused by wind.

## 2.4 Circuit and Experimental Setup

**Fig. 2.3** respectively shows circuits for the thermistor and thermopile sensor employed. Because the voltage that the thermopile outputs is measured in only milli-volts, in order to have a detectable output voltage, high gain amplifiers are employed to boost the voltage to the detectable level. Combining the features of precision, low power, and low bias current, two OPAmp497 and a OPAmp297 are implemented, as shown in **Fig. 2.3**, while in order to reshape, modify or reject all unwanted frequencies of an electrical signal, a low pass filter circuit also be employed, the sensor will filter out frequencies below 3Hz. and the voltage output can be controlled by adjusting the offset. Moreover, the thermopile sensor has a built-in thermistor that provides measurement of the ambient temperature, thus allowing the temperature of the target to be calculated and making temperature compensation easy. However, because the sensor circuit has a high gain amplifier, the output produces some drifts. **Fig. 2.4** shows the drift condition of the sensor used, and **Fig. 2.5** shows the flow of magnified process, and **Fig.2.6** shows the characteristic of thermistor. And experimental setup is shown as **Fig.2.7**.

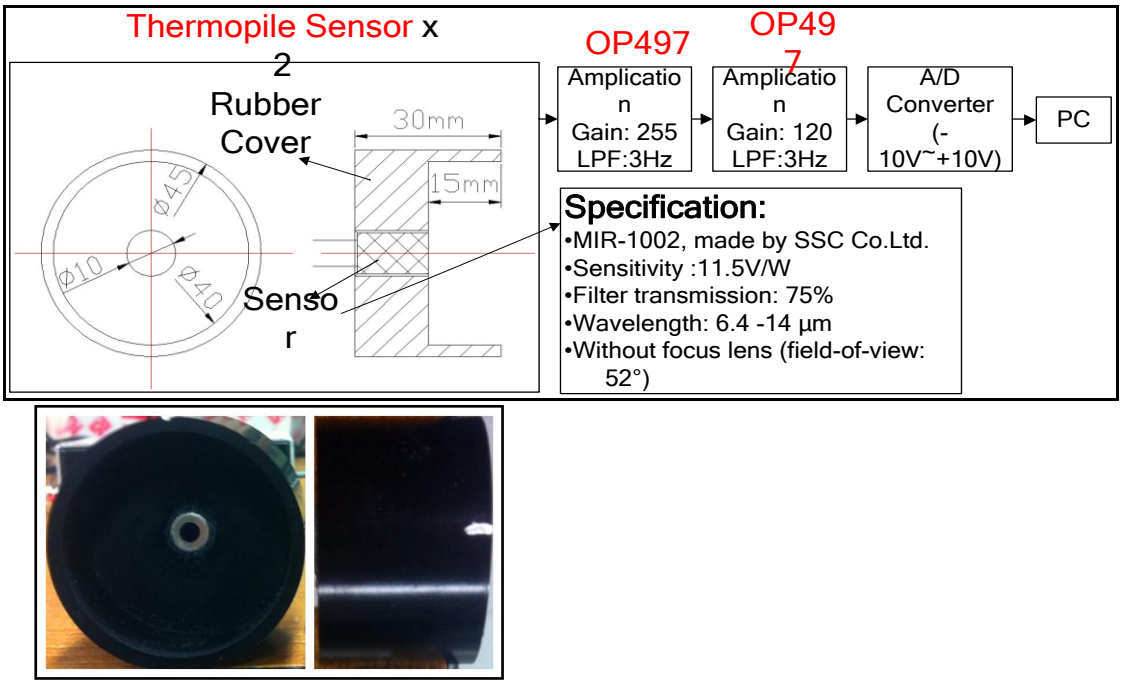


Fig. 2.3 Flow of magnified process

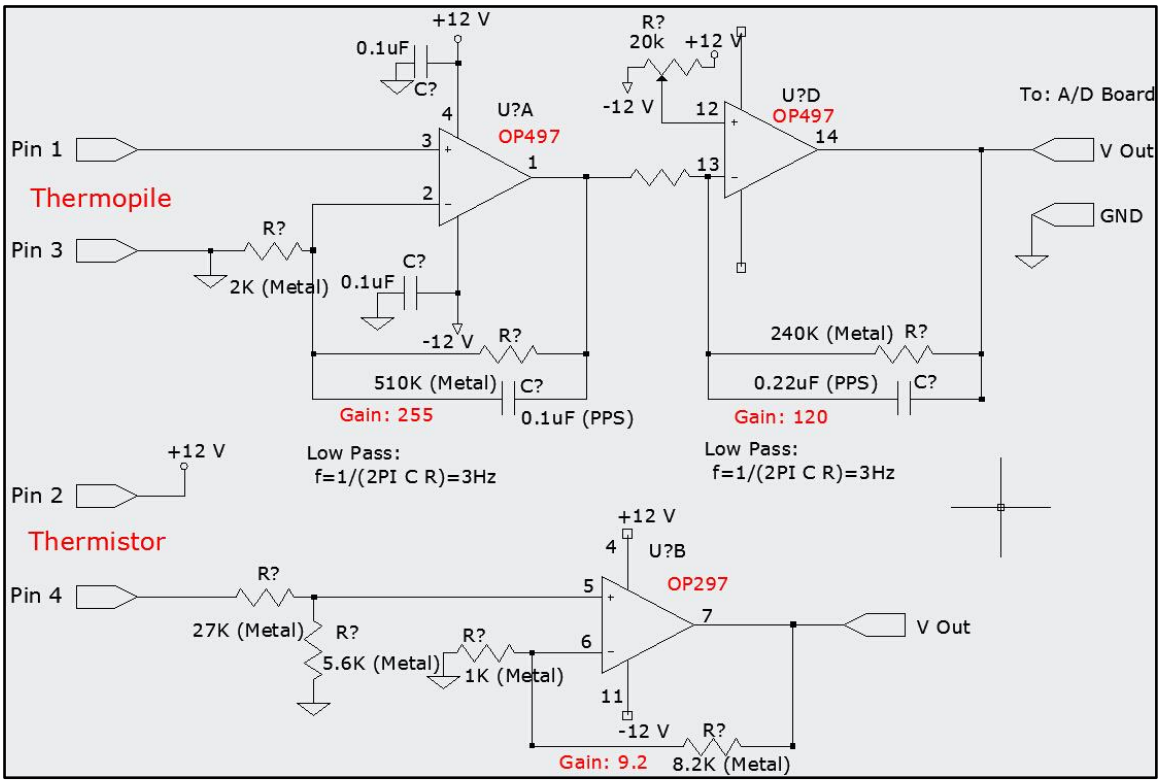


Fig. 2.4 Circuit of thermopile sensor

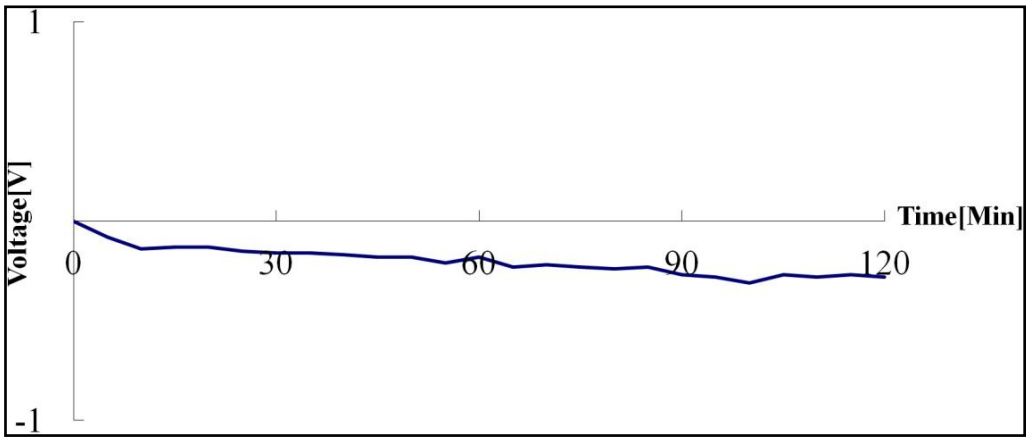


Fig. 2.5 Drift of sensor output

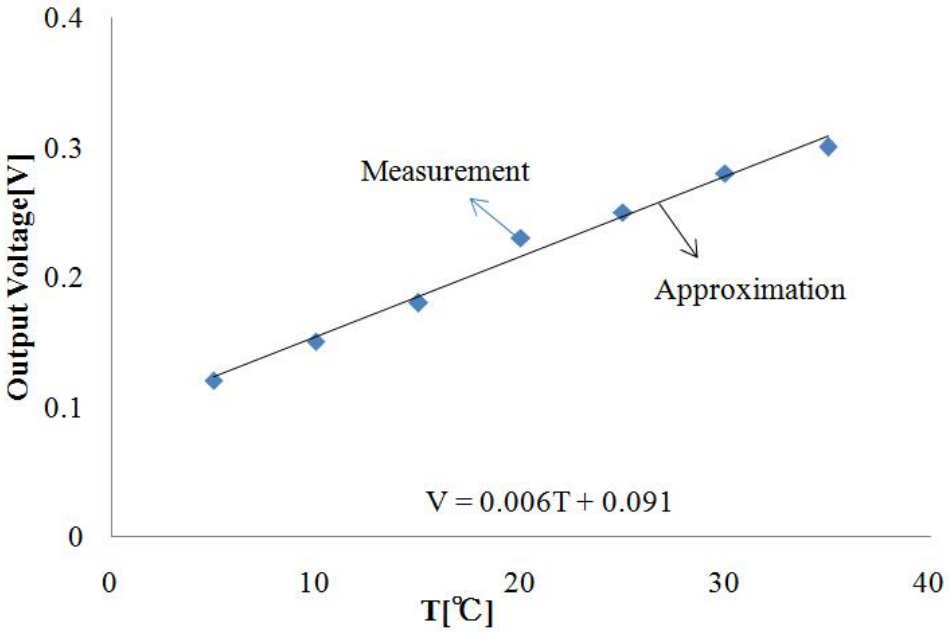


Fig. 2.6 Characteristic of thermistor

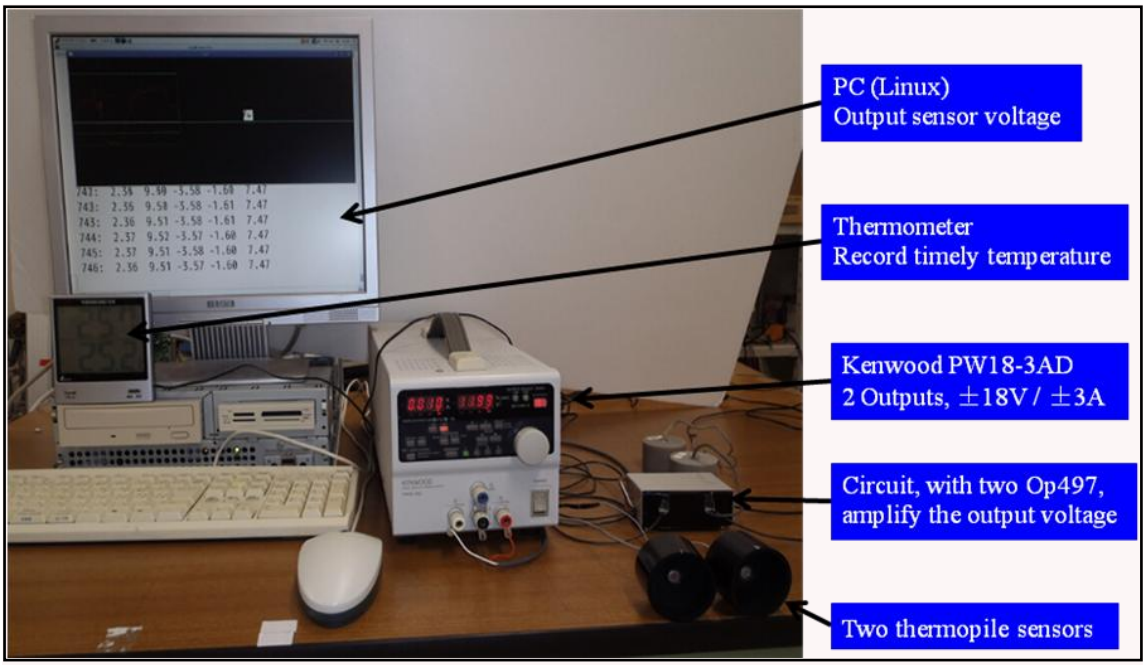


Fig. 2.7 Experimental setup

# CHAPTER 3. MESASUREMENT AND APPROXIMATION OF SENSOR CHARACTERISTIC

In order to detect human position, some basic characteristics about sensor and some factors between human and sensor be considered, including the distance (r), directivity namely angle (θ) from sensor to human, and ambient temperature (T) (**Fig. 3.1**). In the meanwhile, based on the sensor theory as mentioned, we can understand some approximate relationships between sensor output voltage and the factors through measurements.

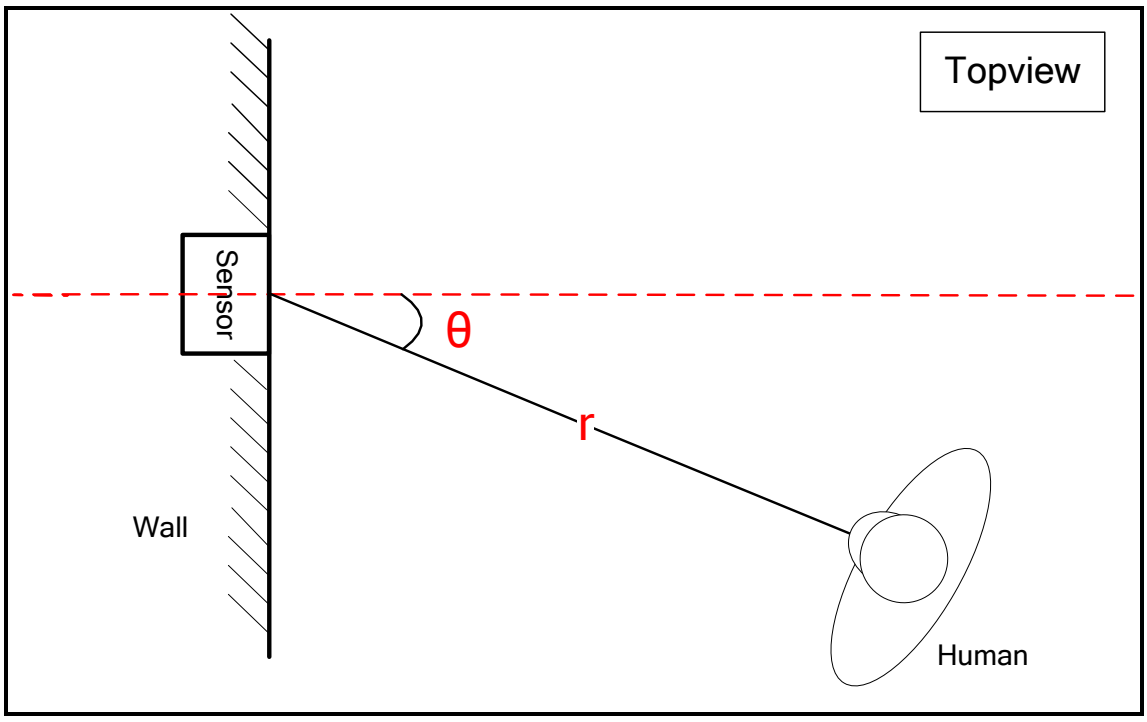


Fig. 3.1 Relationship between sensor and human

## 3.1 Measurement and approximation of distance and ambient temperature

### 3.1.1 Measurement

By the Stefan-Boltzmann law [38], the heat flux is proportional to $T_h^4 - T_a^4$ (with index 'h' denoting the human and 'a' the ambient). In the simplest case, we can therefore use the following relation for the output voltage $U_o$ of a thermopile sensor:

$$U_0 = K'(\varepsilon_0 T_h^4 - T_a^4) \tag{3.1}$$

where K' = K $\sin^2$ ($\varphi$/2) is a constant that depends on the FOV of the sensor, and $\varepsilon_o$ is the object's emissivity.

From (1), because $T_h$ is almost changeless, so we can generally infer that there is an inversely proportional relationship between ambient temperature $T_a$ and sensor output $U_o$.

For verifying its validity, I did the experiment stated as follows: fixed the sensor on the table, and kept it in front of human body, and then measured when standing in some positions from 0.2m to 2m by every 0.2m (**Fig. 3.2**). However, as already mentioned, the sensor output itself has some drifts, so we utilized the method that got the difference of output voltage measured between manned and unmanned shown as **Fig. 3.3**, moreover, each experiment was measured 5 times in order to reduce errors. The difference between manned and unmanned shown as **Fig. 3.4**.

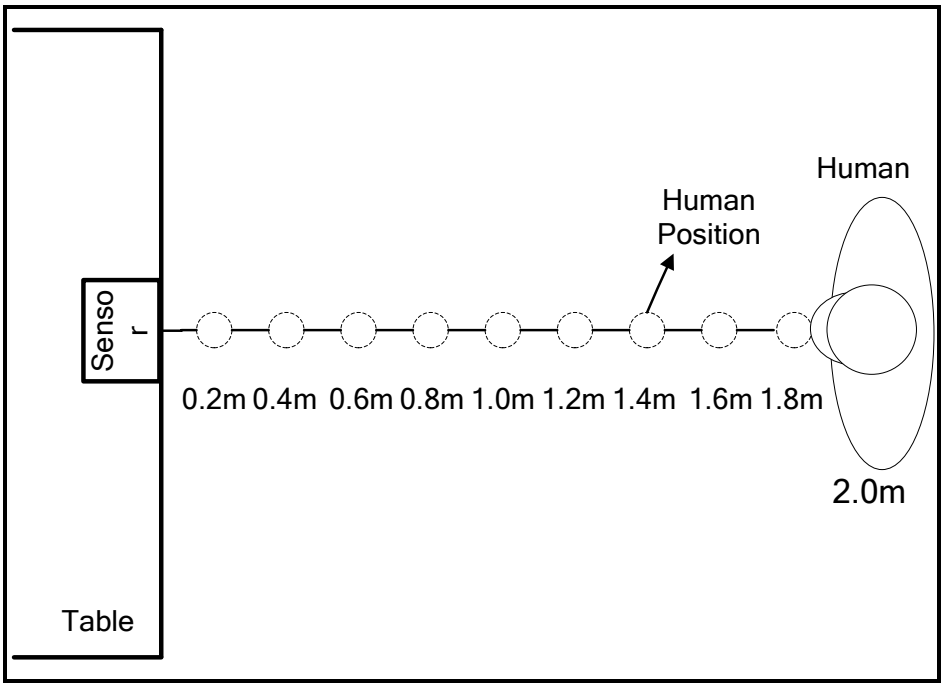


Fig. 3.2 Picture imagination for experiment

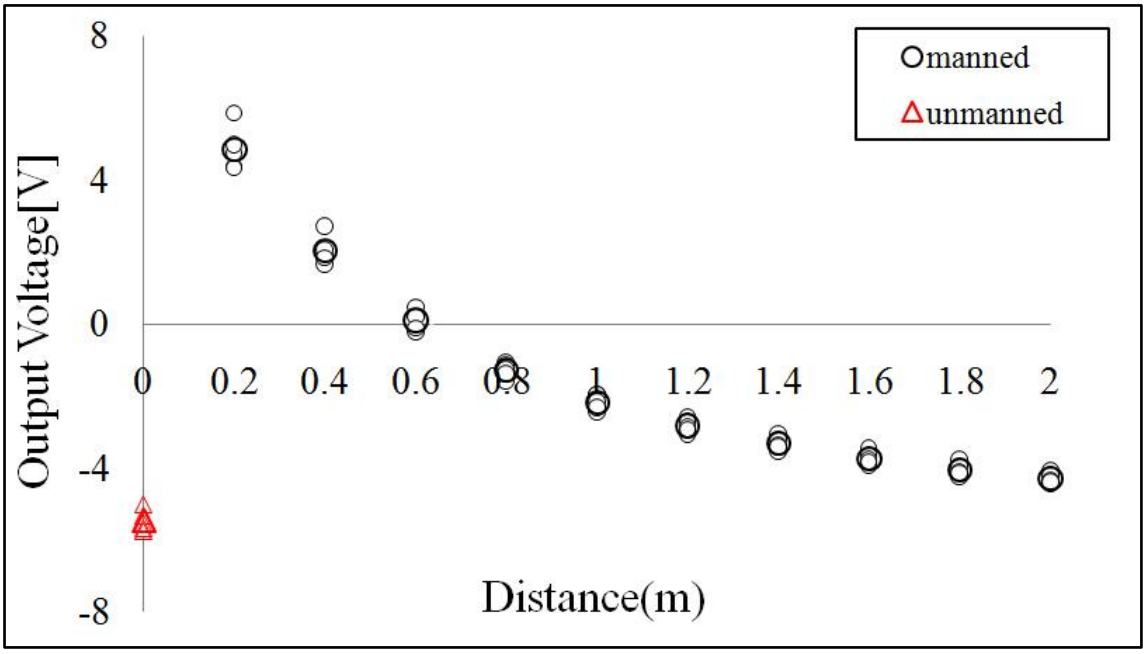


Fig. 3.3 Measurement results between manned and unmanned

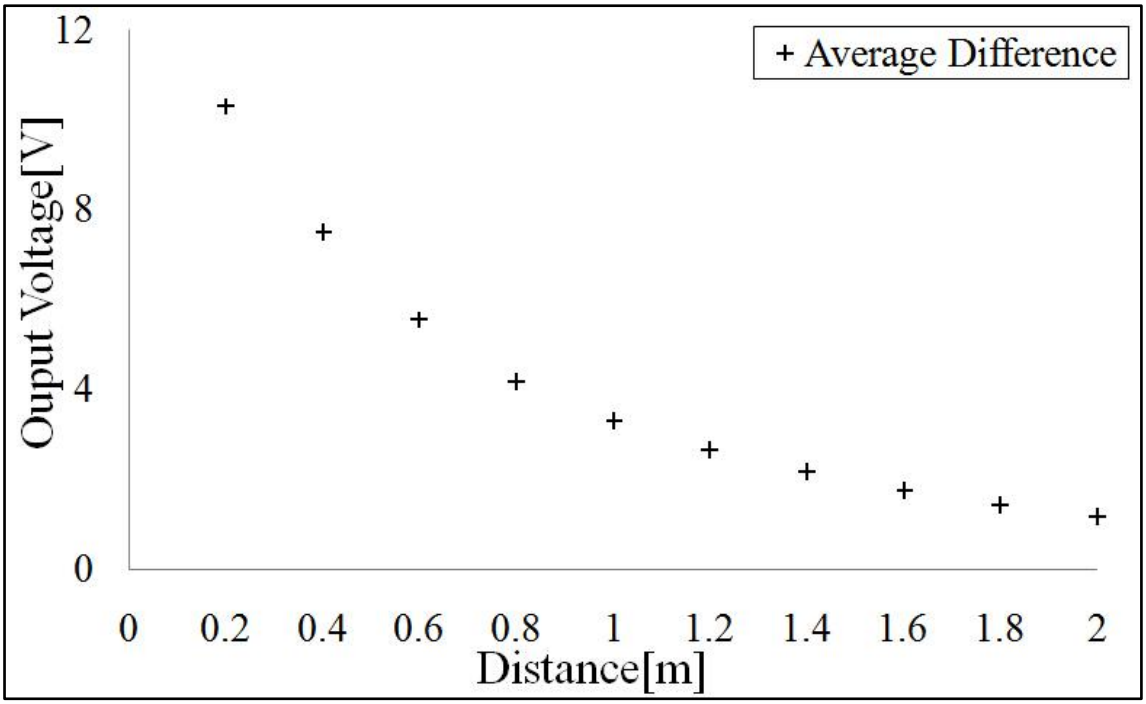


Fig. 3.4 Difference between manned and unmanned

The experiment was repeatedly measured many times respectively at different temperatures. Some results are shown in **Fig. 3.5**.

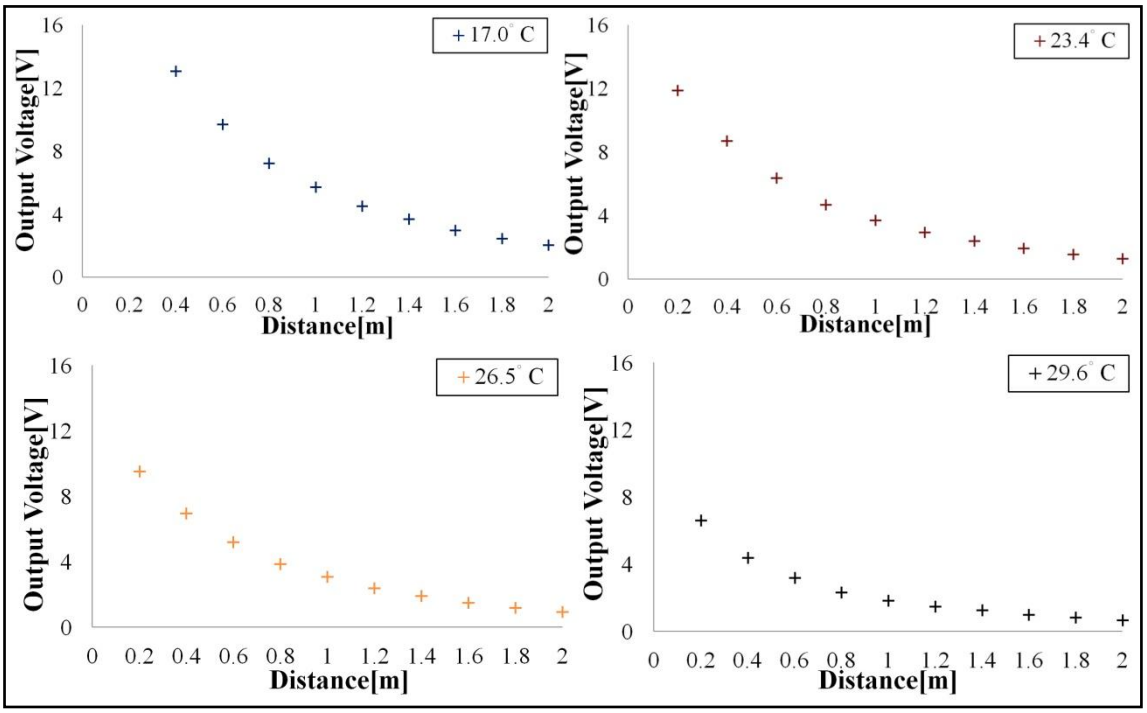


Fig. 3.5 Output results of one sensor at some temperatures

Above mentioned figures show results about one sensor. Similarly, the results of the other sensor show as **Fig. 3.6**:

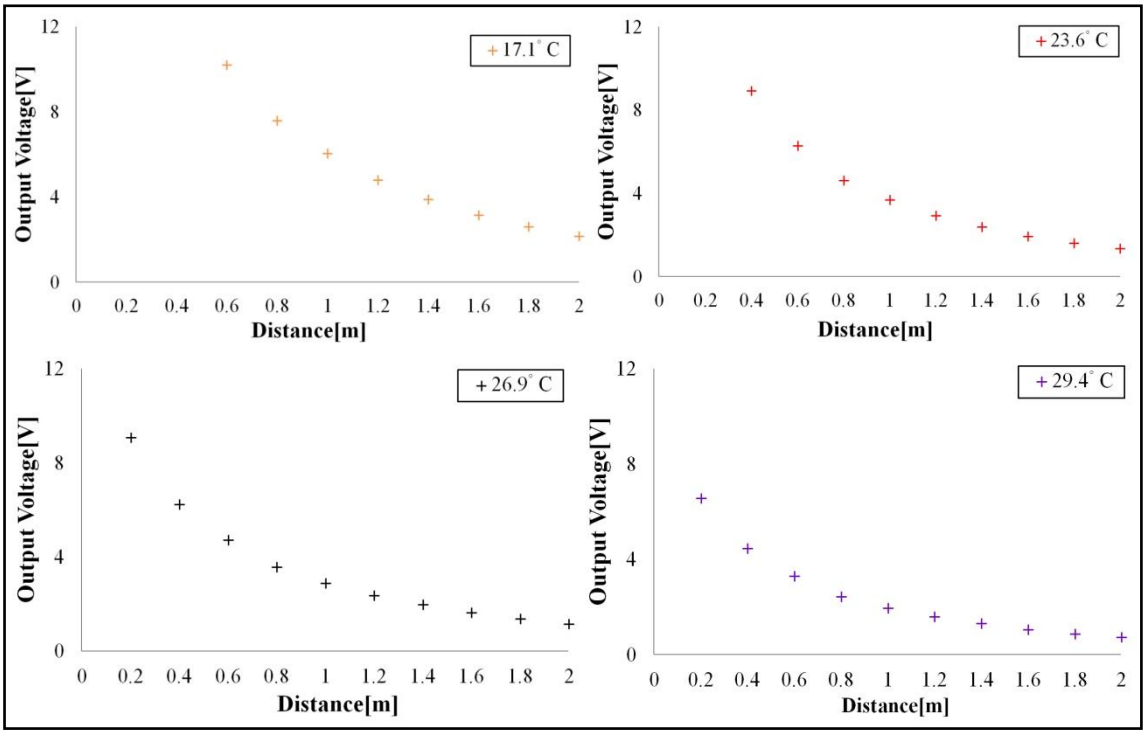


Fig. 3.6 Output results of the other sensor at some temperatures

Through observing the **Fig. 3.5** or **Fig.3.6**, we were aware that each output curve has similar shape. Hence, we compared results between different temperatures, shown as **Fig. 3.7**.

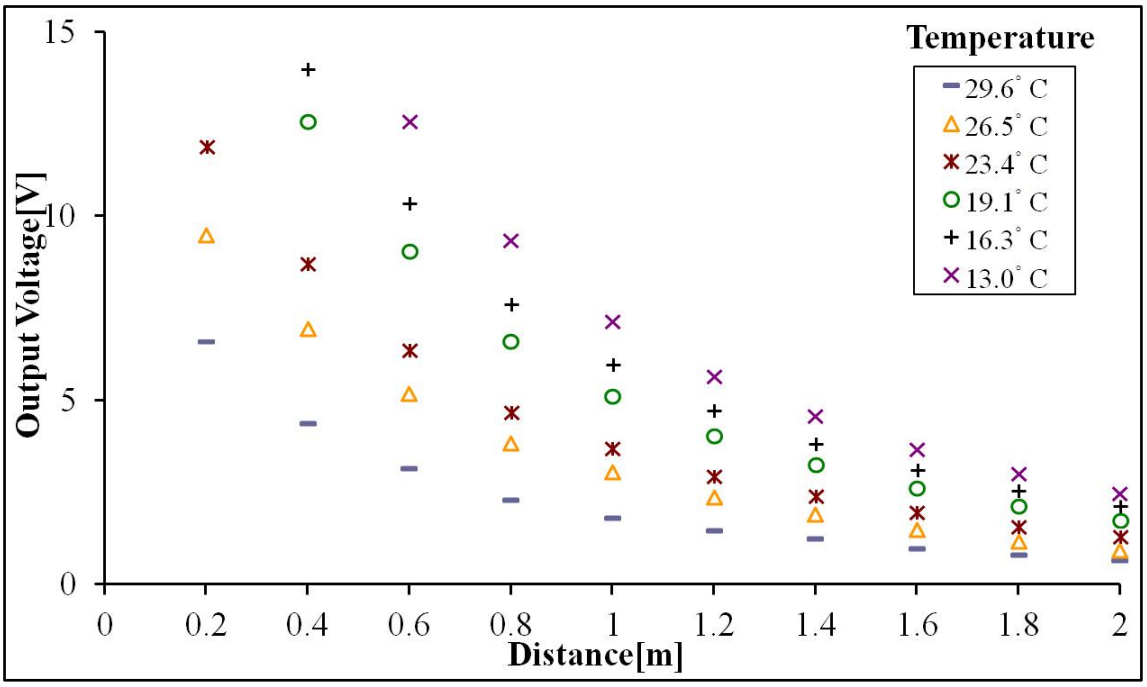


Fig. 3.7 Relationship between distance, temperature and sensor output

We can also see clearly that not only illustrates the correctness of the conjecture in the first part of this section, but also shows that distance(r) from sensor to human is inversely proportional to sensor's output from **Fig. 3.7**.

### 3.1.2 Approximation

Based on the results shown as **Fig. 3.7**, because of what the output curves have certain similarity, we assumed that each curve should have a corresponding equation belong to the curve itself, and all of the equations maybe have a common equation. Based on the assumption, we can utilize the approximation to obtain output curves' common equation. The process of approximation is stated as follows:

1. According to the output style of the curve, we can generally infer the equation's relational expression which could show some types like the following:

$$V_r(r) = a_0/(r^2 + a_1) \quad (3.1)$$

$$V_r(r) = a_0/(r + a_1)^2 \quad (3.2)$$

where $a_0$ and $a_1$ denote constant and $V_r(r)$ is output voltage.

2. By comparing curves drawn by equation with curves drawn by experiment, compared results about two sensors at each temperature are shown in **Fig. 3.8** and **Fig. 3.9**, and through slightly altering the values of parameters ($a_0$ and $a_1$) in the equation to make the difference value as small as possible at each distance.

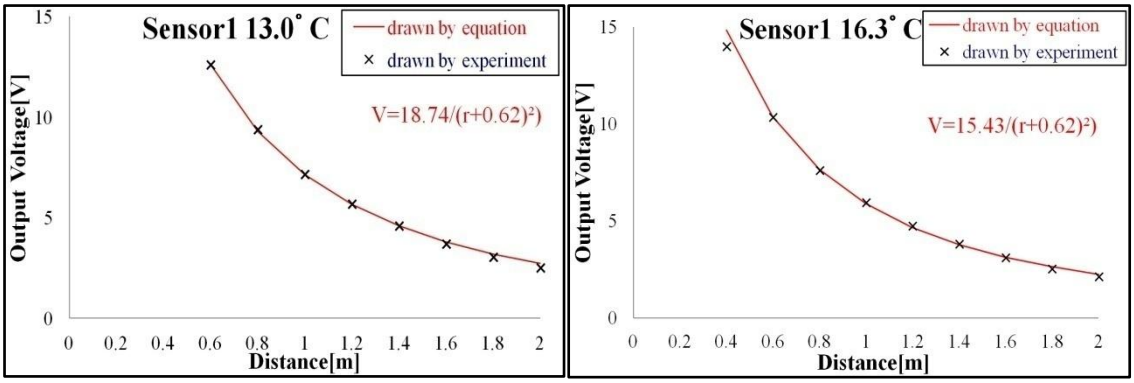


(a) 13.0℃




(b) 16.3℃

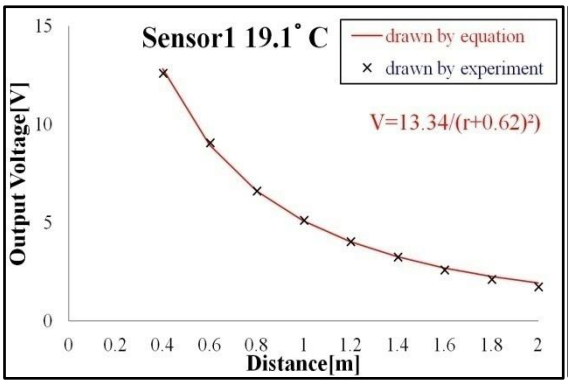


(c) 19.1℃

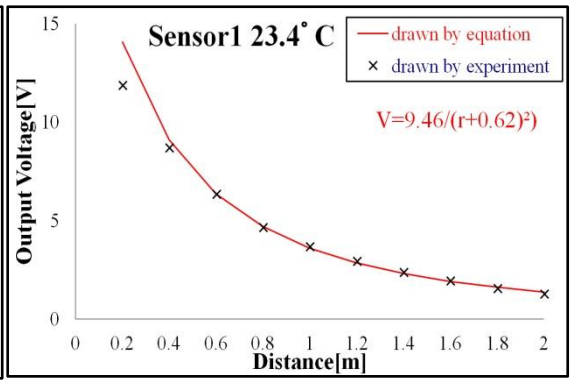


(d) 23.4℃

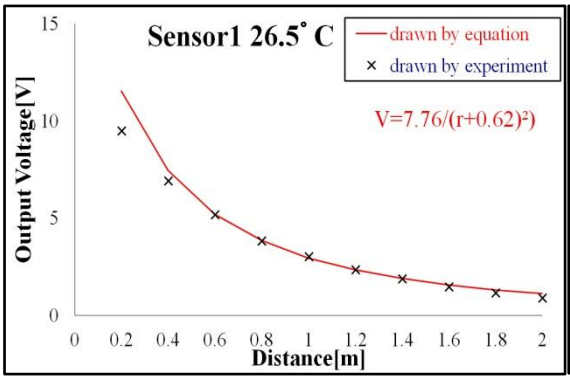


(e) 26.5℃

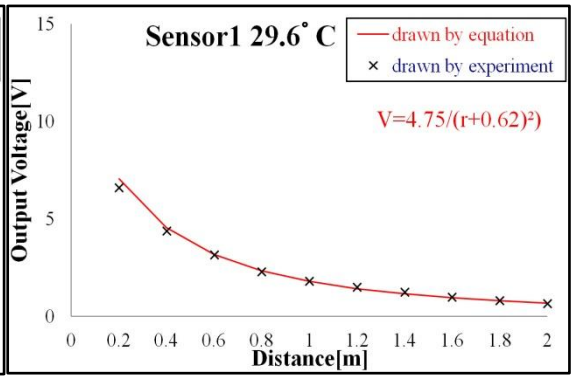


(f) 29.6℃

Fig. 3.8 Comparison between experimental and calculative at some temperatures (sensor1)

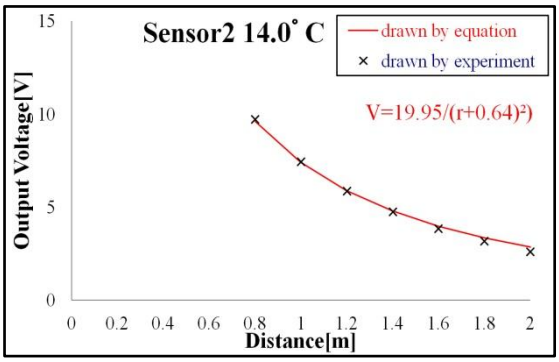


(a) 14.0℃

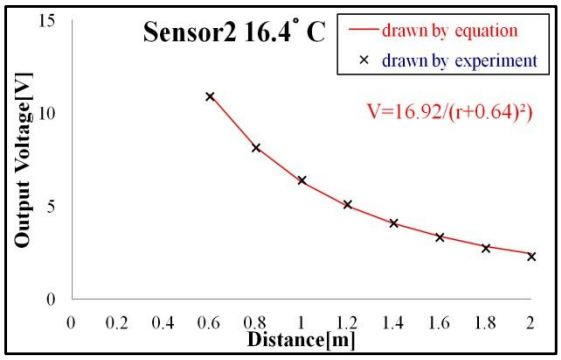


(b) 16.4℃

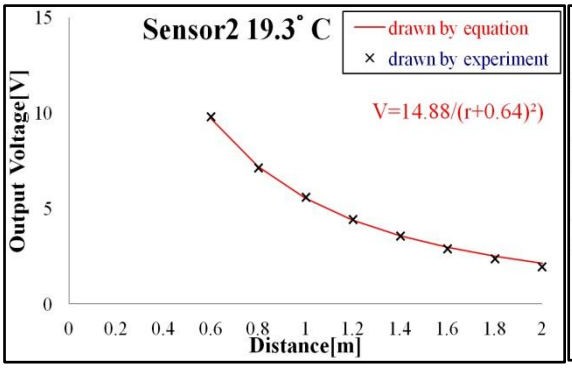


(c) 19.3℃

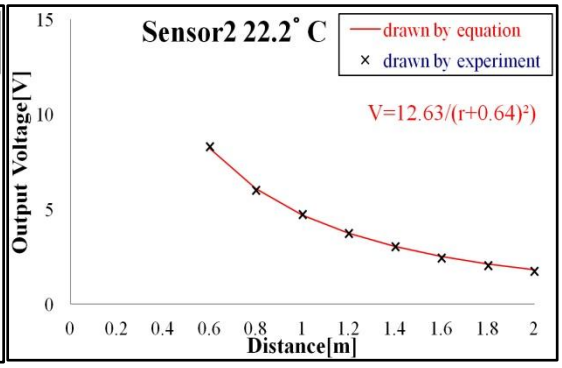


(d) 22.2℃

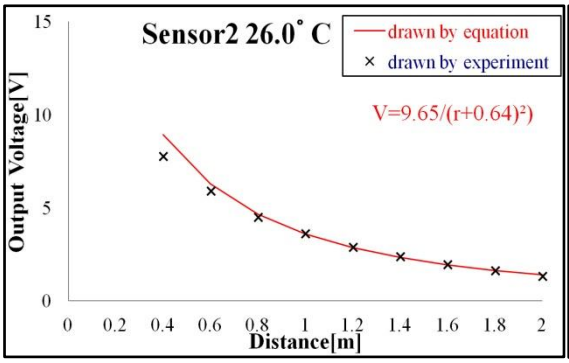


(e) 26.0℃

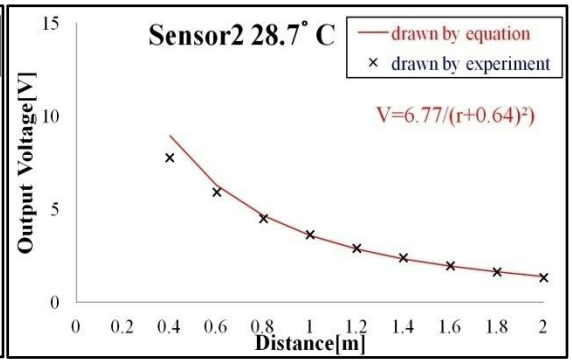


(f) 28.7℃

Fig. 3.9 Comparison between experimental and calculative at some temperatures (sensor2)

From the comparison results among them, we awarded that any equation could find suited parameter ($a_0$ and $a_1$), which making curve fitting. We should find which equation is the optimal one, that is, the optimum equation should ensure that no matter at which temperature, it could find suited parameter ($a_0$ and $a_1$) to make curve fitting.

### 3.1.3 Evaluation of Approximation

Utilizing programming to seek out the most suitable equation that can make the difference value smallest at all temperatures, Specific practices are as follows:
The total Error can be expressed by the difference between experimental data and theoretical data at all temperatures. Through calculating and comparing, finally we can ensure the eq.(3.2) as the curve's equation. The comparison result shows as **Table 3.1**.

TABLE 3.1
COMPARISONS BETWEEN DIFFERENT APPROXIMATION EQUTIONS

| Temp. [℃] | Error [V] | |
|---|---|---|
| | $V_r = a_0 / (r^2 + a_1)$ | $V_r = a_0 / (r + a_1)^2$ |
| 13.0 | 0.09 | 0.082 |
| 13.7 | 0.09 | 0.084 |
| 14.1 | 0.089 | 0.068 |
| 15.0 | 0.089 | 0.077 |
| 16.3 | 0.203 | 0.14 |
| 17.0 | 0.156 | 0.171 |
| 19.1 | 0.26 | 0.089 |
| 20.6 | 0.173 | 0.096 |
| 21.7 | 0.185 | 0.075 |
| 23.4 | 0.352 | 0.302 |
| 25.9 | 0.207 | 0.668 |
| 26.5 | 0.286 | 0.312 |
| 28.0 | 0.203 | 0.198 |
| 28.7 | 0.222 | 0.205 |
| 29.6 | 0.248 | 0.094 |
| Yellow means smaller value | | |

Meanwhile, we could get the optimum values of $a_0$ and $a_1$. It was found that the value of $a_1$ is constant and depends on the sensors, different sensors have different values. The specific values are listed in Table 3.2 later in this chapter. Moreover, $a_0$ has an approximate linear relationship with temperature (T) (**Fig. 3.10**), we finally obtained the linear equation expressed like $a_0 = a_5T + a_6$, where $a_5$ and $a_6$ are constant.

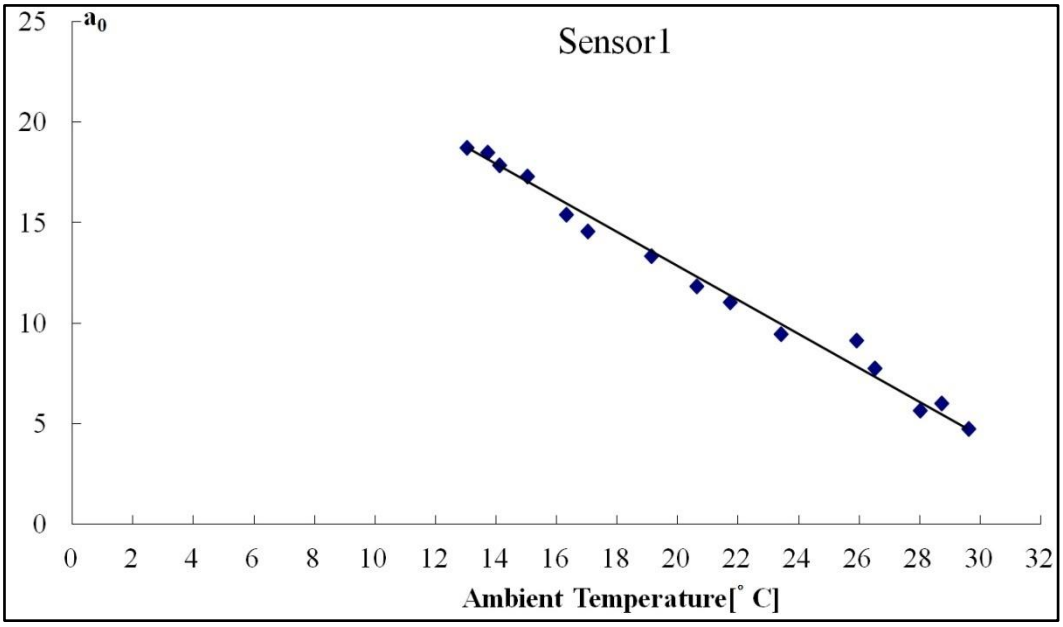


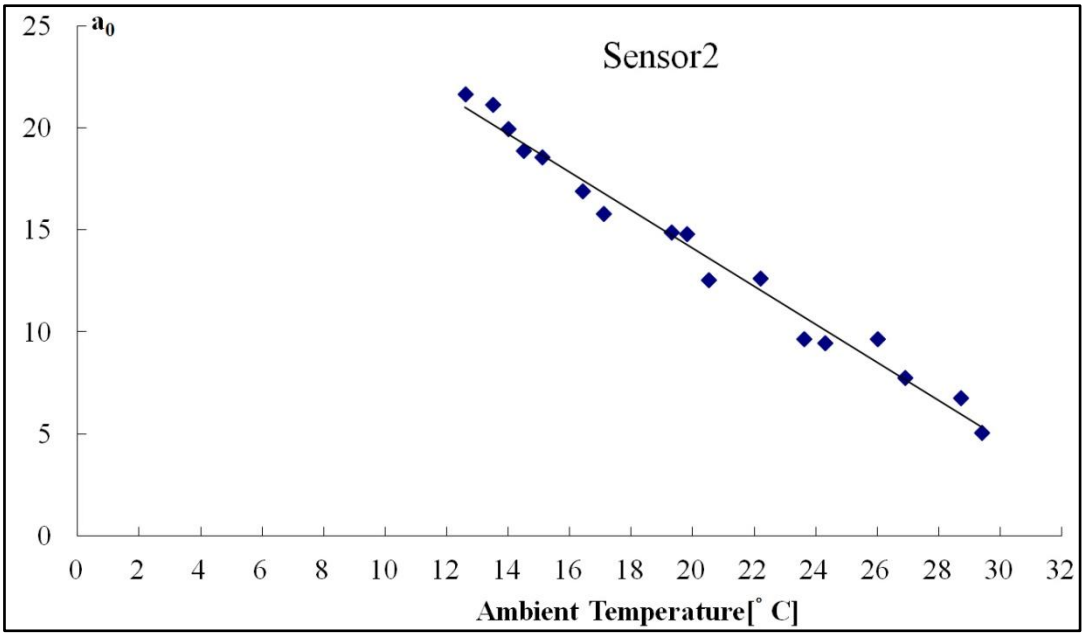


Fig. 3.10 Relationship between $a_0$ and ambient temperature at each sensor

## 3.2 Measurement and approximation of directivity

### 3.2.1 Directivity

Thermopile sensor has directivity, that is, it is effective for detecting human position in some areas, and effective area can be mainly realized through measurement. We

respectively kept body standing at different angles but equidistant distance with sensor and measured, the method of measurement is similar to distance experiment of Section 3.1.1 shown as **Fig. 3.11**.

Meanwhile, we respectively did the same experiment, which put the sensor on the table, separately measured when distance = (1m, 2m). The results are represented as shown in the **Fig. 3.11**. From this graph, we can see that there are almost similar output curve shapes between them, and the effective area could probably be measured from -50 degree to 50 degree.

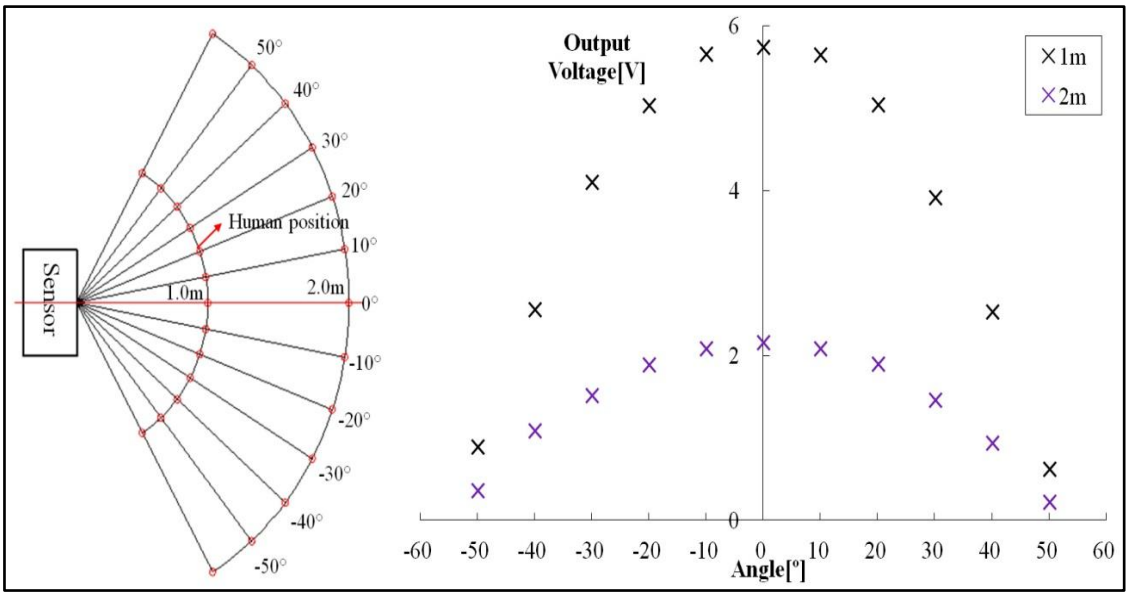


Fig. 3.11 Measurement for sensor directivity

### 3.2.2 Approximation

The equation of curve can be obtained by approximation, and method of obtainment is the same to distance, so it will not be described in detail. **Fig. 3.12** separately shows the comparison results measured at 1m and 2m. Their approximation equations are very close, hence, finally the equation obtained is expressed approximately to:

$$V_\theta(\theta) = a_2(1 - a_3\theta^2 + a_4\theta^4) \quad (3.3)$$

where $V_\theta$ denotes voltage output, values of $a_2$, $a_3$, $a_4$ are constant and depend on sensors.

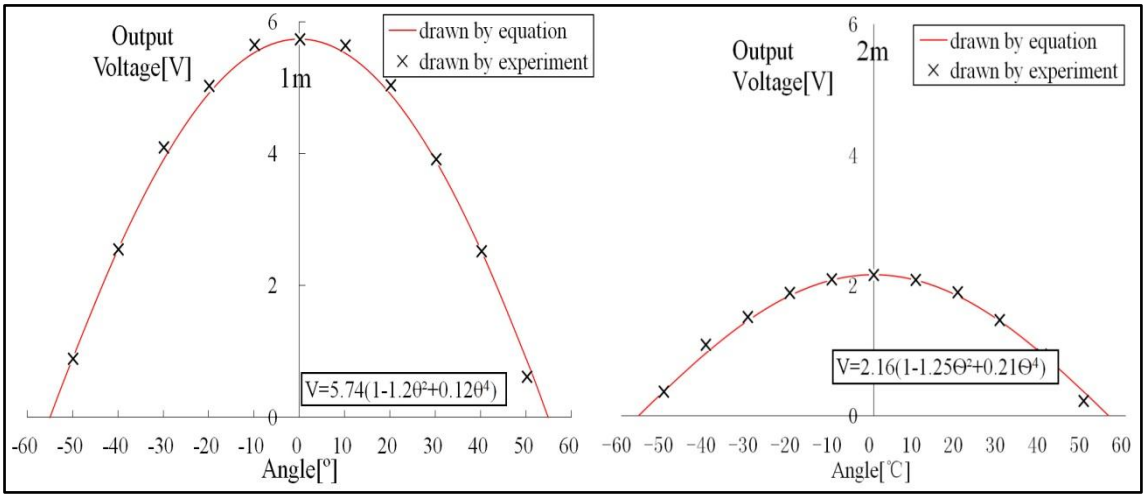


Fig.3.12 Comparison between experimental and calculative at different angles

Moreover, the measurement result of the other sensor is almost same with the sensor we listed.

Together, a general equation can be approximately built from the relationship equation among them, that is:

$$V(r,\theta,T) = (a_5 T + a_6)[1 - a_3\theta^2 + a_4\theta^4]/(r + a_1)^2 \tag{3.4}$$

and each sensor corresponds to the same equation but different parameters. All of the specific values are listed in **Table 3.2**.

TABLE 3.2 APPROXIMATED PARAMETER VALUES OF TWO SENSORS

| Parameter<br>Sensor | a1 | a2 | a3 | a4 | a5 | a6 |
|---|---|---|---|---|---|---|
| Sensor1 | 0.62 | 1 | 1.20 | 0.12 | -0.90 | 31.65 |
| Sensor2 | 0.64 | 1 | 1.45 | 0.44 | -0.93 | 31.87 |

## 3.3 Experiments about influence factor to sensor

In the process of measuring, we found that sensor was influenced by some factors, for example, human wearing different clothes, rotation of body, different human, and sensor at different heights. We specially did some experiments about these factors to see what kind of impact they can produce. All the experiments were measured in a certain

conditions, for instance, in the same ambient temperature, human standing on the same position and keeping same situation, and so on. Experiment setup shows as **Fig. 3.11**.

### 3.3.1 Clothes

We did some experiments when human respectively wear T-shirt and jacket shown as **Fig. 3.13**. We just used one of the two sensors, which were located on the table and human stood in front of the sensor, then measured every 0.2m from 0.2m to 2m. Each experiment was measured by 5 times, and **Fig. 3.13** shows the average value of the output voltage. We could infer the results that the output voltage values when human wear jacket are smaller than the values when wear T-shirt. This conclusion also verified the Stefan-Boltzmann law mentioned in the foregoing, which the less the heat radiation, the smaller the output voltage. When wear more, cause heat radiation decreasing, thus the output voltage becomes smaller.

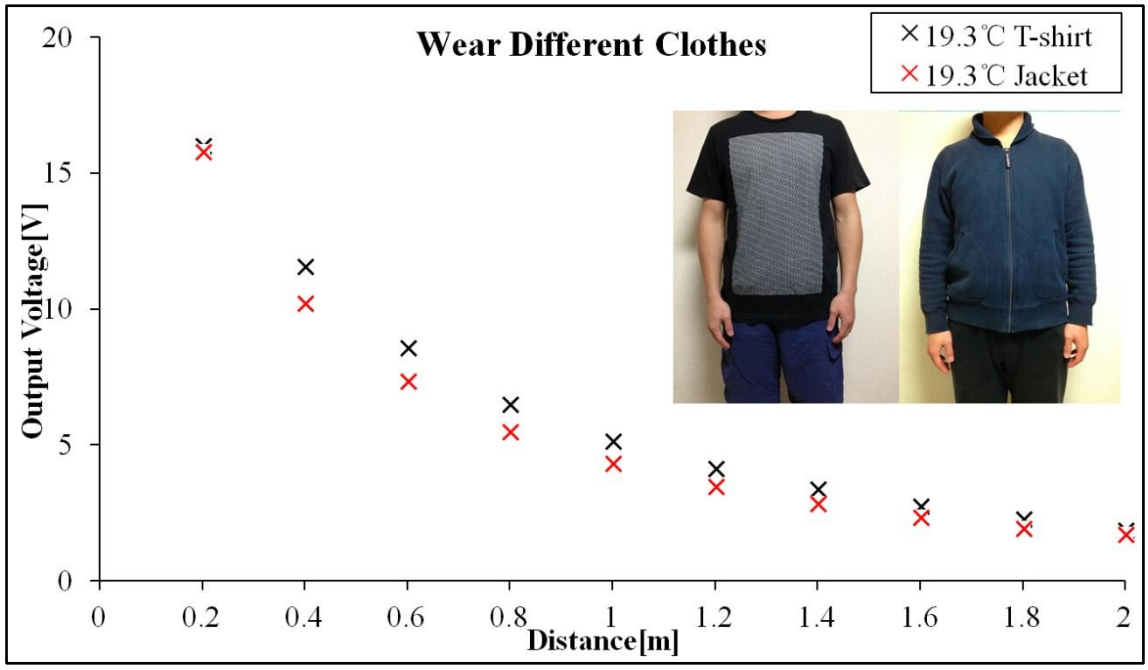


Fig. 3.13 Comparison between different clothes

### 3.3.2 Rotation of Body

This experiment was measured when keeping human's body at different angles but same distance relative to the sensors. We respectively measured in three distances (1m,1.5m,2m) by every 30°. **Fig. 3.14** shows the relationship between them, we could

understood that the output when body face to the sensor was almost symmetric with the output when body back to the sensor, meanwhile the output voltage values depended on the area of human' body, and it illustrates that the area of body is proportional to the sensor output voltage.

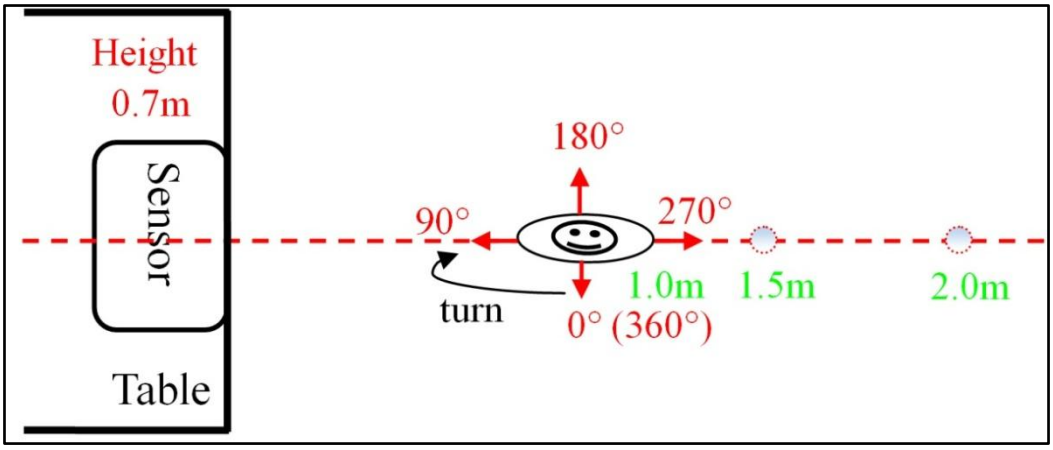


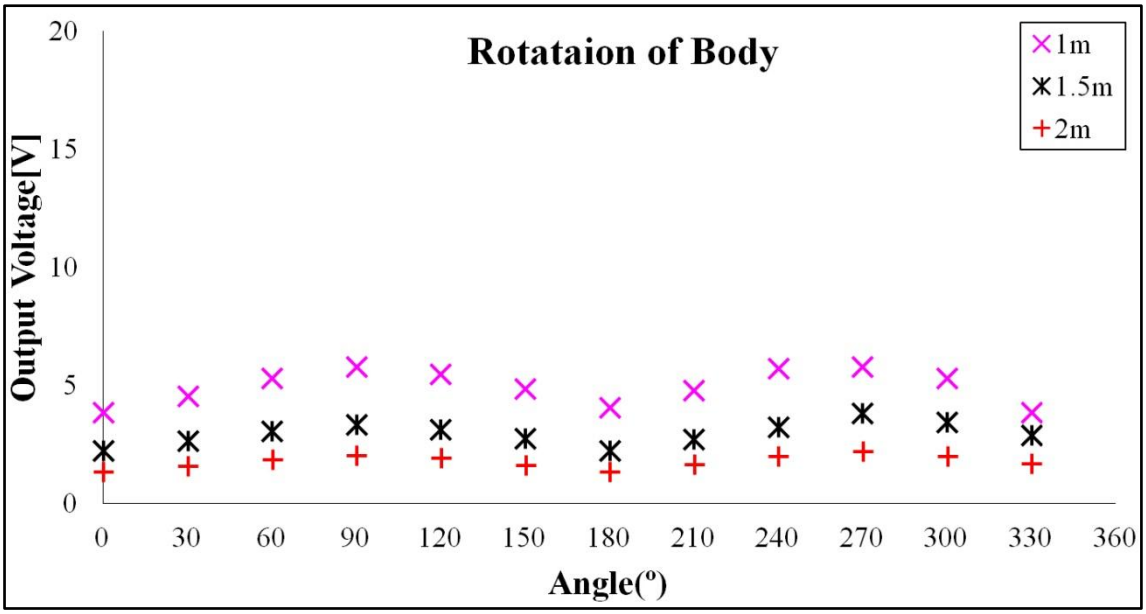


Fig. 3.14 Comparison between different angles of human's body

### 3.3.3 Different Humans

This experiment was separately measured on three persons. **Table 3.3** shows some specific parameters of their bodies. The process of the measurement was the same to the clothes experiment. **Fig. 3.15** shows output relationship among them. We could generally got the conclusion that the taller and heavier the person, the bigger the output voltage.

TABLE 3.3 THE SPECIFIC PARAMETERS ABOUT DIFFERENT HUMAN

| Parameter<br>Human | Height<br>[cm] | Weight<br>[kg] | Hipline<br>[cm] | Waistline<br>[cm] | Bust<br>[cm] |
|---|---|---|---|---|---|
| Human1 | 170 | 65 | 103 | 85 | 88 |
| Human2 | 183 | 85 | 114 | 93 | 98 |
| Human3 | 175 | 70 | 110 | 90 | 90 |

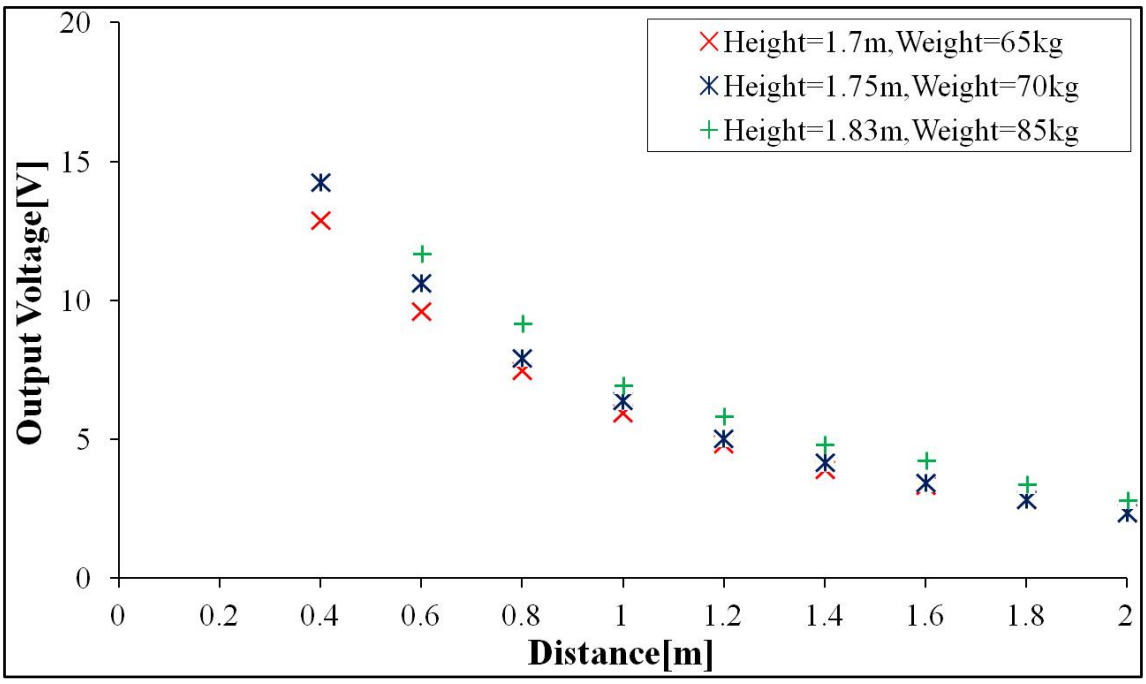


Fig.3.15 Comparison between different persons

### 3.3.4 Sensor height

This experiment was measured through keeping the sensor at different heights, which separately measured at a height of 0.76m, 0.98m and 1.15m shown as the picture of **Fig. 3.16**. From the picture, we can understand that height 0.76m is corresponding to the crotch of body, while height 0.98m is corresponding to the belly of body, and height 1.15m is generally located on the chest of body. The measurement process was also the same to the clothes experiment. See the result from **Fig. 3.16**. We could infer that the value of output voltage completely depends on the area of the body detected, and an obviously direct proportion relationship between them.

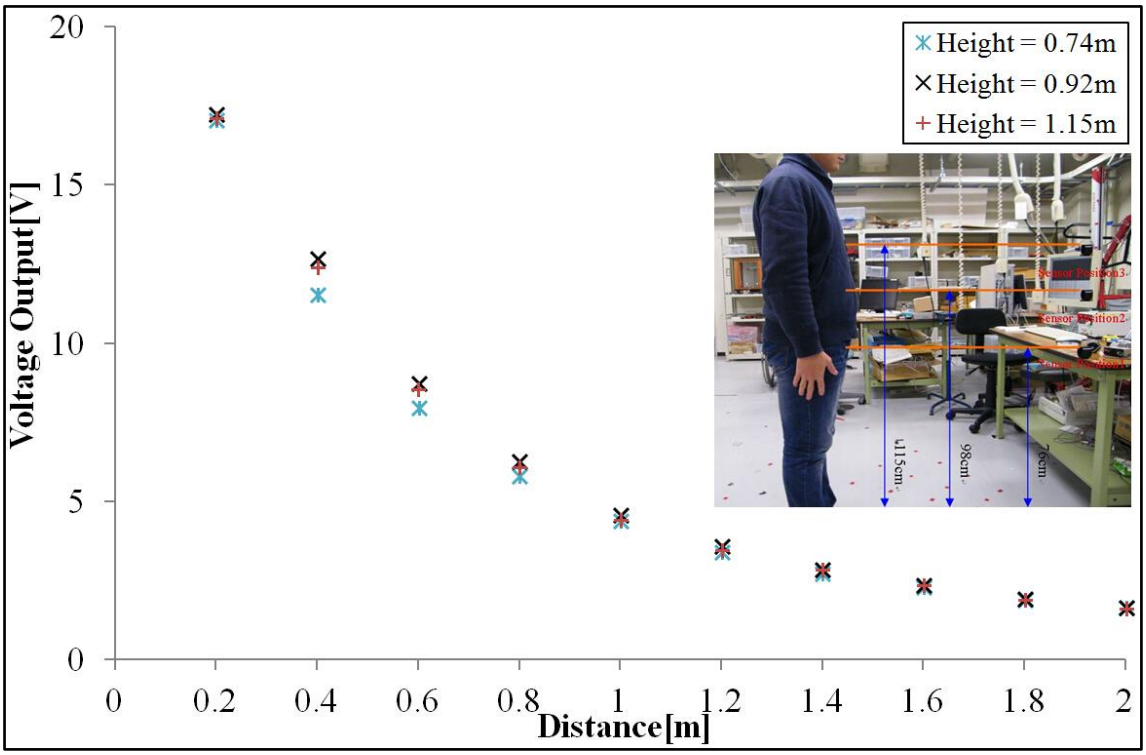


Fig. 3.16 Comparison between different sensor heights

### 3.3.5 Light

In addition, we also did some other experiments. We have mentioned that sensor cannot be influenced by the lighting in the room. So we did an experiment to verify whether is true or not. We separately kept lighting on and off to measure at some same positions under same temperature. Comparison results are shown as **Fig. 3.17**.

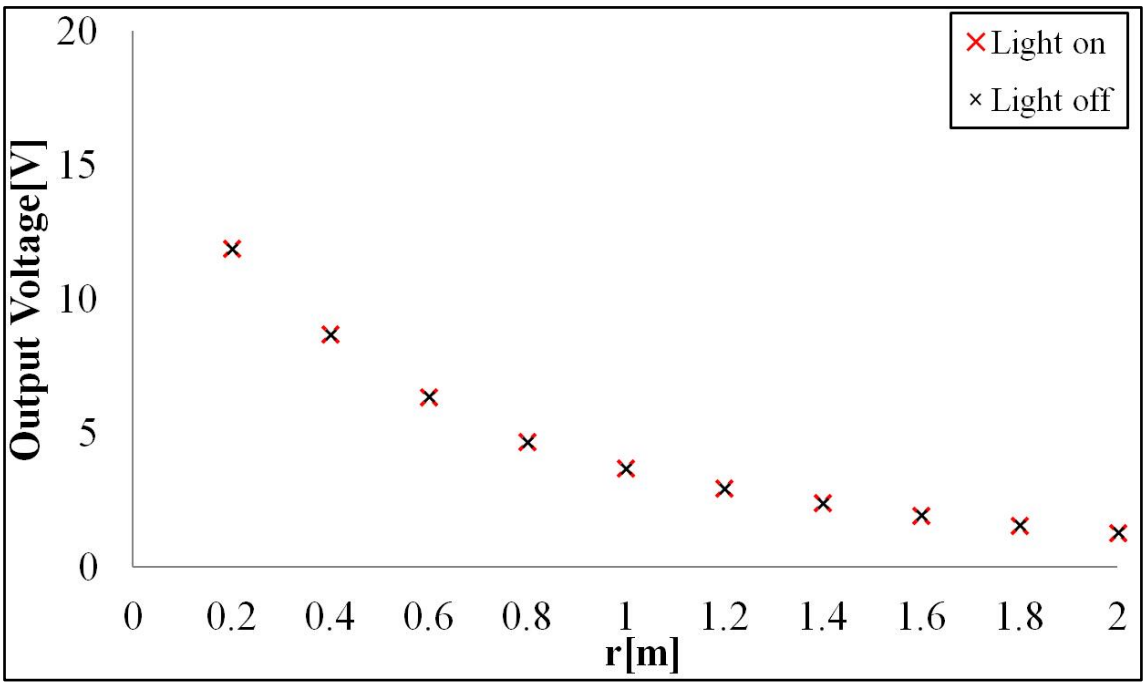


Fig. 3.17 Comparison between lighting on and off

Comparison result shows that it indeed illustrates the characteristic of thermopile sensor.

### 3.3.6 Two persons

Meanwhile, we did an experiment to see how the result is when measured not only by one person. That is, one person still stood at a certain position and the other person move one by one position as previous experiment. Result shows as **Fig. 3.18**.

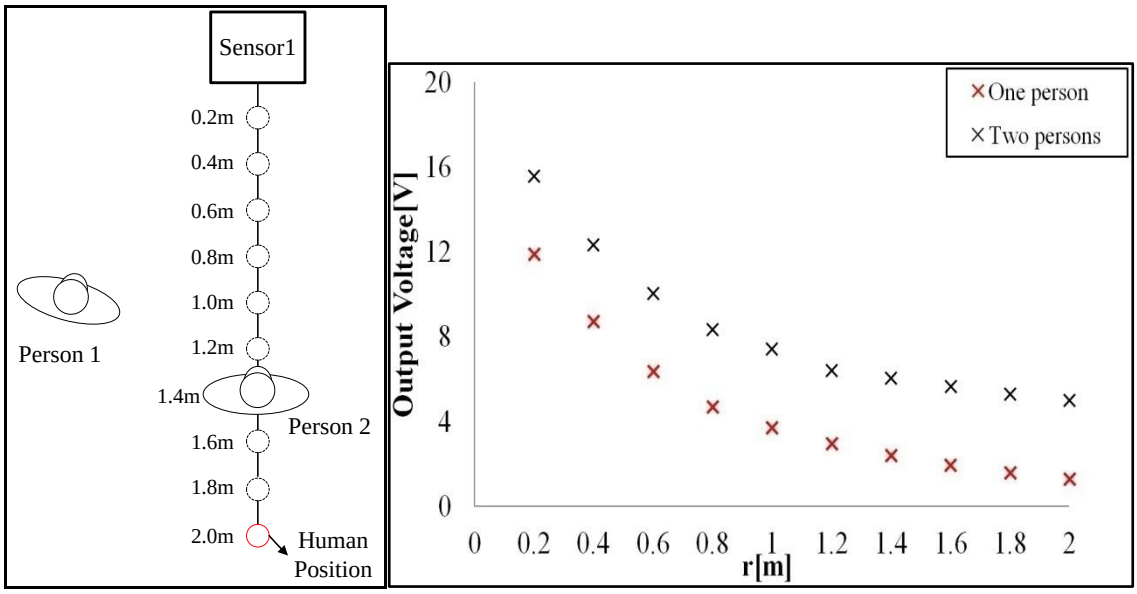


Fig. 3.18 Comparison result between one person and two persons

From the comparison result, we can see that output result by two persons is larger than one person because of more incidence radiations by two persons. Hence, we can conclude that this sensor system we developed only can detect one person.

# CHAPTER 4. HUMAN DETECTION BY SENSORS FROM WALL

## 4.1 Basic method

From the above approximation equation which we obtained in previous chapter, which is

$$V(r,\theta,T) = (a_5T + a_6)[1 - a_3\theta^2 + a_4\theta^4]/(r + a_1)^2 \quad (4.1)$$

only distance r and angle θ are unknown. Therefore, we could intuitively consider that at least two sensors were asked to detect human position, and we imaged a method that using two sensors, putting them together and they are mounted at a certain angle (half angle is α) shown as **Fig. 4.1**, to detect human position.

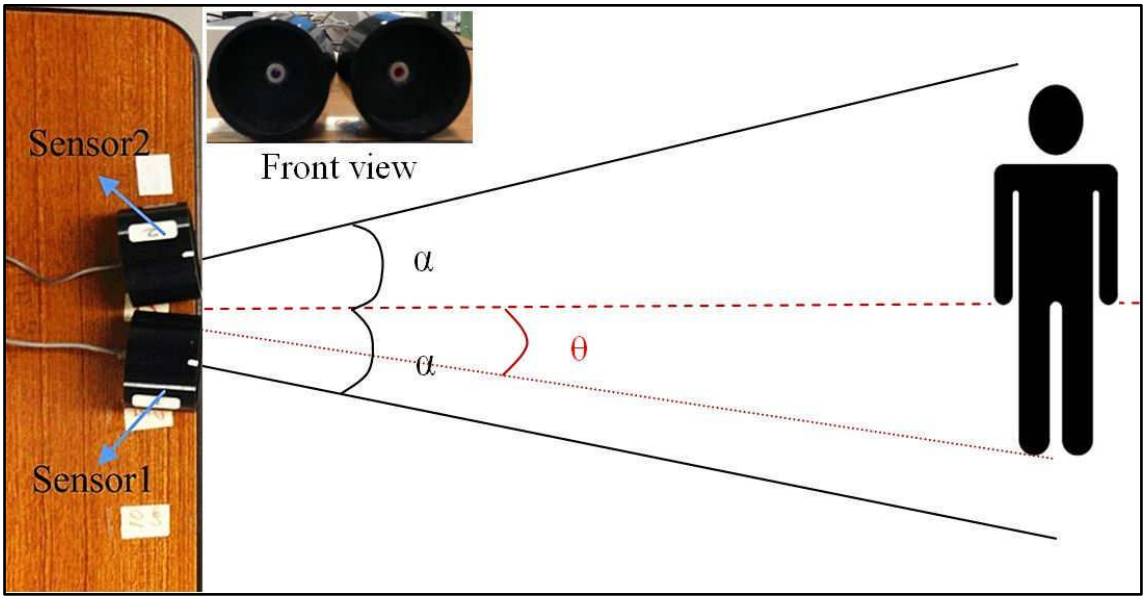


Fig. 4.1 Detecting human by two thermopile sensors

Based on the directivity of the sensor we have known, we can imaged that if we put two sensors together and kept a certain angle, the output image will show as **Fig. 4.2**, we can clearly looked out that the θ is respectively corresponding to a unique pair of output voltage values in the measurable range, in other words, we should get the θ by using this method. Based on the assumed conclusion, we can further ideally understood that used the equation above to draw an image graph shown as **Fig. 4.2** below, each curve represents the same output voltage curve. Normally there should be numerous curves in some effective range, but just few curves be drawn in **Fig. 4.2**. Because many

intersections are formed by many different curves, and each intersection consists of a pair of output voltage values [$V_1$, $V_2$], meanwhile it was also considered as human position.

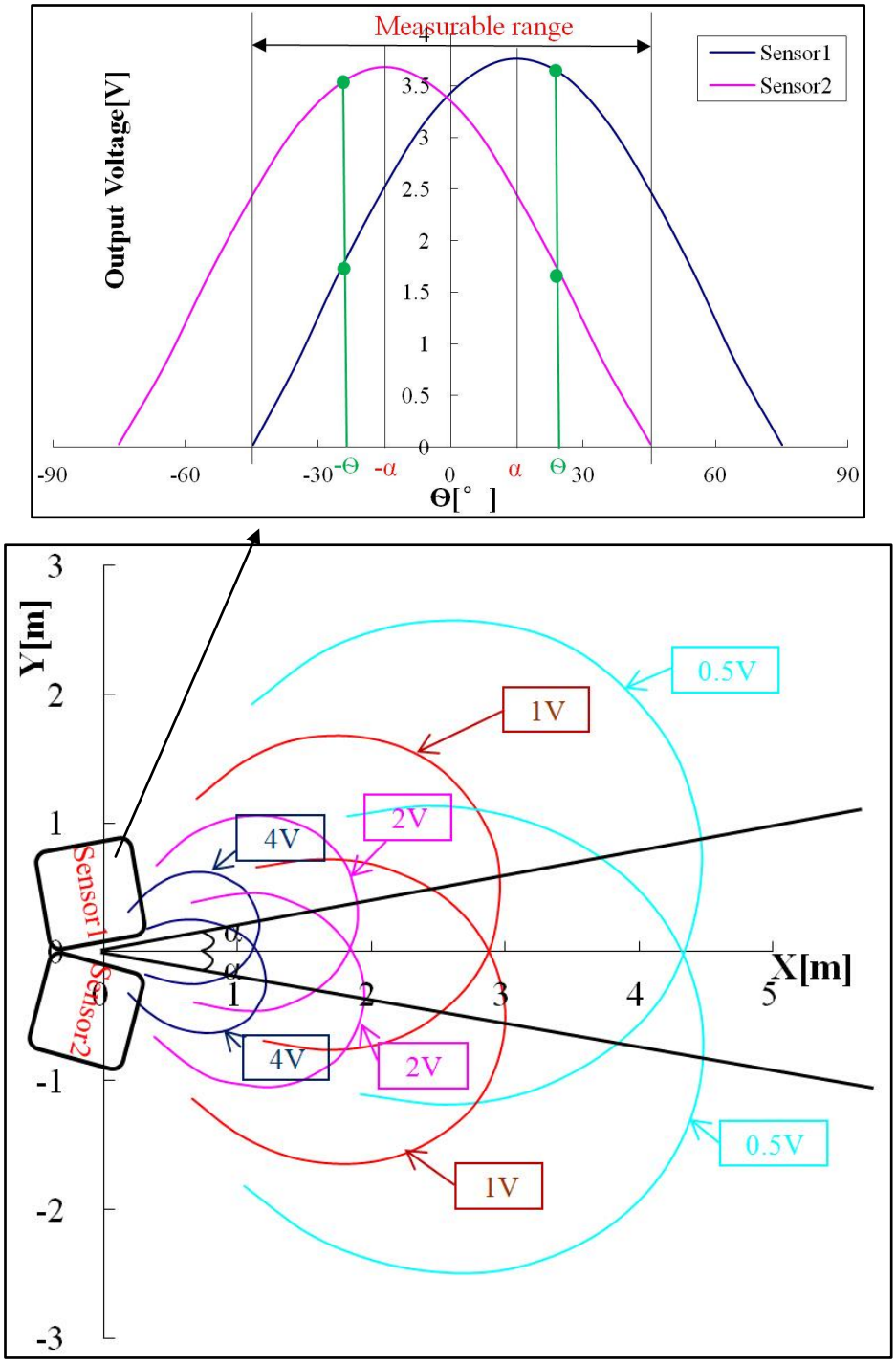


Fig. 4.2 Outline of detection by two sensors

In conclusion, we can generally detect human position by using two sensors, and could build an equation set by the eq.(4.1) is given as following:

$$V_1 = (a_{51}T + a_{61})[1 - a_{31}(\alpha - \theta)^2 + a_{41}(\alpha - \theta)^4] / (r + a_{11})^2 \quad (4.2)$$

$$V_2 = (a_{52}T + a_{62})[1 - a_{32}(\alpha + \theta)^2 + a_{42}(\alpha + \theta)^4] / (r + a_{12})^2 \quad (4.3)$$

(All the values of $a_{11}$, $a_{12}$, $a_{31}$, $a_{32}$, $a_{41}$, $a_{42}$, $a_{51}$, $a_{52}$, $a_{61}$, $a_{62}$ are listed in **Table 3.2**.)

In other word, detecting human position becomes a problem concerning on how to solve the solution of unknown r and θ in the equation set (4.2) and (4.3). Two proposed methods will be introduced as follows.

## 4.2 Analytical method

In order to solve the binary quartic equation set mentioned above, because T in the equation set (4.2) and (4.3) can be known, we transformed the equation set into the form below:

$$V_3 = V_1 / (a_{51}T + a_{61}) = [1 - a_{31}(\alpha - \theta)^2 + a_{41}(\alpha - \theta)^4] / (r + a_{11})^2 \quad (4.4)$$

$$V_4 = V_2 / (a_{52}T + a_{62}) = [1 - a_{32}(\alpha + \theta)^2 + a_{42}(\alpha + \theta)^4] / (r + a_{12})^2 \quad (4.5)$$

in order to transform binary equation into unary equation, we considered that all the parameters in the right parts of equation (**4.4**) and equation **4.5**) same (i.e., $a_{11} = a_{12}$, $a_{31} = a_{32}$, $a_{41} = a_{42}$), and then through (**4.4**) dividing (**4.5**), thus cancel out r in the denominator and transform into a form below:

$$\frac{V_3}{V_4} = \frac{[1 - a_{31}(\alpha - \theta)^2 + a_{41}(\alpha - \theta)^4]}{[1 - a_{31}(\alpha + \theta)^2 + a_{41}(\alpha + \theta)^4]} \quad (4.6)$$

thus, we could get a function named f (θ) just about unknown θ by (**4.6**), that is:

$$f(\theta) = A\theta^4 + B\theta^3 + C\theta^2 + D\theta + E \quad (4.7)$$

where A, B, C, D, E are made up of some parameters (i.e., α, $a_{31}$, $a_{41}$). In other word, we need to extract a root of f (θ) = 0.

Dichotomy method [39], [40] is generally used for numerical solution of the equation

in an unknown, which is a method of separator halves, which is approximately the arithmetic equation. So we used this method to solve f (θ) and got the solution of θ.

Continuous dichotomy using a completely different approach to the problem of the index. The minimum and maximum values of the constants A to E equation is allocated such that for a given θ value $f(\theta)_{min}$ and maximum value $f(\theta)_{max}$ can be calculated. All input lines must be located in one of these ranges f(θ), but not more than one line for each range. The program then successively halved constant range for upper and lower range, and again f(θ) ranges were calculated. Now if some of the line does not fall within a smaller f(θ) range, then either the upper or lower limit of the range may be rejected. Thus, constants A and E are sequentially reduced, thereby increasing its accuracy. The method may be exhaustive, but consuming the minimum time of crystal symmetry.

Though utilizing the principle of dichotomy method, the value of θ can be worked out, and then r can be calculated, furthermore human coordinate position (x, y) could be obtained. Moreover, the sensors outputs continually changed along with human motion, that is, we could get human position in real-time. However, we assumed that some parameters in the right part of the equation same, which necessarily led to large errors, so we reduced the errors by correcting the temperature parts in (**4.4**) and (**4.5**) (for example, change the values of $a_{51}$, $a_{61}$, $a_{52}$, $a_{62}$).

The method is easy to impurity peaks from the pattern, but the benefits can be achieved at the expense of their more computer time. This method works well in low-parameter space, i.e. when testing cube, square and triangular / hexagonal lattice of time, a significant increase in computer time monoclinic and triclinic systems. Therefore, we need to consider an alternative approach to the problem of low symmetry indexing powder diffraction pattern.

## 4.3 Steepest Descent method

Although dichotomy method [41],[42] can be used to measure human position as an effective method, but no matter what we adjusted the parameter to make a better result, it still produced a large error in actual measurement process. Therefore, we considered another approach, that is, steepest descend method.

Algorithm to find the nearest local minimum of a function presupposes gradient function can be calculated. Steepest descent method, also known as the gradient descent method, which is based on the observation that if a multivariable function F(y) is defined and micro-neighborhood of a point, then F(y) decreases fastest if an entry from a negative gradient in the direction of F in b, $-\nabla F(b)$. It follows that, if

$$a = b - C\nabla F(b) \tag{4.8}$$

for C small enough, then F(b) $\geqslant$ F(a). With this observation in mind, one starts with a guess $y_0$ for a local minimum of F, and considers the sequence $y_0, y_1, y_2, \cdots$ such that

$$y_{n+1} = y_n - C_n \nabla F(y_n), n = 0,1,2,3 \ldots \ldots \tag{4.9}$$

here we knew

$F(y_0) \geqslant F(y_1) \geqslant F(y_2) \geqslant \cdots$,

so the number of columns ($y_n$) converges to the desired local minimum. Note that the value of the step C is allowed to change in each iteration. And on certain assumptions function F (for example, F convex $\nabla$F Lipschitz) and specific selection C (for example, through a line search conditions are selected to meet the Wolf), converges to a local minimum can be guaranteed. When the function F is convex, all of the local minimum is a global minimum, so in this case, the gradient descent can converge to the global solution.

This process is illustrated in the picture below as **Fig. 4.3**. Where F is assumed to be defined on the plane, and which pattern has the shape of a bowl. Blue contour curves, namely, F value thereon is constant region. The red arrow indicates the direction of the starting point in a negative gradient is shown as a point in **Fig. 4.3**. Note that the (negative) gradient of a point perpendicular to the contour line through that point. We see that the gradient descent leading to the bottom of our bowls, that is, to the point where the value of the function F is minimal.

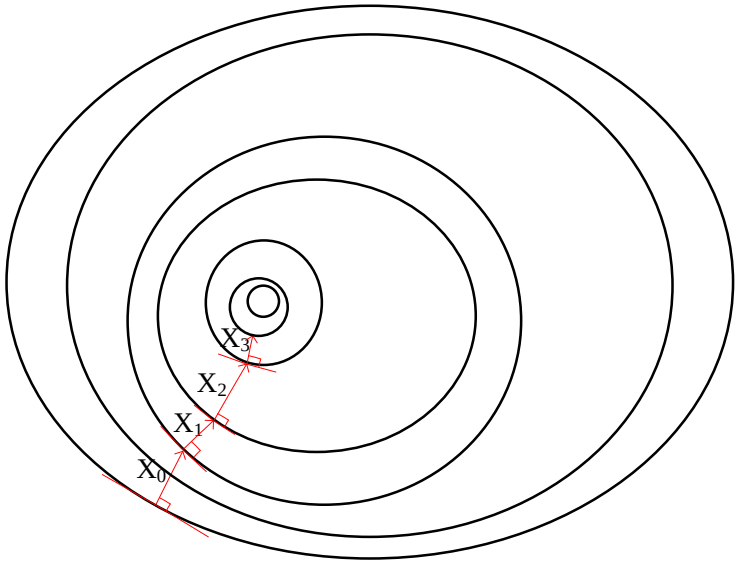


Fig. 4.3 Illustration of gradient descent

The specific process for detecting human position stated as follows:

First, we built the function like this:

$$E(r,\theta) = \Delta V_1^2 + \Delta V_2^2 \tag{4.10}$$

the $\Delta V_1$ and $\Delta V_2$ were respectively defined as the following form:

$$\Delta V_1 = V_1 - (a_{51}T + a_{61})[1 - a_{31}(\alpha - \theta_k)^2 + a_{41}(\alpha - \theta_k)^4]/(r_k + a_{11})^2 \tag{4.11}$$

$$\Delta V_2 = V_2 - (a_{52}T + a_{62})[1 - a_{32}(\alpha + \theta_k)^2 + a_{42}(\alpha + \theta_k)^4]/(r_k + a_{12})^2 \quad (k = 0,1,2.....) \tag{4.12}$$

where $V_1$ and $V_2$ denote measured voltages.

We also defined that the search starts at the initial point ($r_0$, $\theta_0$) ($r_0$=1, $\theta_0$=0), we therefore set the iterative form below:

$$r_{k+1} = r_k - C\left(\frac{\partial E}{\partial r}\right)_{\substack{r=r_k \\ \theta=\theta_k}} \tag{4.13}$$

$$\theta_{k+1} = \theta_k - C\left(\frac{\partial E}{\partial \theta}\right)_{\substack{r=r_k \\ \theta=\theta_k}} \tag{4.14}$$

and continue the process, by searching from ($r_k$, $\theta_k$) to ($r_{k+1}$, $\theta_{k+1}$). The most suitable point was found when function E(r, θ) reaches certain accuracy (i.e., E(r, θ) < 1e-5) through continually adjusting the value of C, and finally we got C =0.005 when a fixed point is reached shows as **Fig. 4.4**. Here, we want to make some explanations, that is, steepest decent method can be combined with a line search, finding the locally optimal step size C on every iteration. Performing the line search can be time-consuming. Conversely, using a fixed small C can yield poor convergence. Hence, finding the optimum C is most important in the process of using steepest decent method.

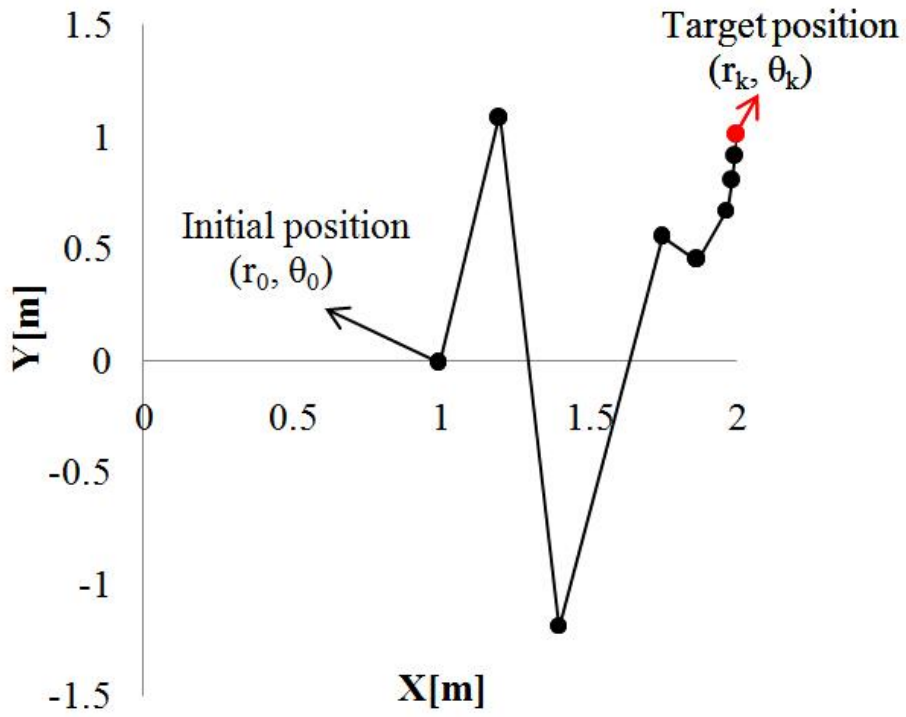


Fig.4.4 Example of convergence graph

For some examples, the steepest descent method is relatively slow close to the minimum: Technically, this is the asymptotic convergence rate better than many other methods. Convex problem for poor air conditioning, the steepest descent method increasingly "zigzags" as nearly orthogonal gradient point to the lowest point in the shortest direction.

Although the advantages of the steepest descent method lies in the fact: it is guaranteed to find the smallest by numerous iterations as long as it exists, but it also has some drawbacks, for example, it takes a lot of iterations before the minimum functional orientation, because the steps taken in the iterative process are very small, the convergence speed is quite slow. Although large steps will increase the convergence speed, but it also may lead to large errors in the estimates.

## 4.4 Accracy

After some experiments of detecting human position at different temperatures, we can clearly see that the error distributions have a similar output condition by comparing the measured results, that is, the farther the distance, the larger the error. Because accuracy indicates the level that how close a measured value to the actual value, therefore, the farther the distance, the lower the accuracy. In order to verify the possibility of

generating this cause, we analyzed the errors like this. According to the detected position coordinate value (x, y), we worked out the corresponding sensor output voltage value ($V_1$, $V_2$) through the equation set Eq.(4.10) and Eq.(4.11), and then changed ($V_1$, $V_2$) into ($V_1 \pm \Delta V$, $V_2 \pm \Delta V$)(i.e., $\Delta V = 0.1v$), thereby we could get new detected position like ($x \pm \Delta x$, $y \pm \Delta y$) once again by the equation set. So positions ($\pm\Delta x$, $\pm\Delta y$) presented the degree of deviation from the detected position. **Fig. 4.5** shows the distribution of errors, and which illustrates the fact that the farther the distance, the lower the accuracy.

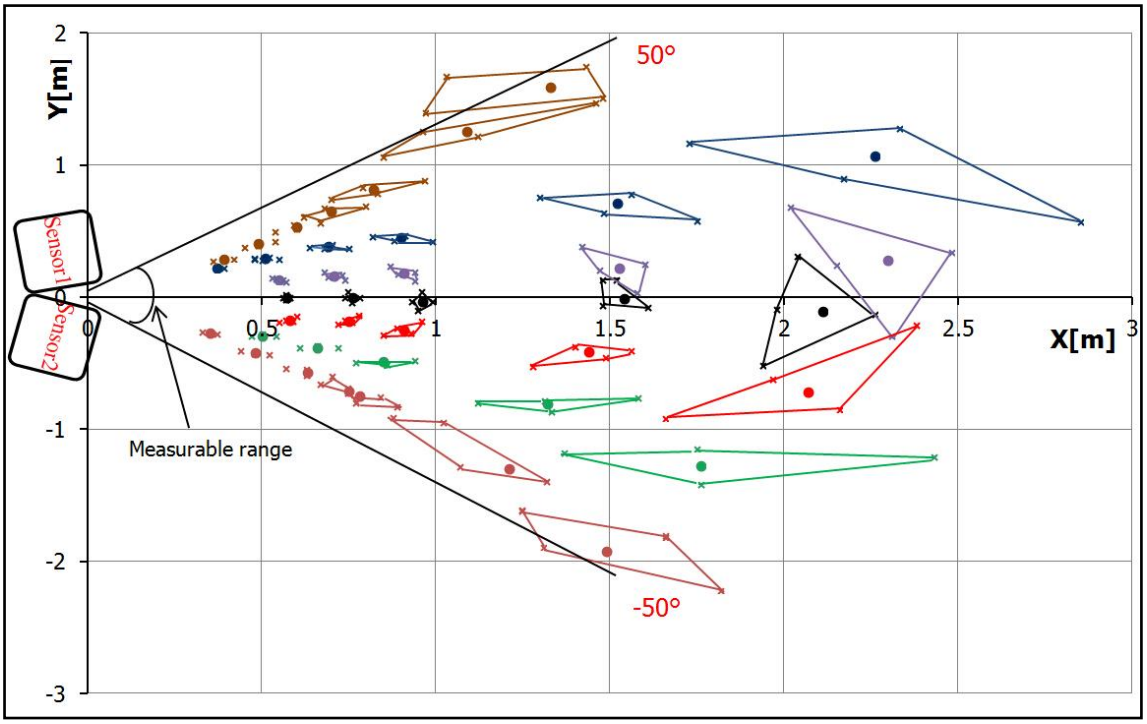


Fig. 4.5 Distribution of errors (dots mean detected position and nodes mean position errors).

## 4.5 Experiment results

The experiments were respectively discussed in two situations. Situation 1 shows as **Fig. 4.6 (a)**, that is, keep two sensors together and make the angle between them is 10°, 15°, 30° etc. Situation 2 shows in the same scene as **Fig. 4.6 (b)** just keep two sensors a slight apart, and sensor1 is fixed face to the front direction, sensor2 was fixed at a certain distance from the sensor1 and keep 10°,20°,30° etc with the front direction show as **Fig 4.6**, and **Fig. 4.7** shows experimental scene.

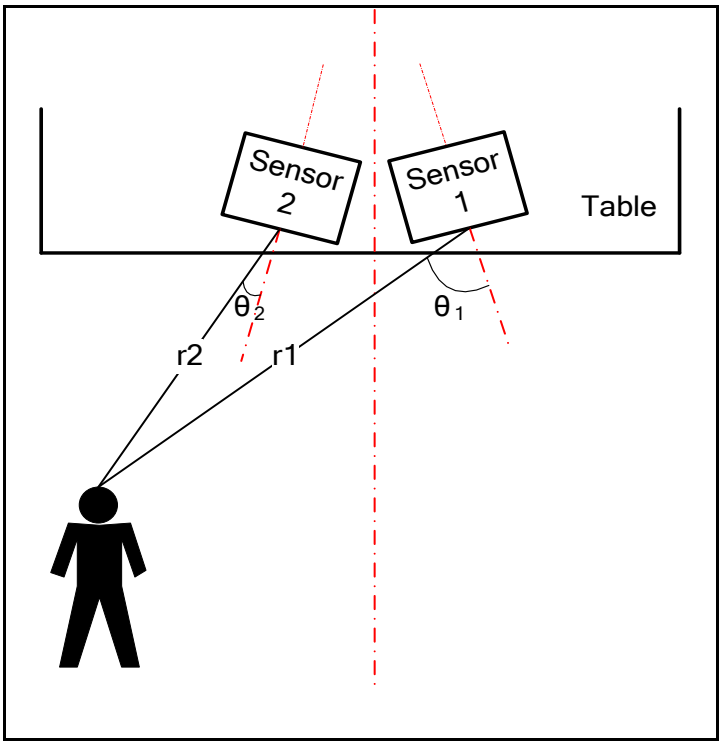


(a)

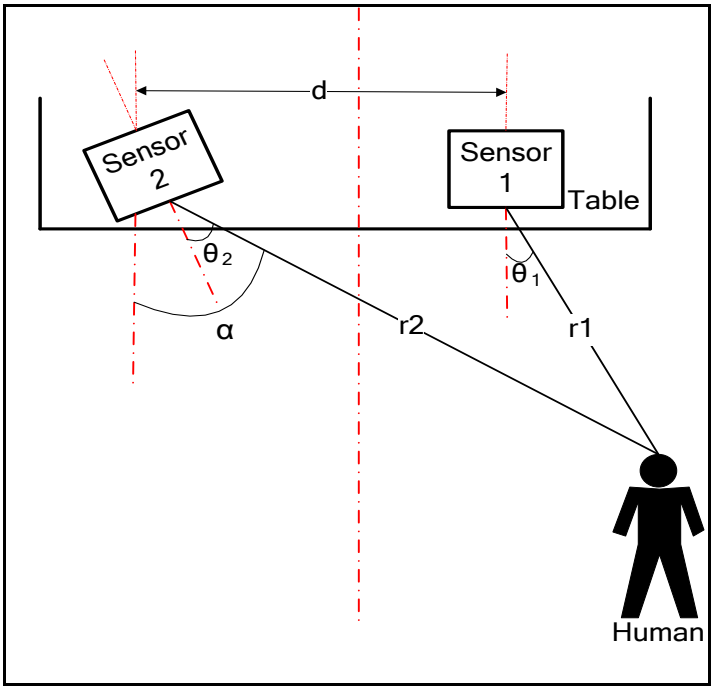


(b)

Fig. 4.6 Two types of arrangement to detect human

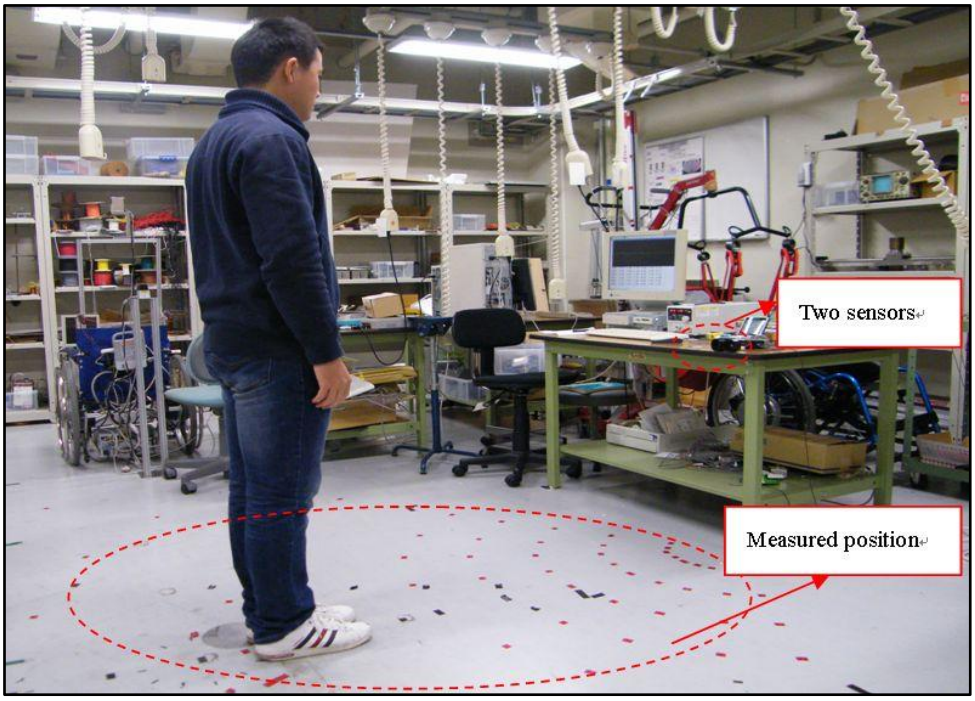


Fig. 4.7 A photo of experimental scene

The detailed description of situation 1 as follows. Two sensors were located on the table at a height of 0.7m above the ground, and the measured positions on the ground were arranged like this: We defined increment of θ was 15° and measurable range was [-45° ,45° ], while the increment of r was 0.2m within 1m and 0.5m beyond 1m, measurable range was [0.2m,2.5m]. The detected positions can be directly read by computer screen. In any case, all the experiments were done in this scene. As previously described, we respectively detected human position by two methods, that is, analytical method (dichotomy) and steepest descend method. Though doing a mass of experiments at different temperatures, it has been found that utilizing the steepest descend method can acquire the optimal results until now. We respectively did some experiments at some different ambient temperatures and they had a similar output result.

**Fig. 4.8** shows that the result through applying a method of analytical method, and relatively, **Fig. 4.9** shows the result after adjusting some parameters.

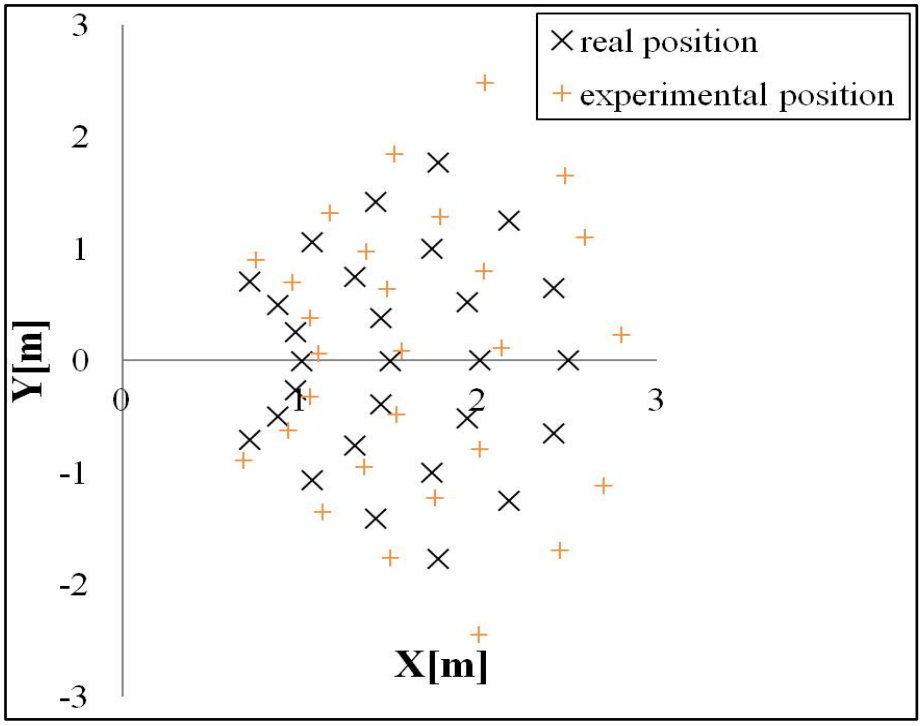


Fig. 4.8 Result measured by analytical method

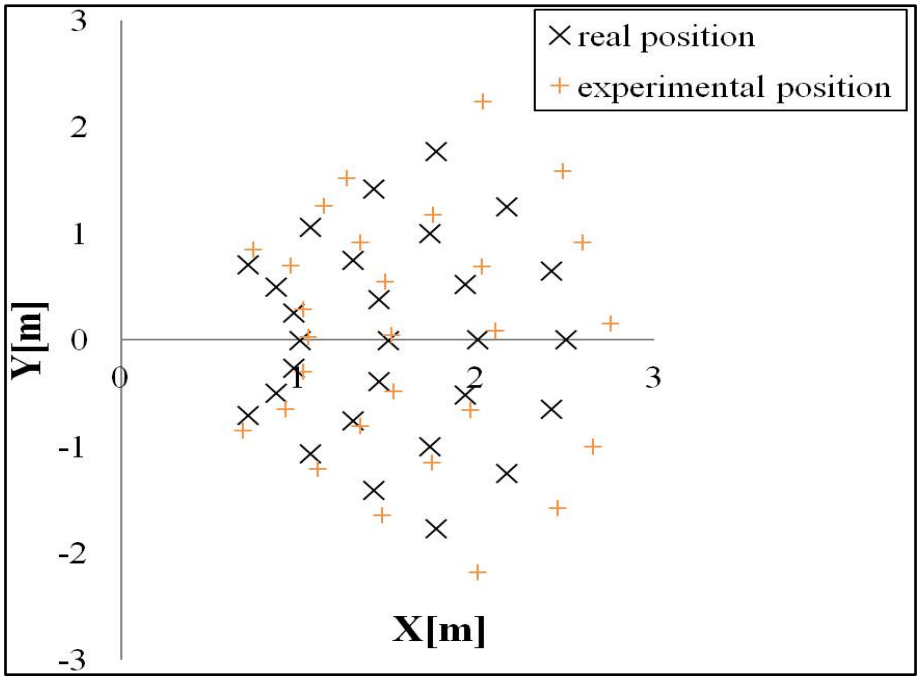


Fig. 4.9 Result measured by analytical method after adjusting some parameters

From the comparison results, we can know that there are large errors by using analytical method. After adjusting, although errors are reduced, it still has large errors.

**Fig. 4.10** and **Fig. 4.11** separately show the comparison results measured at 26.3℃ and 14.0℃ by the steepest descend method. Comparing to the result by using analytical

method, the error is obvious reduced. Hence, we decided to detect human by this method.

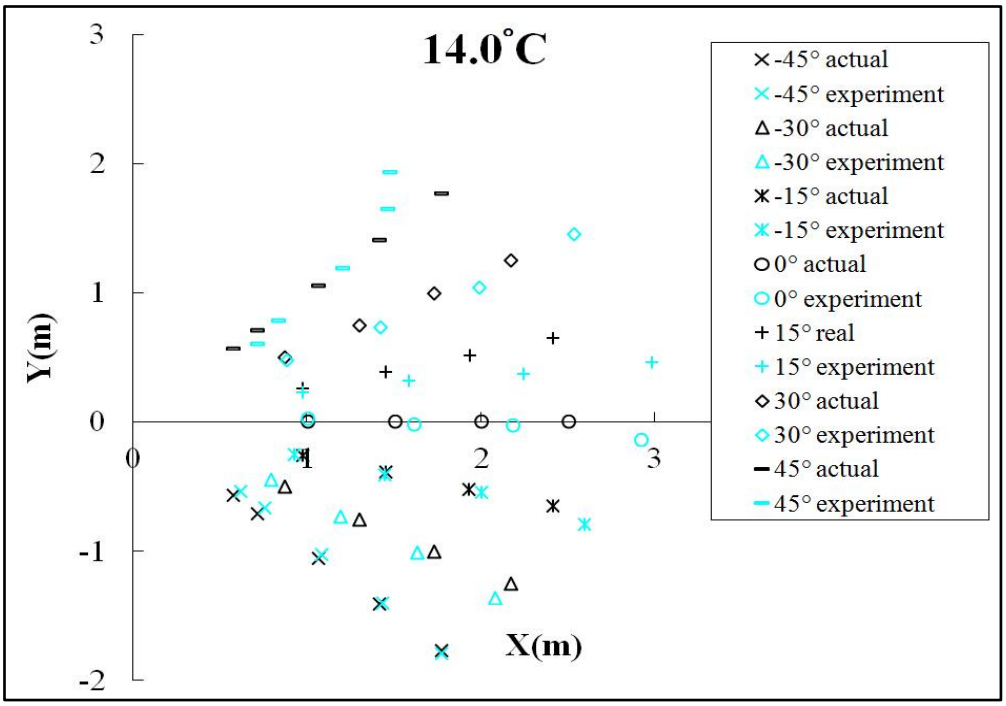


Fig. 4.10 Results measured at 14.0℃ by steepest decent method (dark points mean actual positions while light points mean detected positions)

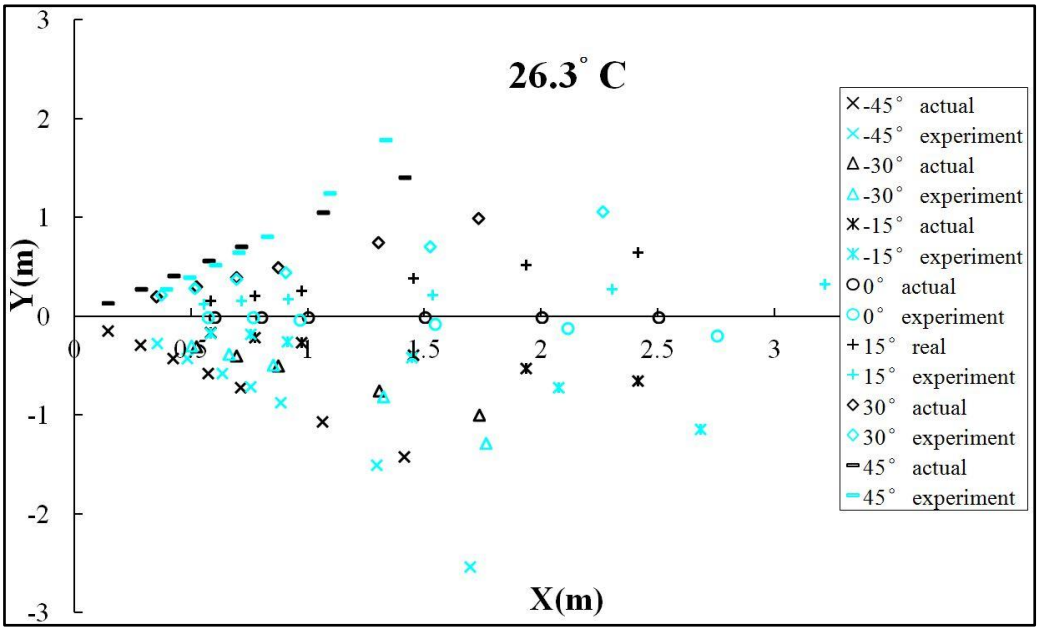


Fig. 4.11 Results measured at 14.0℃ and 26.3℃ by steepest decent method (dark points mean actual positions while light points mean detected positions)

After discussed the measurement arranged like **Fig. 4.6 (a)**, we continued to measure by **Fig. 4.6 (b)**, we did experiments while fixing the angle α of sensor2, separately keeping distance d = 0.1m or d = 0.4m, which measured at same temperature. Results show as **Fig. 4.12** and **Fig. 4.13**.

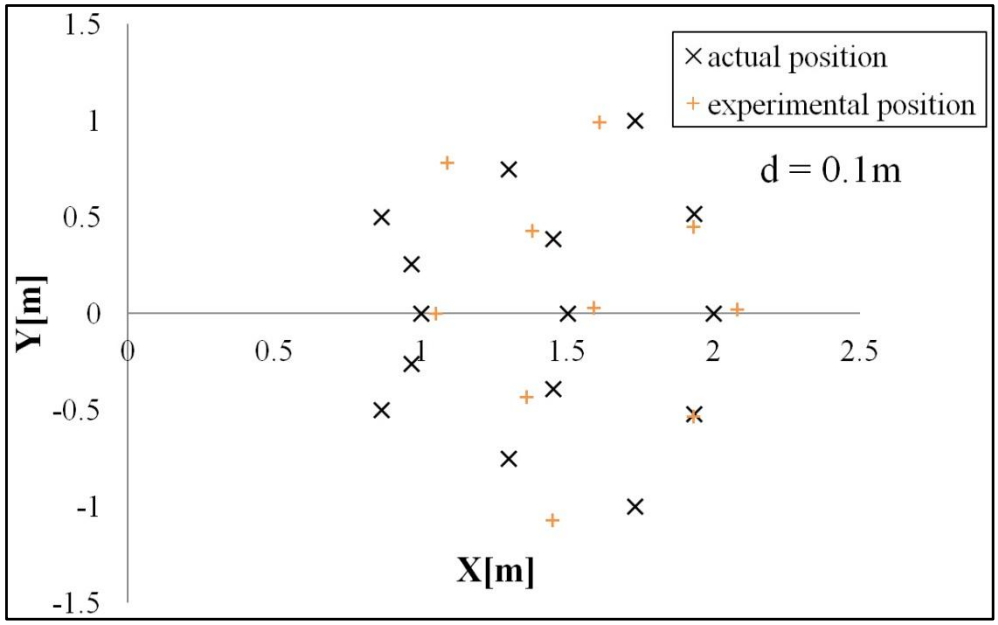


Fig. 4.12 Results measured according to Fig. 4.5 (b) (d = 0.1m)

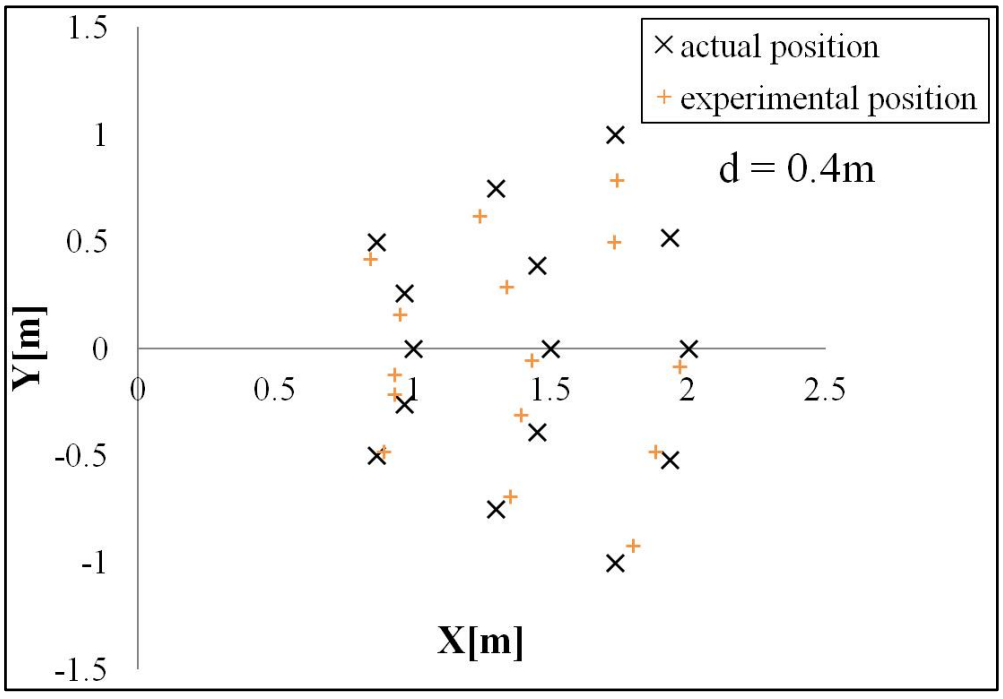


Fig. 4.13 Results measured according to Fig. 4.5 (b) (d = 0.4m)

We got that result measured when d = 0.4m is better than result measured when d = 0.1m, as well as the larger the distance the better the result after some other experiments when d is different. But if d is too large, that will lead a bad result, which is because the common detected area is reduced. Meanwhile, we also found that result measured under **Fig. 4.6 (a)** is better than result measured under **Fig. 4.6 (b)**, we can clearly see that the detected area in **Fig. 4.8** is larger than detected area in **Fig. 4.12**.

In addition, **Fig. 4.13** and **Fig. 4.14** shows the comparison results separately calculated by simulation when step size C=0.1 and C = 0.005. From the comparison results, we can know that some positions cannot be solved and errors are also large when C = 0.1. It was verified that a larger step size will increase the convergence speed, but it could also result in an estimate with large error.

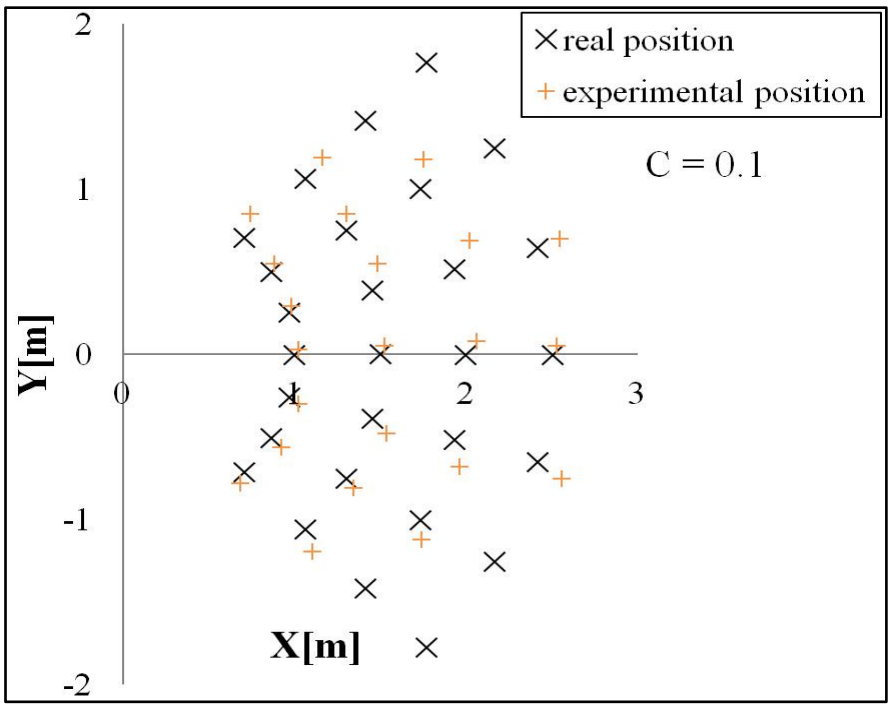


Fig. 4.13 Results when C = 0.1 through simulation by steepest decent method

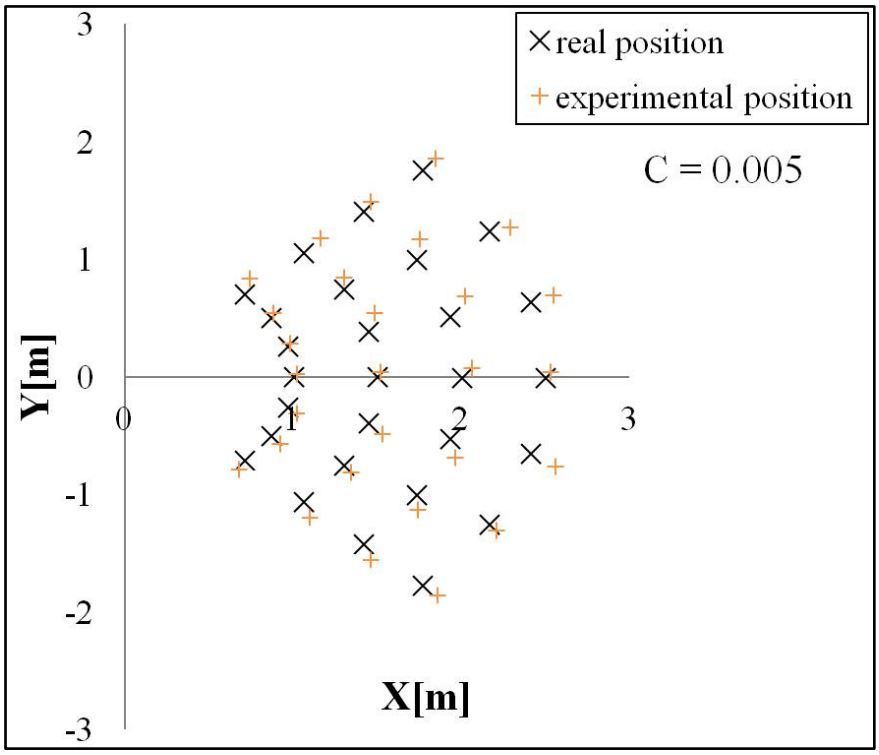


Fig. 4.14 Results when C = 0.005 through simulation by steepest decent method

In addition, in order to test the sensors system can detect human position in real-time, we did an experiment for moving human. Human walked slowly at a speed of about 0.5m/s from one side to the other side (**Fig. 4.15(a)**) at a distance 1m to the sensors, and we also measured along the direction shown as **Fig. 4.15(b)**. The response time of system is 0.1s. We collected several data by random in the detection range. It was verified that the system can well be used to detect moving human by the experiment as expected. [43]

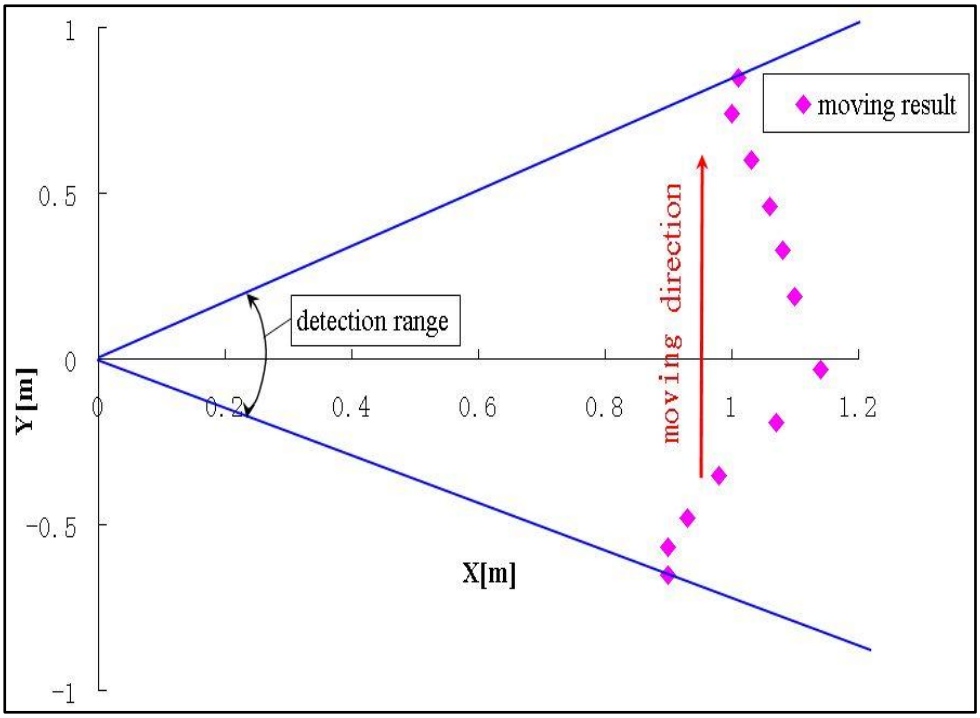


(a)

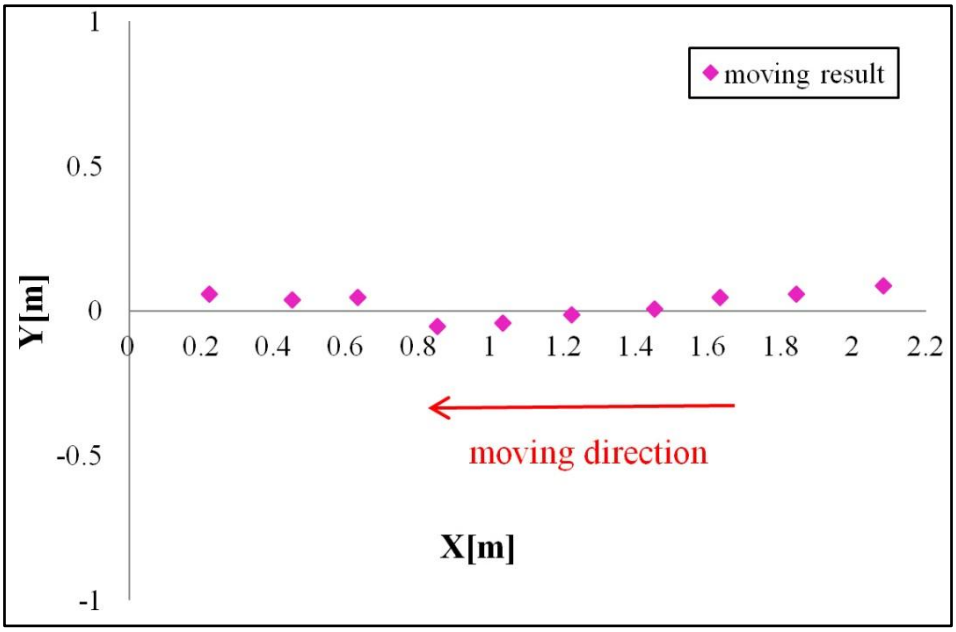


(b)

Fig. 4.15 Detected position for moving human

## 4.6 Conclusion

This chapter presented an approach for detecting human position by using two thermopile sensors that are put together and mounted at a certain angle on the table.

Through measuring, built an approximate equation between output voltage, distance and angle from each sensor to human, and two methods be introduced to solve the equation set, that is, analytical method and steepest descend method. It has proved that the best way to obtain human position in real-time is the steepest descend method through comparing the output results, and which has been confirmed that the proposed system can work steadily by some experiments. At the same time, after analyzing some factors which has influence on the sensors, we could conclude that temperature of human measured is directly determine the sensor output, that is, the higher the human temperature, the larger the sensor output and vice versa at a certain ambient temperature.

On the basis of the experiment method, we prepare to detect human position or motion when the sensors are in vertical direction, so we will apply the thermopile sensor system to the human monitoring from ceiling.

# CHAPTER 5. HUMAN DETECTION BY VERTICAL SENSORS FROM CEILING

Based on the theory and measurement method by two thermopile infrared sensor in the horizontal direction, we started to consider the method for detecting human when put the sensors on the ceiling, that is to say ,to detect human in the vertical direction. We thought that there also should be some relationships between human and sensors, besides, in the process of detecting human on the table, it just can detect position of human in real-time, in this chapter, we will introduce the contents about which not only human position but also human motion. Because there are two situations when detecting human on the ceiling, that is,

A) Detecting human when sensors are only put in the vertical direction (sensor angle = 0°).

B) Detecting human when sensors are only put in any directions (sensor angle is tilted).

Hence we will introduce in this two situations. While, we thought situation A is simple than situation B, this chapter for introducing situation A, and chapter 7 will be used for introducing B. Please follow us and see what will happen in the following.

## 5.1 Measurement and approximation of some factors

In order to detect human position and body orientation, some basic characteristics about sensor and some factors between human and sensor be considered shown as **Fig. 5.1**, including the height difference h from sensor to top of human's head, horizontal distance r between human position and projection position of suspended sensor, body orientation namely angle α, and ambient temperature T. The idea of basic measurement for detecting human is based on the human detection on the table, so after obtaining some approximate relationships between sensor output voltage and the factors through measurements, we can get the equation of sensor output including all effects like:

$$V = V_T(T) \cdot V_h(h) \cdot V_r(r) \cdot V_\alpha(\alpha) \qquad (5.1)$$

where $V_T(T)$ denotes relationship between ambient temperature (T) and sensor output.

$V^{h(h)}$ denotes relationship between height (h) and sensor output.

$V_r(r)$ denotes relationship between distance (r) and sensor output.

$V_\alpha(\alpha)$ denotes relationship between body orientation (α) and sensor output.

Here, we want to explain why the factor directivity (θ) is not used to calculate for sensor

output, because the factor $V_r(r)$ has contained the $V(\theta)$.

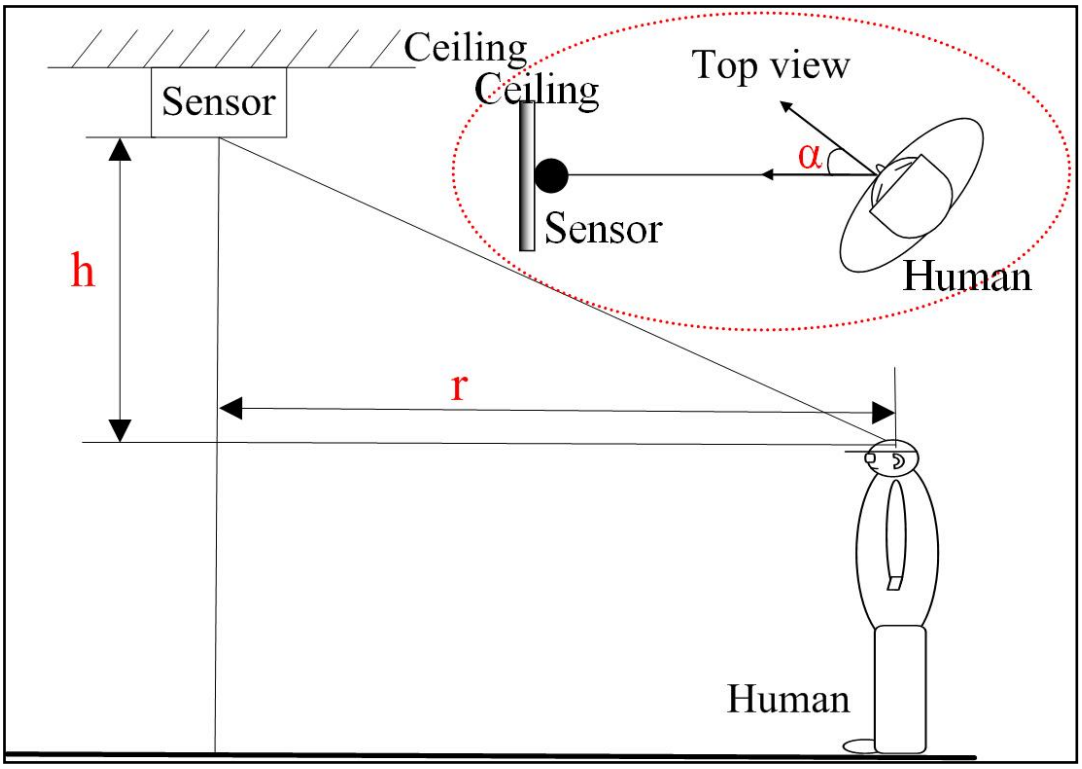


Fig. 5.1 Relationship between human and sensor

5.1.1 Height and Ambient Temperature

By the Stefan-Boltzmann law, the output voltage of a thermopile sensor is given by:

$$U_0 = K'(\varepsilon_0 T_h^4 - T_a^4) \tag{5.2}$$

where $T_h$, $T_a$ is human temperature and ambient temperature, $K' = K \sin^2(\varphi/2)$ is a constant that depends on the FOV of the sensor, and $\varepsilon_o$ is the object's emissivity. However, we can't use this equation because the FOV is larger than target (human) in our system.

We did the experiments about temperature effect on sensor output stated as follows: fixed the sensor at 2.5m height on the ceiling and kept it a vertically downward direction (this experimental setup is applicable to all the experiments about measuring sensor characteristics, so later will not be introduced), human stood just below it, and then separately measured when standing at some heights (h) from 0.2m to 0.8m by every 0.2m shown as **Fig. 5.2**. Every experiment was measured 5 times in order to reduce errors. The experiment was repeatedly measured many times respectively at

different temperatures. The results are shown in **Fig. 5.3**.

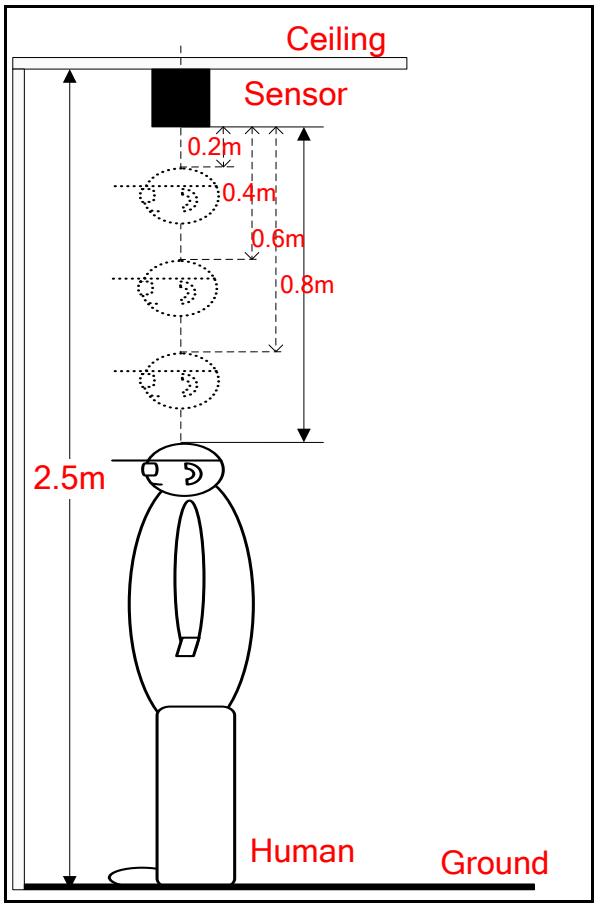


Fig. 5.2 Measurement at different h

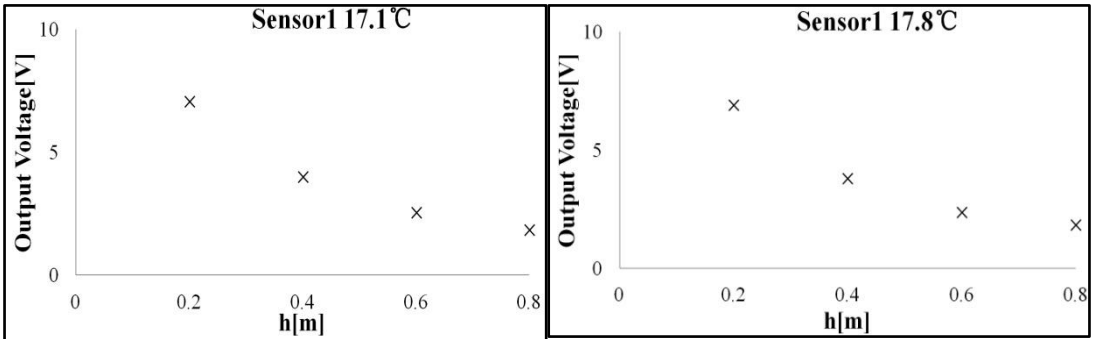


A. 17.1℃




B. 17.8℃

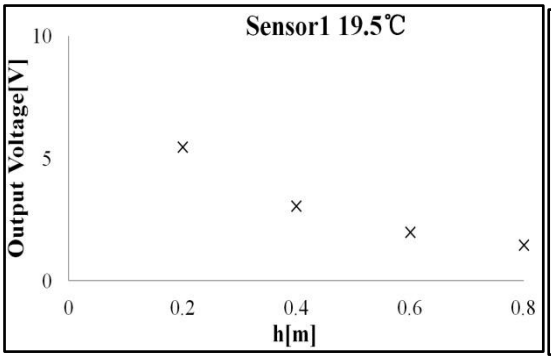


C. 19.5℃

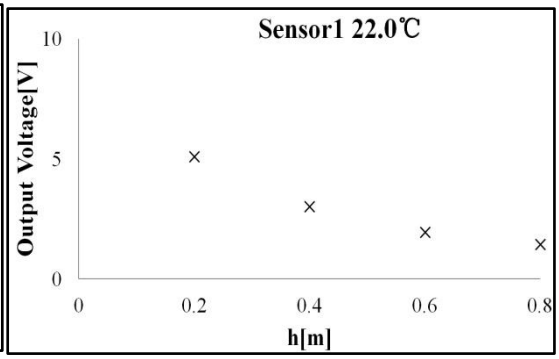


D. 22.0℃

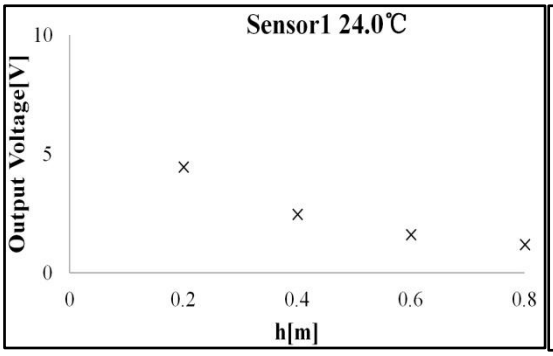


E. 24.0℃

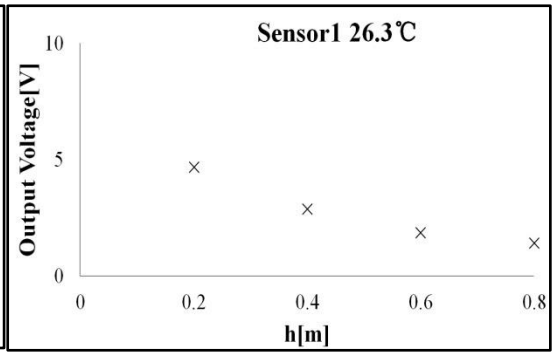


F. 26.3℃

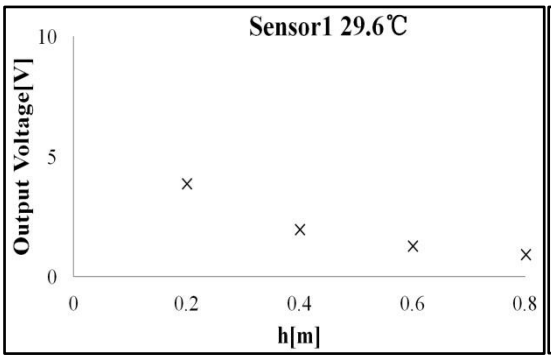


G. 29.6℃

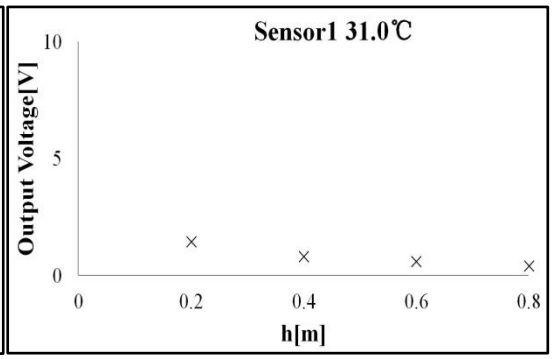


H. 31.0℃

Fig. 5.3 Results between h and V at different temperatures (sensor1)

Which shows that height difference h is inversely proportional to sensor's output.
Meanwhile, we also measured the other sensor (sensor2) and results are shown as **Fig. 5.4**.

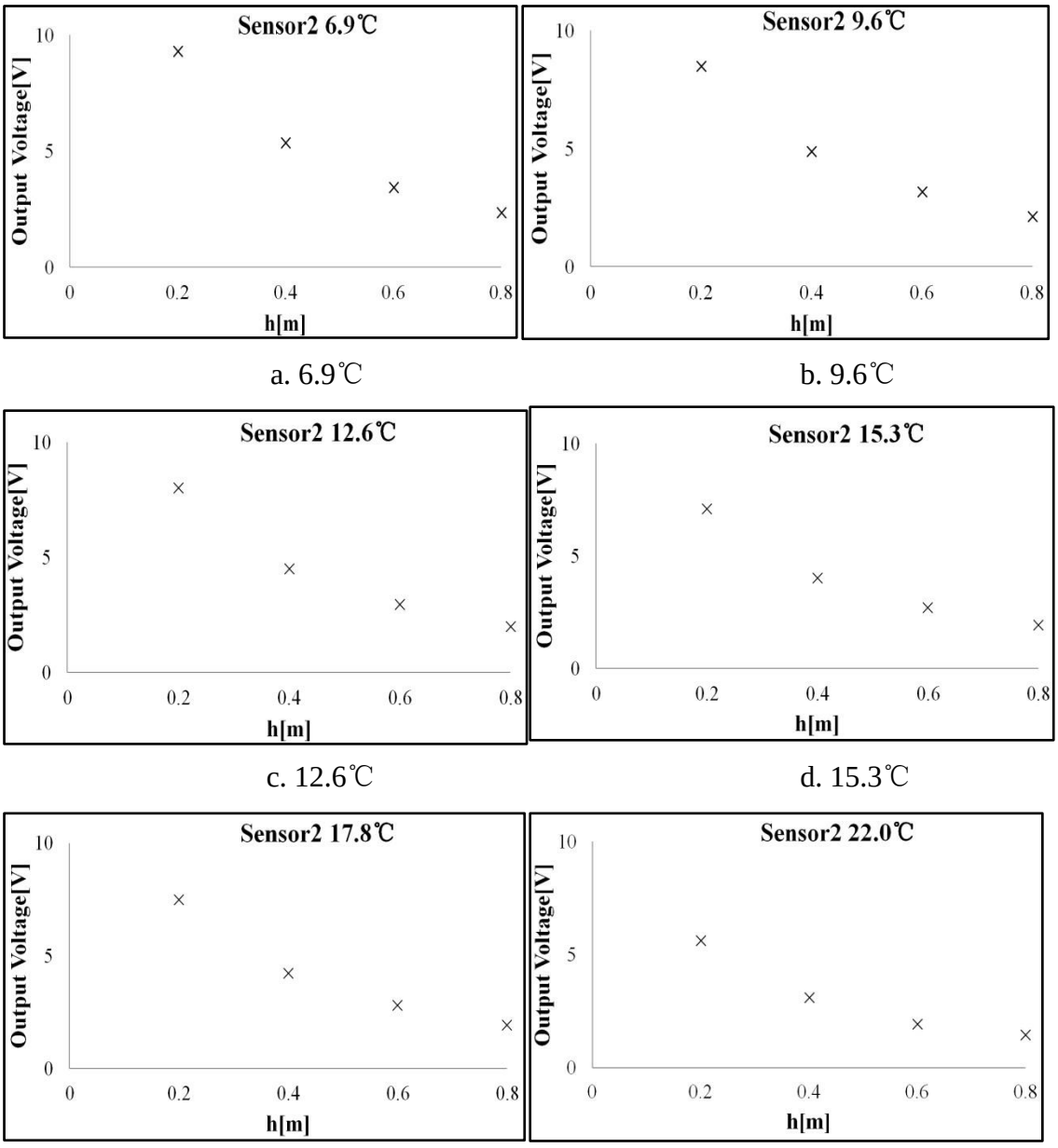


a. 6.9℃ b. 9.6℃

c. 12.6℃ d. 15.3℃

e. 17.8℃ f. 22.0℃

Fig. 5.4 Results between h and V at different temperatures (sensor2)

From the results regardless of which sensor, the output curves have certain similarity and we guessed that maybe they have a common equation.

Because the output shapes are similar with results measured at different distances while detecting human position by attaching sensor on the table, we suspected that they

should have similar approximation equation, that is:

$$V_{T,h} = a_0/(h + a_1)^2 \quad (5.3)$$

Or, maybe it has analogous equation, which can make the curve fitting at all temperatures. Hence we started to try to find it. The specific method for finding the optimum solutions has been introduced in previous Chapter, thus here we will not state it again. After comparing by **Eq. 5.3**, we can make curve fitting, results about sensor1 and sensor2 respectively show as **Fig. 5.5** and **Fig. 5.6**, which separately are corresponding to **Fig. 5.3** and **Fig. 5.4**.

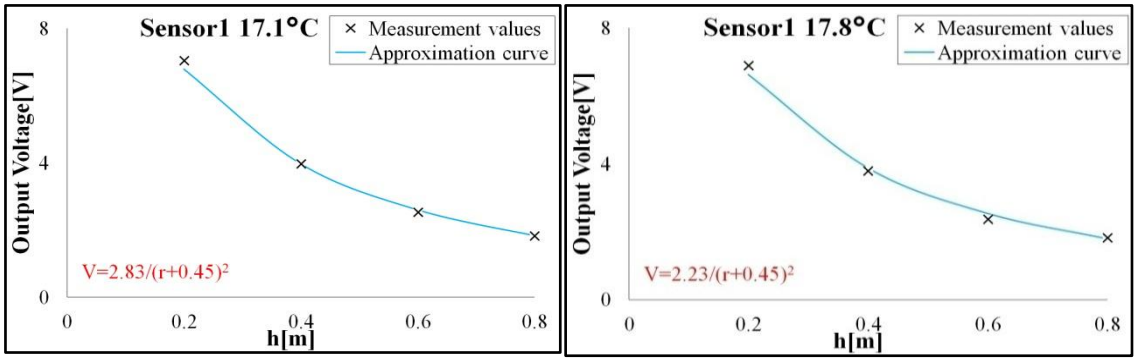


A. 17.1℃ B. 17.8℃

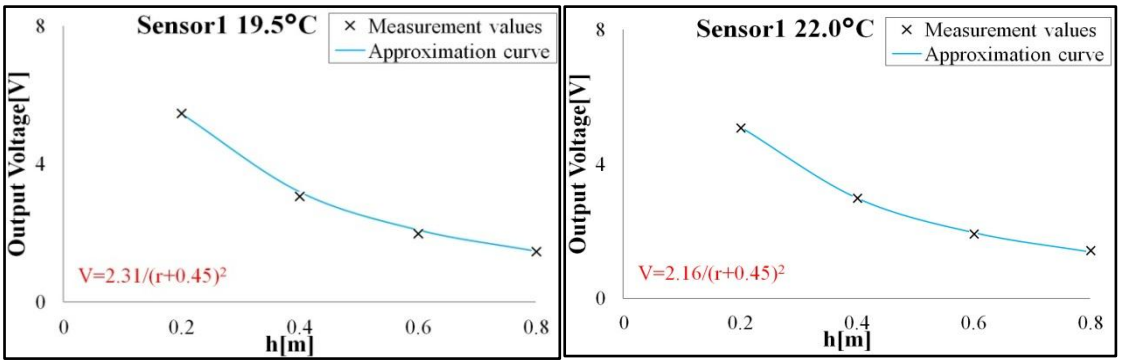


C. 19.5℃ D. 22.0℃

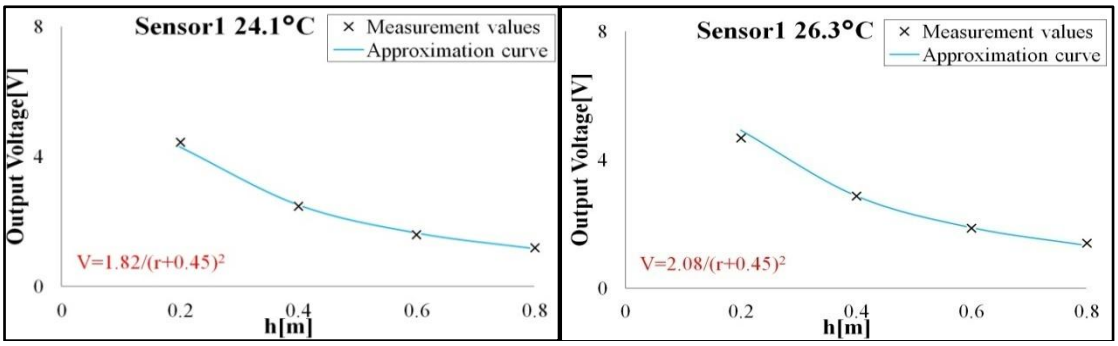


E. 24.1℃ F. 26.3℃

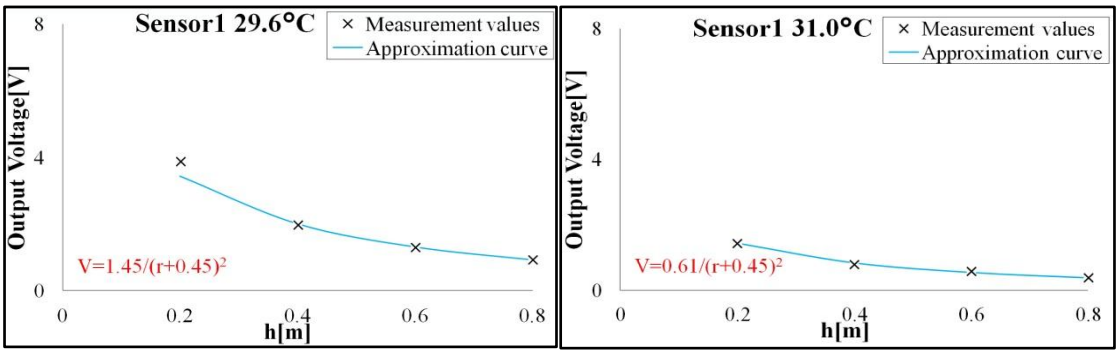


G. 29.6℃ H. 31.0℃

Fig. 5.5 Results by fitting the curve at each temperatures (sensor1)

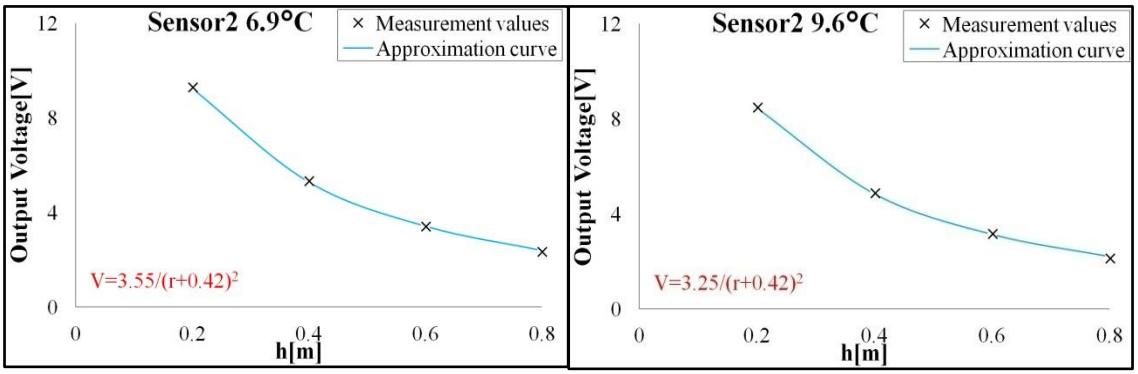


a. 6.9℃




b. 9.6℃

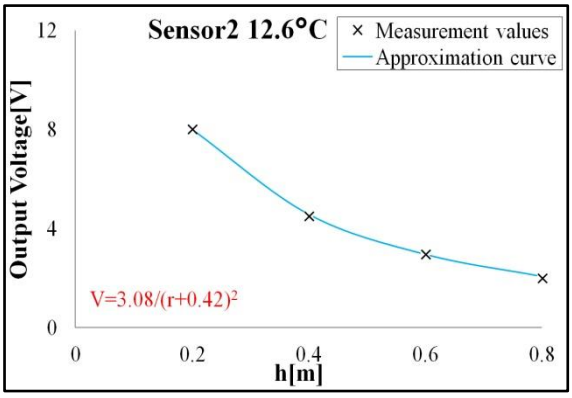


c. 12.6℃

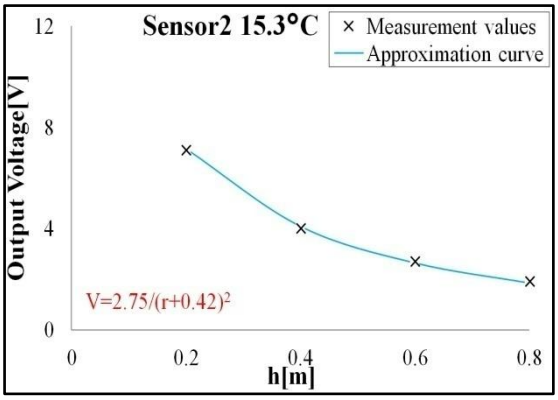


d. 15.3℃

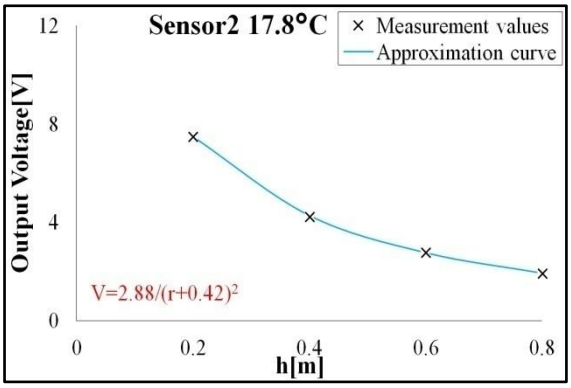


e. 17.8℃

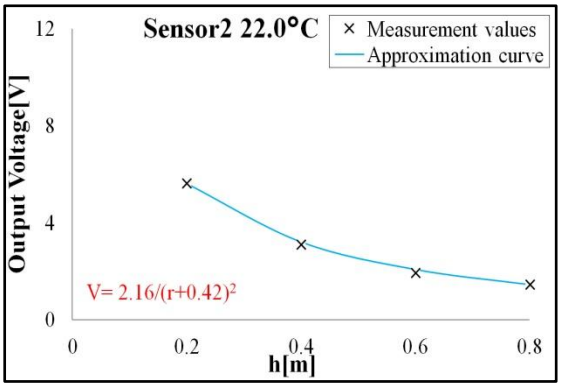


f. 22.0℃

Fig. 5.6 Results by fitting the curve at each temperatures (sensor2)

After integrating all curves into a total graph, they will show as **Fig. 5.7** and **Fig.5.8**.

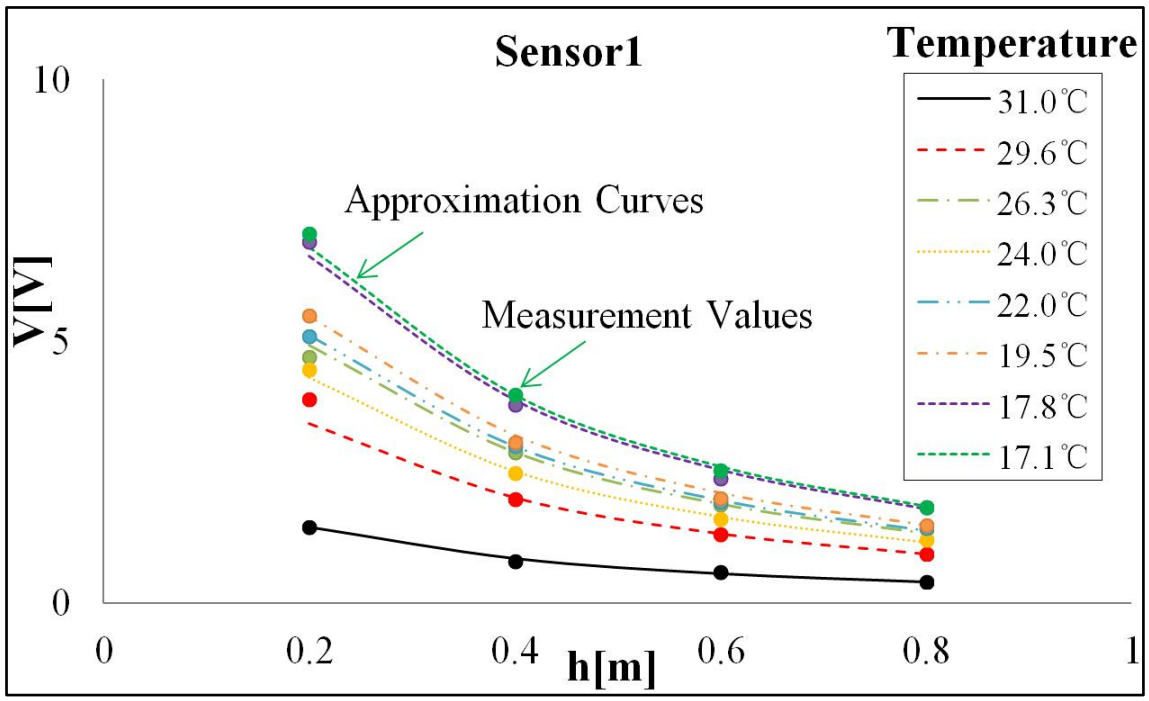


Fig. 5.7 Total results by fitting the curve at all temperatures (sensor1)

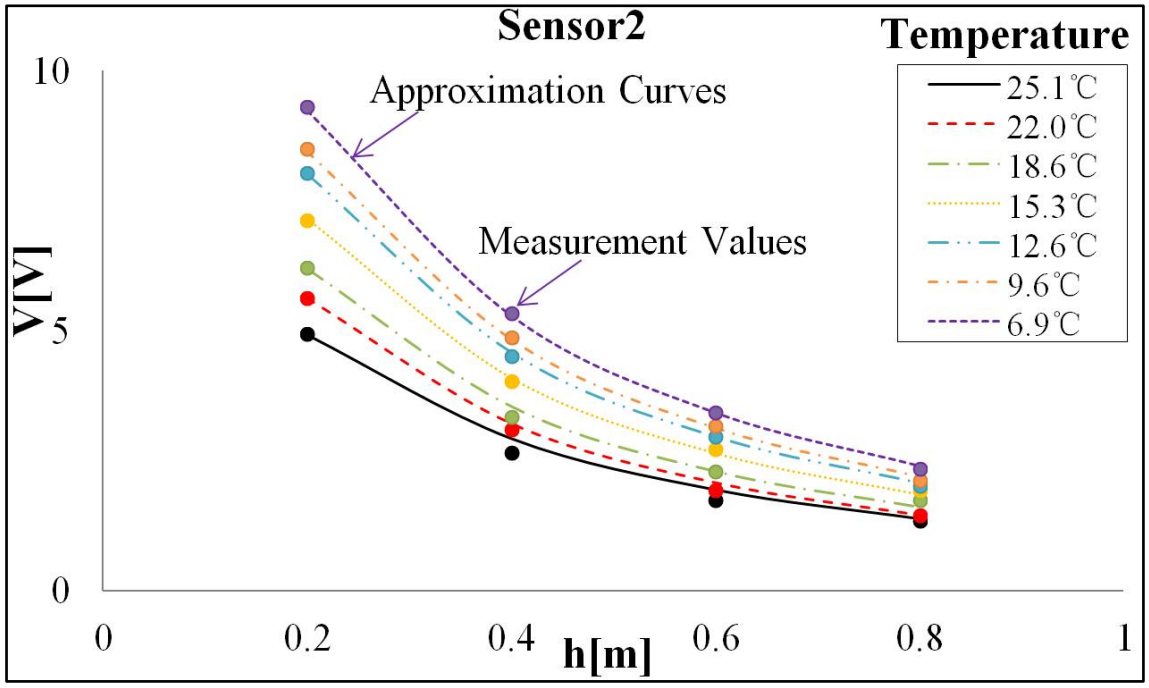


Fig. 5.8 Total results by fitting the curve at all temperatures (sensor2)

Finally we got an optimum approximation equation expressed by **Eq. 5.3**, which is also expressed by:

$$V = V_T(T) \cdot V_h(h) = a_0/(h + a_1)^2 \quad (5.4)$$

Where $a_1$ is constant, $a_0$ has an approximate linear relationship with temperature (**Fig. 5.9**),

$$a_0 = V_T(T) = a_8 T + a_9 \quad (5.5)$$

where $a_8$ and $a_9$ are constant.

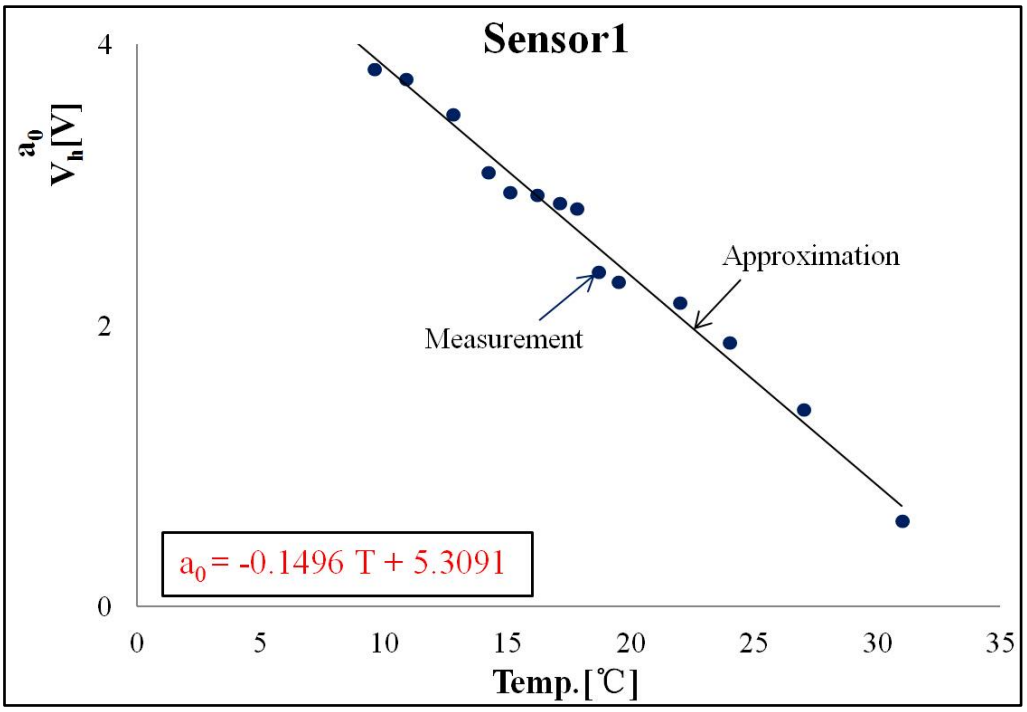

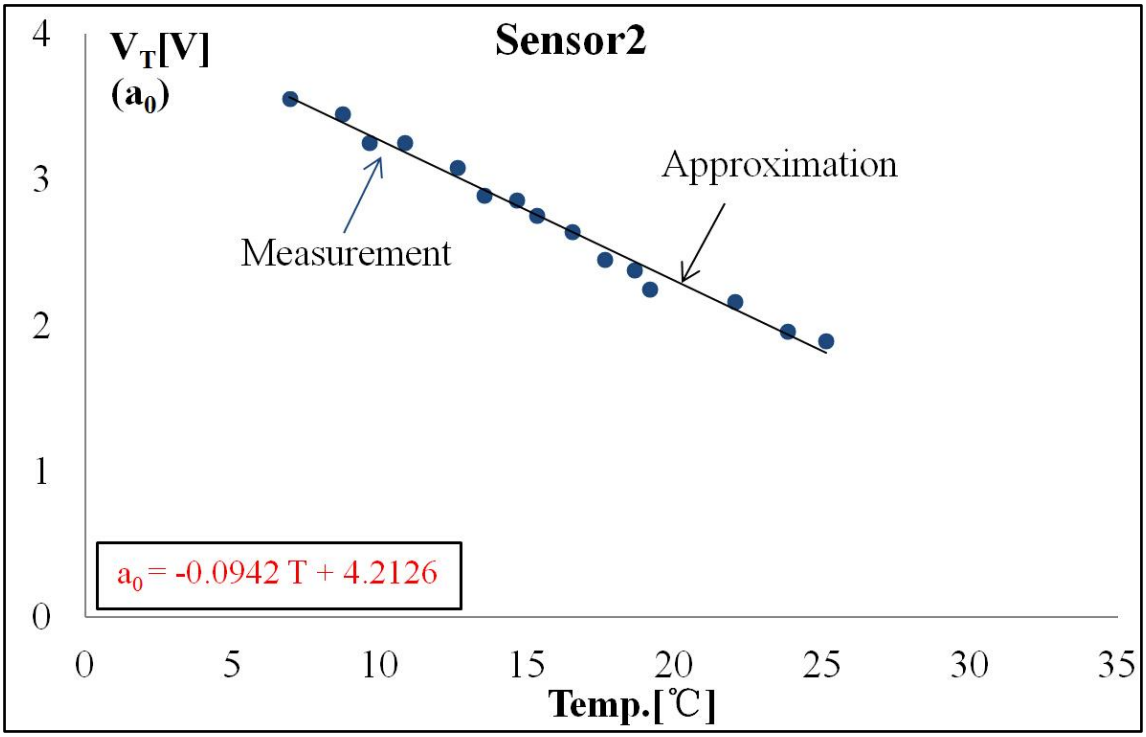


Fig. 5.9 Relationship between $a_0$ and temperature

5.1.2 Distance

We measured the relationship between sensor output and distance r, human position and suspended sensor. Human separately stood in some positions to measure from 0m to 2m by every 0.2m in a line. Meanwhile, in order to verify both sides of the sensor whether symmetrical or not, we measured on both sides shown as **Fig. 5.10**. Also, this measurement was repeatedly measured many times respectively at different temperatures and different height (h=0.2m, 0.4m, 0.6m, 0.8m).

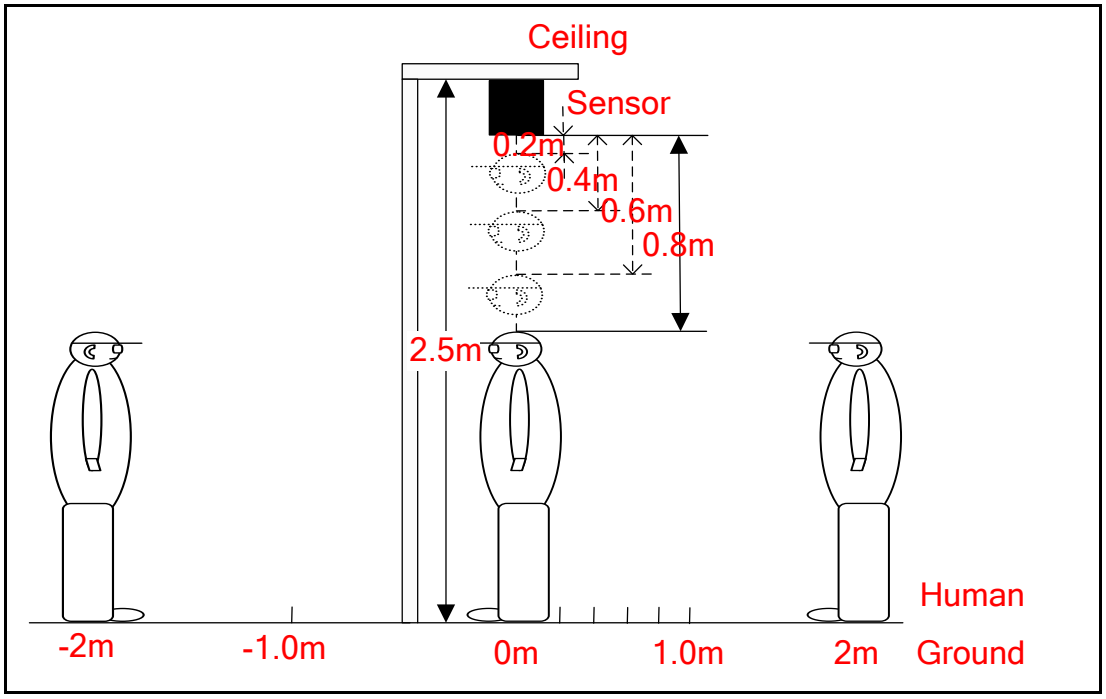


Fig.5.10 Measurement about different distance (r) under different height (h)

The measured results at each height show as following **Fig. 5.11,** and **Fig. 5.12** shows results about sensor2. They have almost same output at same h from results. Because this measurement has been proceeded at many different temperatures, **Fig. 5.11** and **Fig. 5.12** are only one result measured when T = 26.3℃.

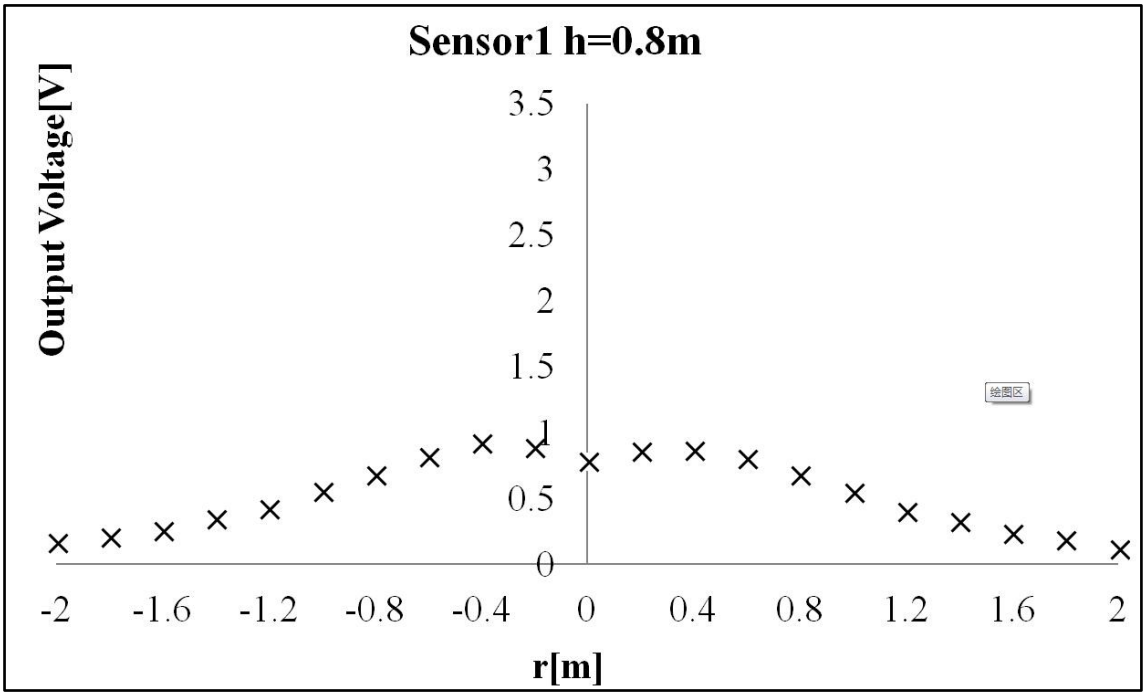
Sensor1 h=0.8m
Output Voltage[V]
3.5
3
2.5
2
1.5
1
0.5
0
-2
-1.6
-1.2
-0.8
-0.4
0
0.4
0.8
1.2
1.6
2
r[m]

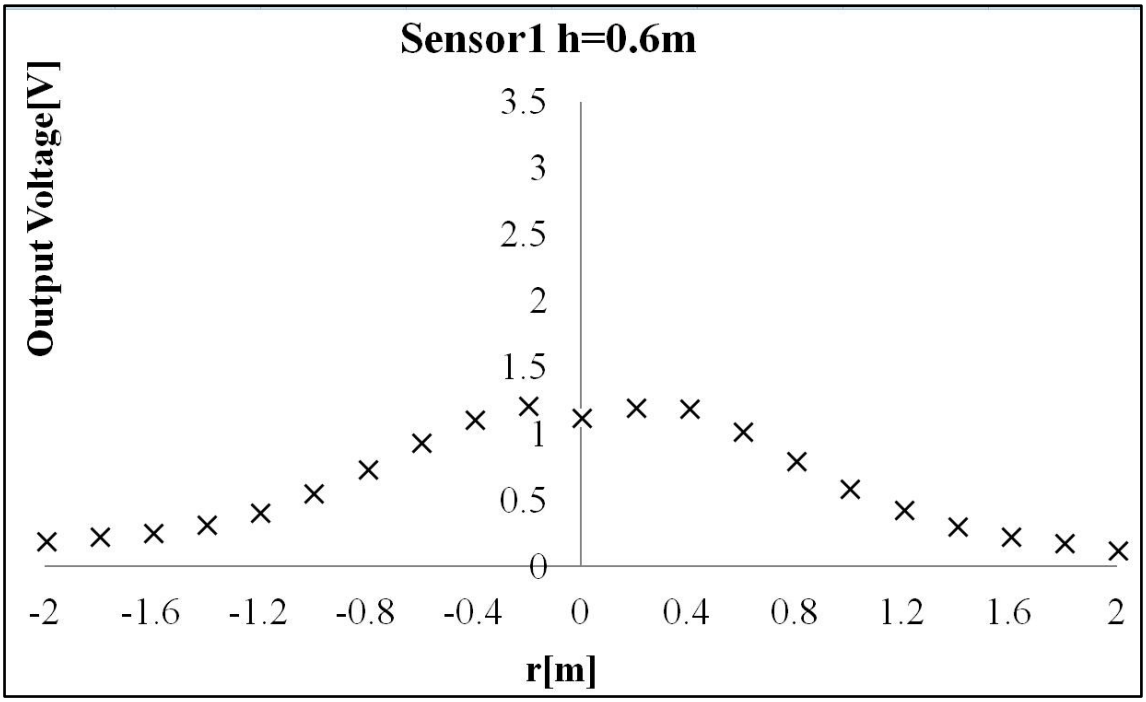
Sensor1 h=0.6m
Output Voltage[V]
3.5
3
2.5
2
1.5
1
0.5
0
-2
-1.6
-1.2
-0.8
-0.4
0
0.4
0.8
1.2
1.6
2
r[m]

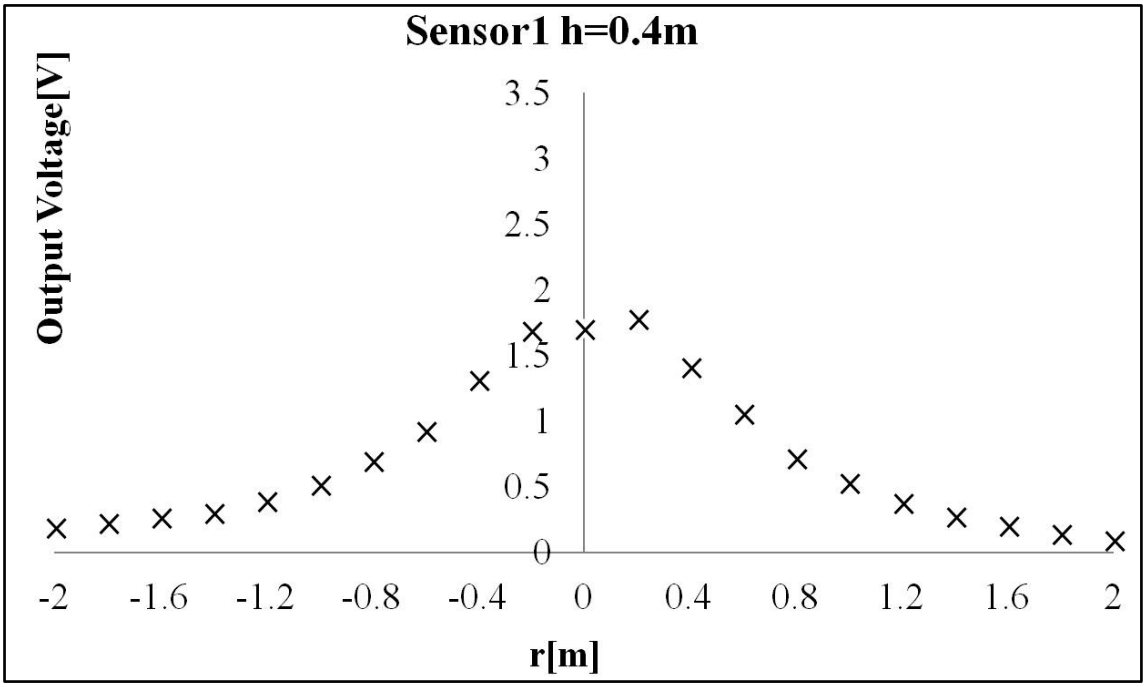


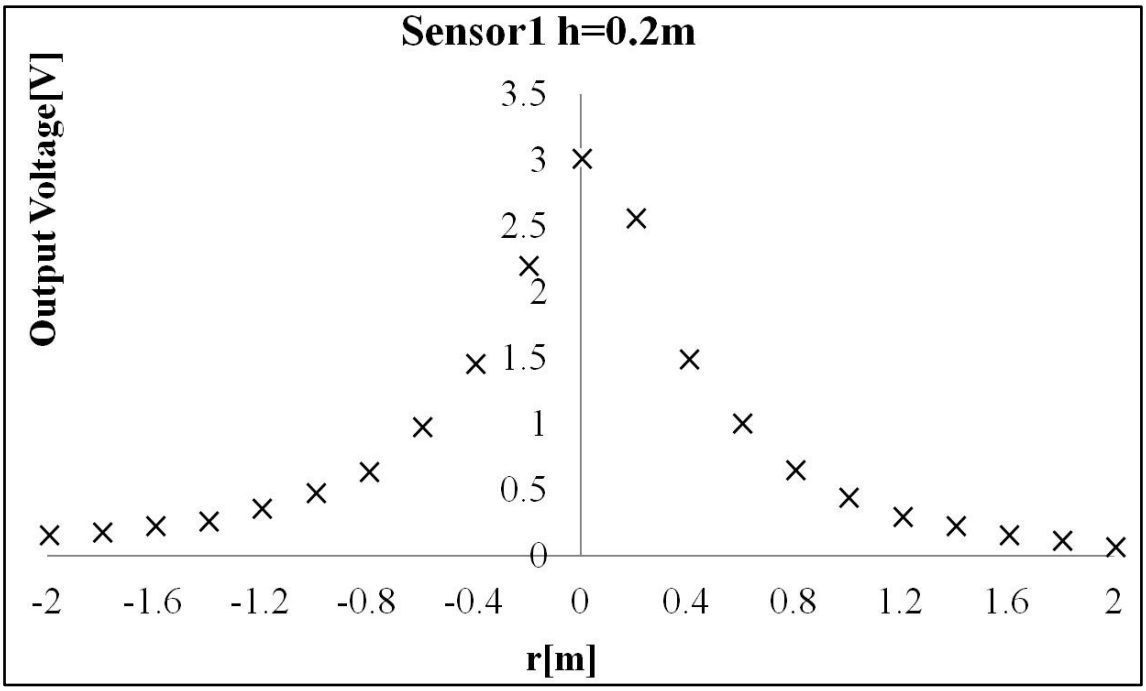


Fig. 5.11 Results about relationship between r and V under different h (sensor1)

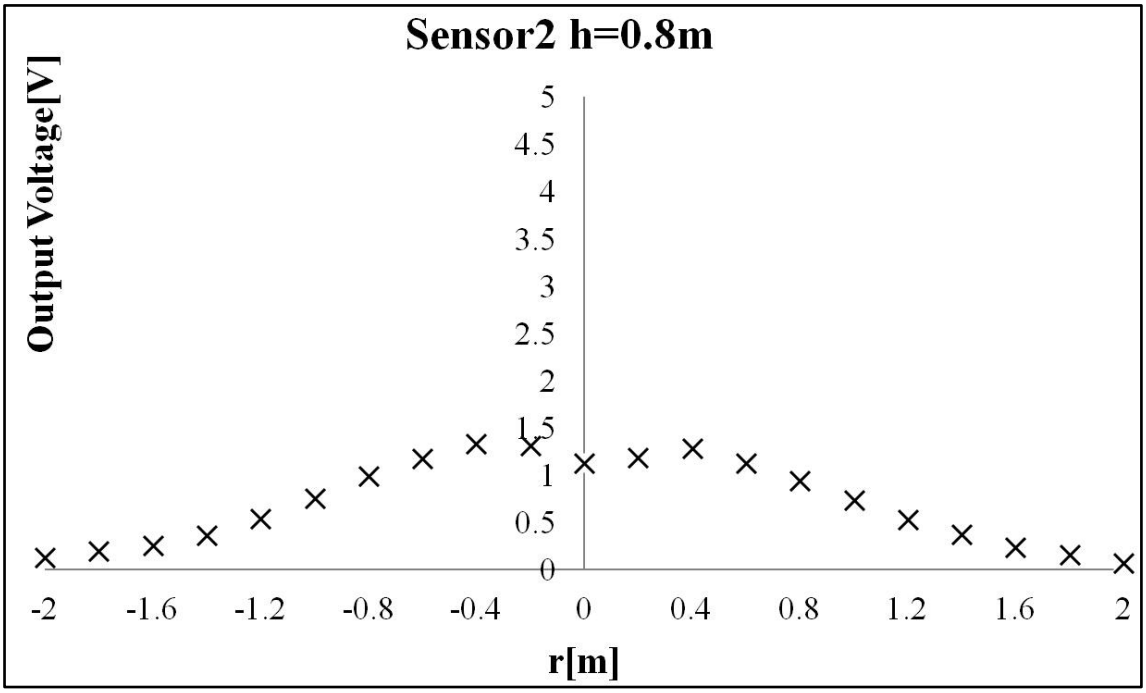
Sensor2 h=0.8m
Output Voltage[V]
5
4.5
4
3.5
3
2.5
2
1.5
1
0.5
0
-2
-1.6
-1.2
-0.8
-0.4
0
0.4
0.8
1.2
1.6
2
r[m]

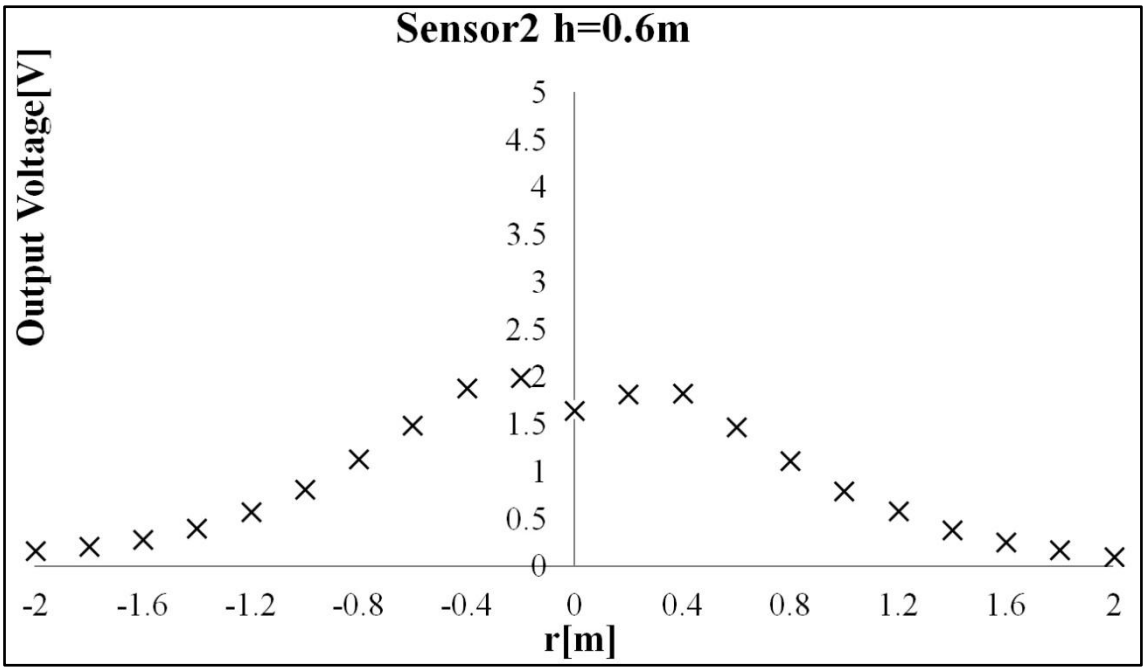
Sensor2 h=0.6m
Output Voltage[V]
5
4.5
4
3.5
3
2.5
2
1.5
1
0.5
0
-2
-1.6
-1.2
-0.8
-0.4
0
0.4
0.8
1.2
1.6
2
r[m]

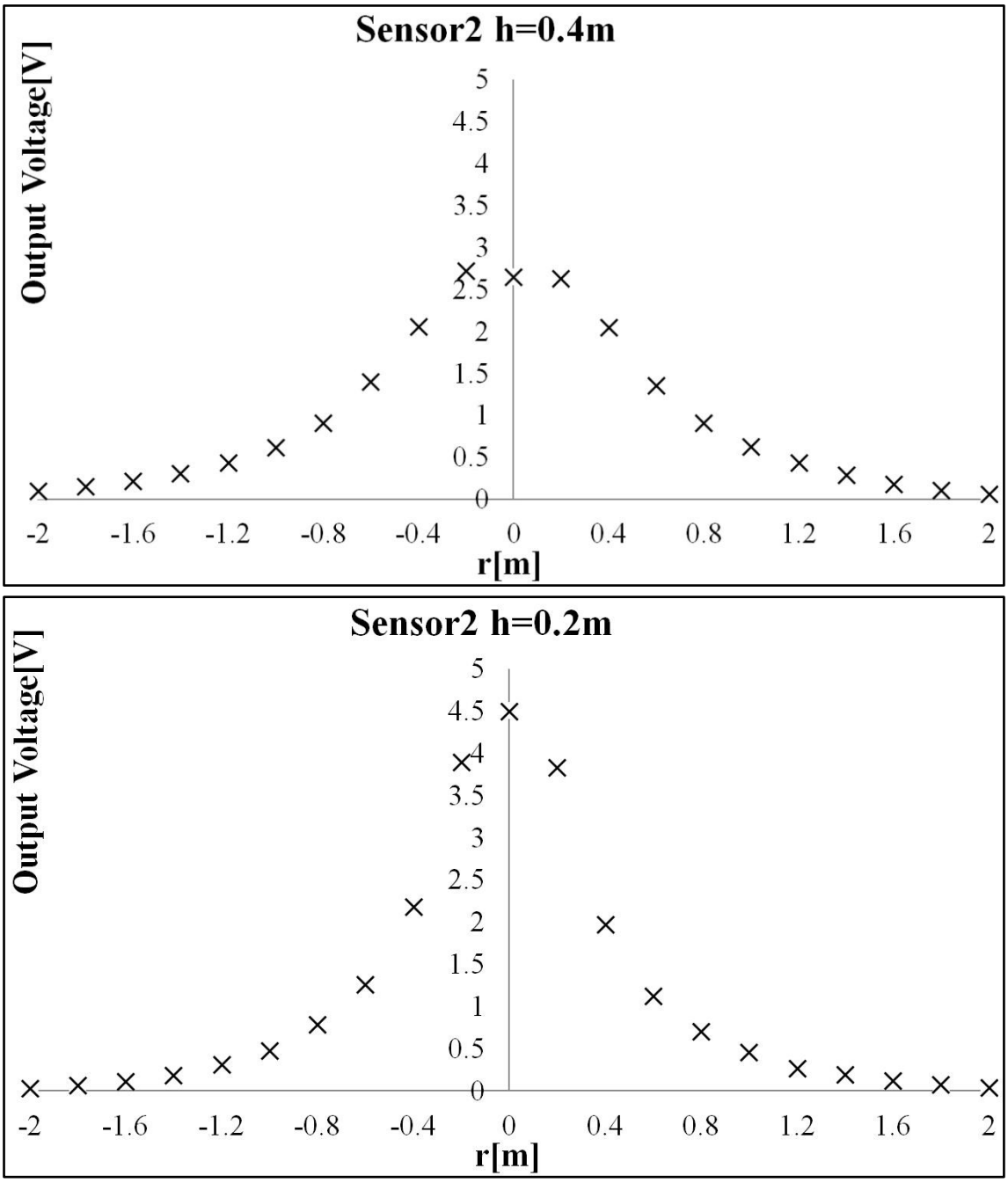


Fig. 5.12 Results about relationship between r and V under different h (sensor2)

According to **Eq. 5.1**, we can convert it into the form of the following form:

$$V_r(r) = V/(V_T(T) \cdot V_h(h) \cdot V_\alpha(\alpha)) \quad (5.6)$$

In **Eq. 5.6**, because we measured under the premise of keeping body face to the sensor, that is to say, body angle always same, here we can ignore this part, consequently **Eq. 5.6** can be turned into the form below:

$$V_r(r) = V/(V_T(T) \cdot V_h(h)) \quad (5.7)$$

We could image that $V_r(r)$ should be very close after calculating by **Eq. 5.7** under many T, results show as **Fig. 5.13**, which separately calculated when h = 0.8m, 0.6m ,0.4m, 0.2m.

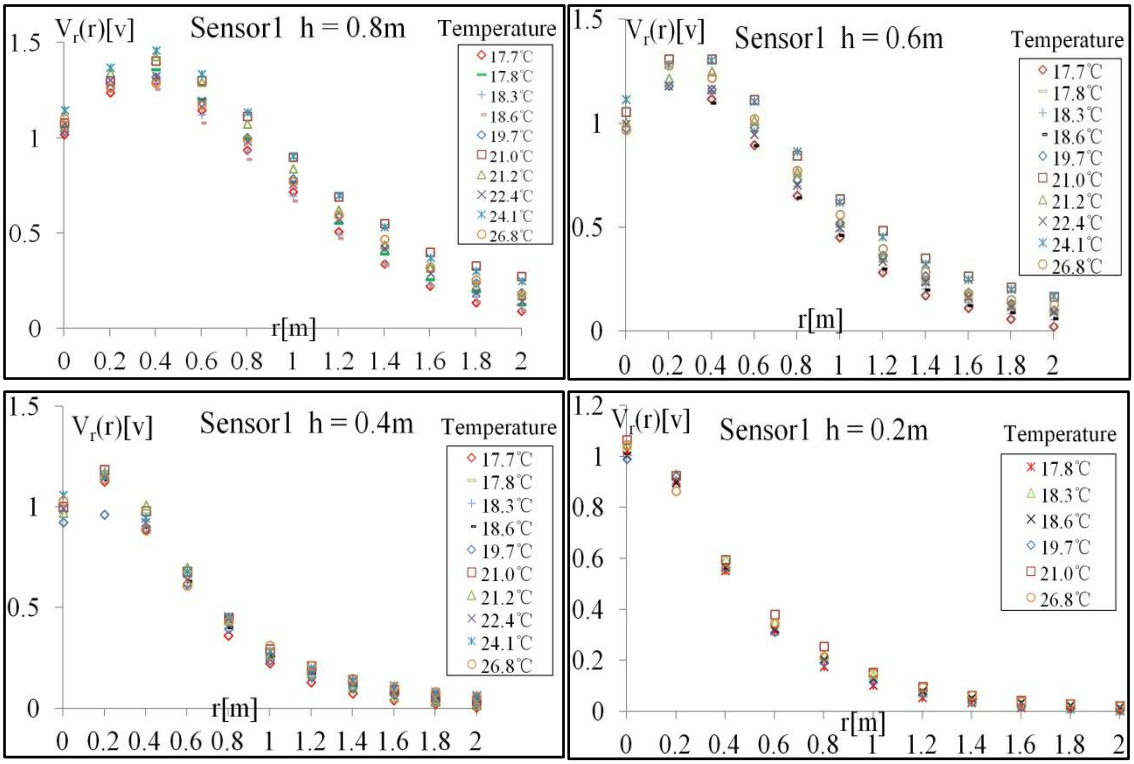


Fig. 5.13 Calculated results for $V_r(r)$

As we envisaged, we can see that results calculated at different T are very approach from **Fig. 5.13**. Then we got the average value of all temperatures. The comparison result shows as **Fig. 5.14.**

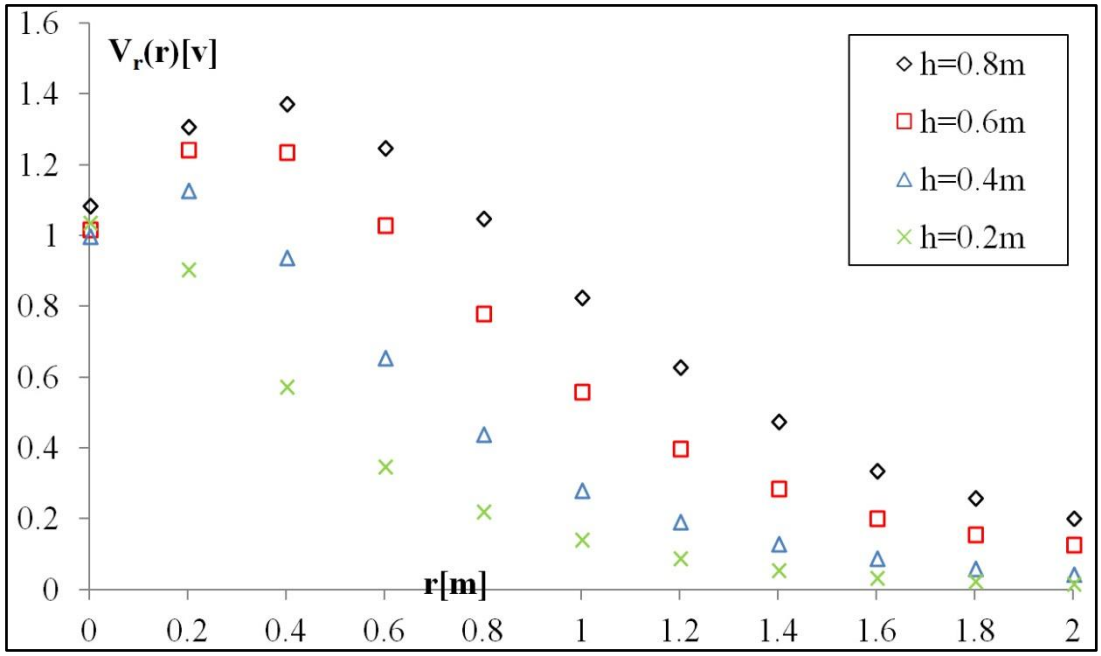


Fig. 5.14 Comparison result at different heights

From the shapes of **Fig. 5.14**, we can see that there are a very big different, that is, the sensor output is almost same when the distance is near to the sensor. Here, we want to explain the reason why it produced this phenomenon. Because when measured just under the sensor, the detected human body is almost fix, in addition, the radiation is very less, and error exists during the measurement.

In order to find the relationship among these heights, we selected the result when h = 0.8m as a standard curve, then through multiplying an coefficient by sensor output to make the curve near to the standard, result shows as **Fig. 5.15**.

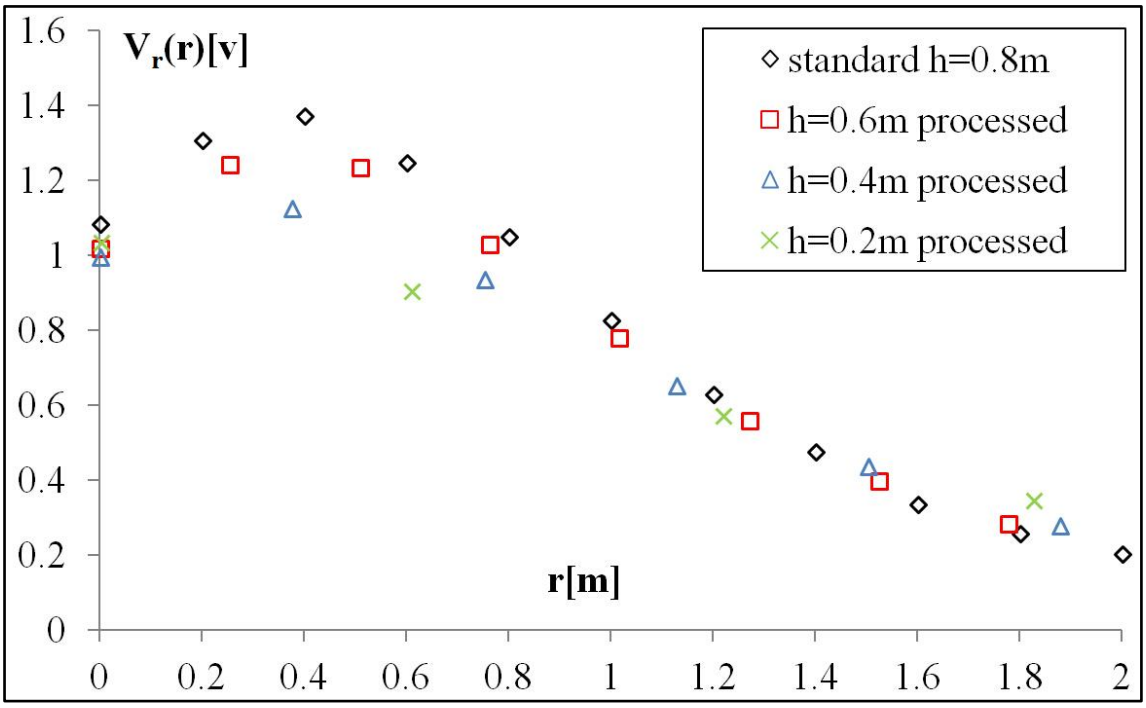


Fig. 5.15 Processed results that come from Fig. 5.14

The result shows that it is very difficult to find appropriate coefficient to make them coincide.

We can discover that there are two same output voltages in some near positions. If we employed all data at any position, there will be produce two solutions in the latter measurement. Hence, we decided to neglect some data within 0.4m, thus the After doing away with some data, based on the method that sensor output times an coefficient, we continued to make the x-axis distance (r) times an coefficient in order to make curves close, after adjusting it again, result shows as **Fig. 5.16**.

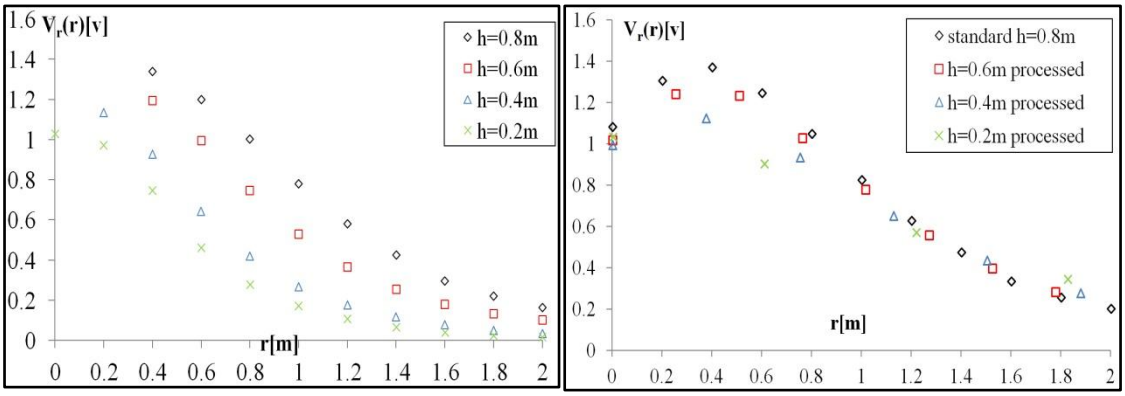


(a) (b)

Fig. 5.16 (a) After ignore some positions (b) Result based on (a) times an coefficient

Although we want to find the relationship between these heights, the result shows that there is no certain relationship among them. Hence, we separately disposed to fitting the curve at each height. We used the polynomial to fitting the curve, so we need to find out that how many powers of the function is the optimal? We separately calculated the theoretical values by using different powers, then compared the theoretical values and experimental values, **Table 5.1** shows the comparison result, here just enumerates the result when height = 0.8m. Obviously, we got the optimal function when power is 5 after comparing. **Fig. 5.17** shows the results at each height when the power is 5.

TABLE 5.1 COMPARISON RESULTS UNDER DIFFERENT POWER

| h = 0.8m | | | | | |
|---|---|---|---|---|---|
| r | $V_r(r) = r^2$ | $V_r(r) = r^3$ | $V_r(r) = r^4$ | $V_r(r) = r^5$ | $V_r(r) = r^6$ |
| 0.4 | 0.056 | 0.014 | 0.0010 | 0.000 | 0.000 |
| 0.6 | 0.043 | 0.022 | 0.0040 | 0.0010 | 0.0020 |
| 0.8 | 0.050 | 0.011 | 0.0010 | 0.0030 | 0.0040 |
| 1 | 0.013 | 0.014 | 0.0060 | 0.0030 | 0.0030 |
| 1.2 | 0.018 | 0.018 | 0.0020 | 0.0020 | 0.0020 |
| 1.4 | 0.025 | 0.0020 | 0.0110 | 0.0070 | 0.0070 |
| 1.6 | 0.034 | 0.0050 | 0.0040 | 0.0070 | 0.0050 |
| 1.8 | 0.004 | 0.017 | 0.0010 | 0.0020 | 0.0040 |
| 2 | 0.031 | 0.011 | 0.0020 | 0.0020 | 0.0020 |
| average | **0.030** | **0.013** | **0.0040** | **0.0030** | **0.0030** |

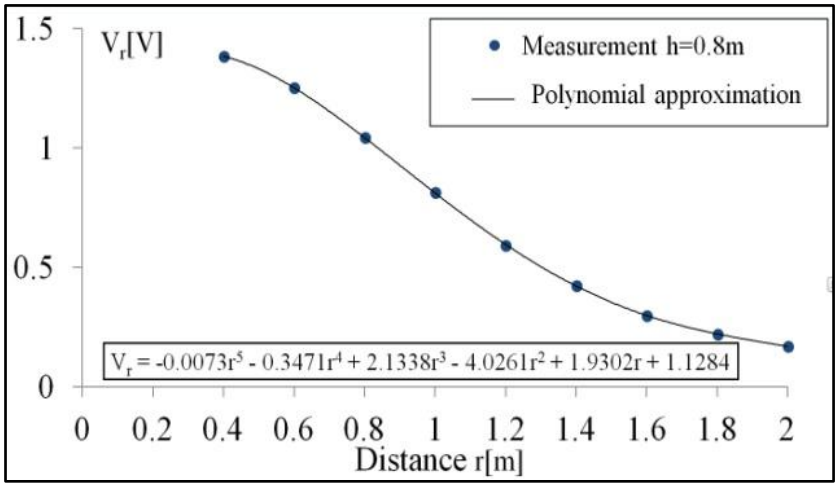
1.5
1
0.5
0
$V_r$[V]
Measurement h=0.8m
Polynomial approximation
$V_r = -0.0073r^5 - 0.3471r^4 + 2.1338r^3 - 4.0261r^2 + 1.9302r + 1.1284$
0 0.2 0.4 0.6 0.8 1 1.2 1.4 1.6 1.8 2
Distance r[m]

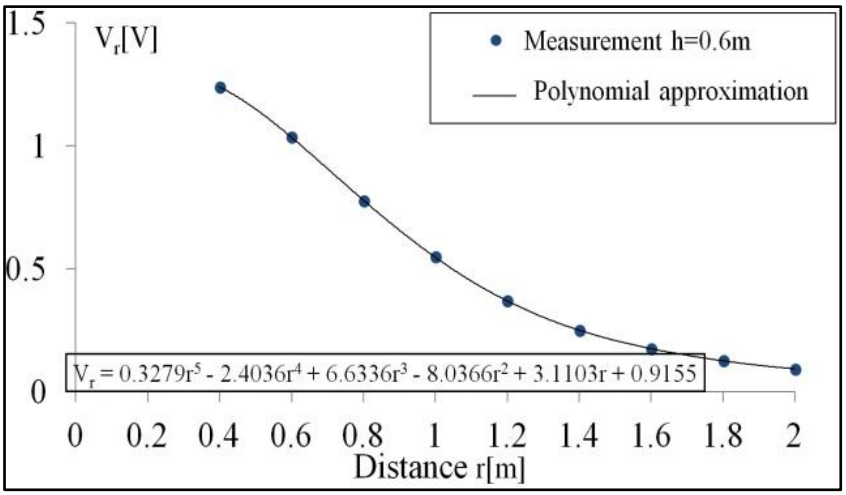
1.5
1
0.5
0
$V_r$[V]
Measurement h=0.6m
Polynomial approximation
$V_r = 0.3279r^5 - 2.4036r^4 + 6.6336r^3 - 8.0366r^2 + 3.1103r + 0.9155$
0 0.2 0.4 0.6 0.8 1 1.2 1.4 1.6 1.8 2
Distance r[m]

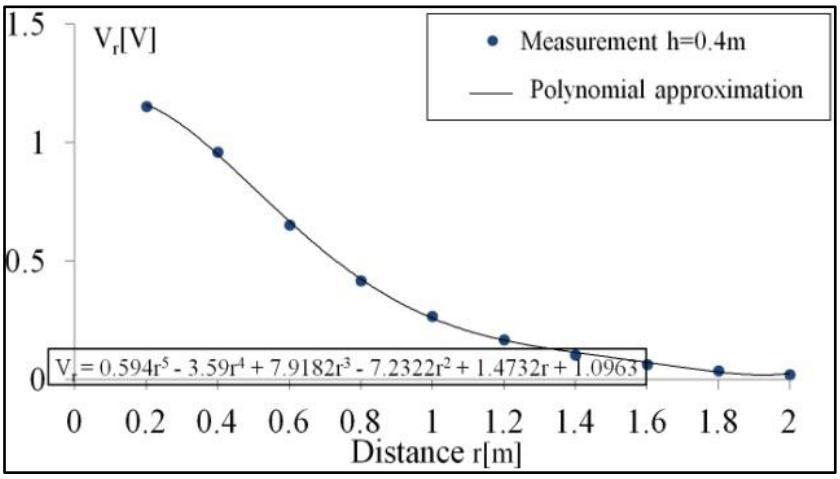
1.5
1
0.5
0
$V_r$[V]
Measurement h=0.4m
Polynomial approximation
$V_r = 0.594r^5 - 3.59r^4 + 7.9182r^3 - 7.2322r^2 + 1.4732r + 1.0963$
0 0.2 0.4 0.6 0.8 1 1.2 1.4 1.6 1.8 2
Distance r[m]

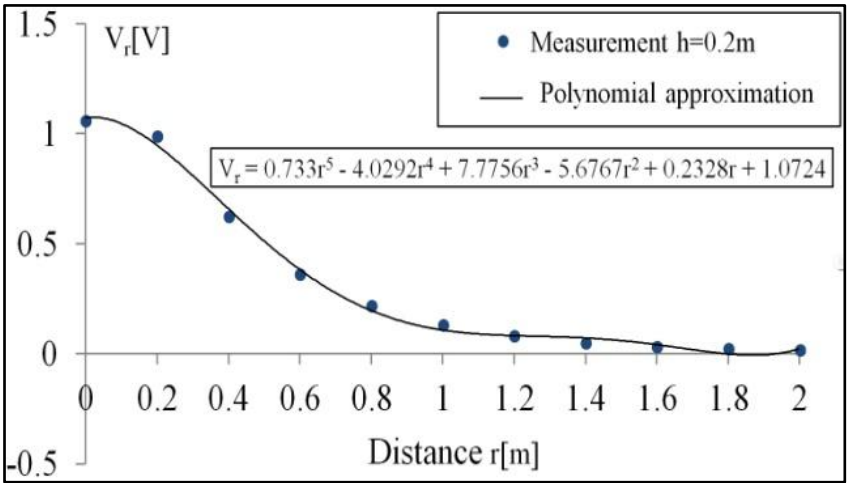


Fig. 5.17 Curve fitting at each h

And the approximated equation expressed like:

$$V_r(r) = a_2r^5 + a_3r^4 + a_4r^3 + a_5r^2 + a_6r + a_7 \quad (5.8)$$

where $a_2$~$a_7$ are constant in **Table 5.3** below.

### 5.1.3 Human body orientation

We did experiment to measure the relationship between sensor output and human body orientation angle α . The experiment is described as follows (see **Fig. 5.18**): human separately stood in some positions to measure from 0.4m to 2m by every 0.2m in a line, we defined the direction that when human is directly facing to the sensor as 0°. Because we realized that sensor output when human face to the sensor is same as that when human back to the sensor, we just measured semi-circle from -90° to 90° by every 30°. **Fig. 5.19** shows the results of two sensors. We found that the output is nearly symmetrical between [-90°,0°] and [0°,90°], and the bigger the orientation angle, the smaller the sensor output.

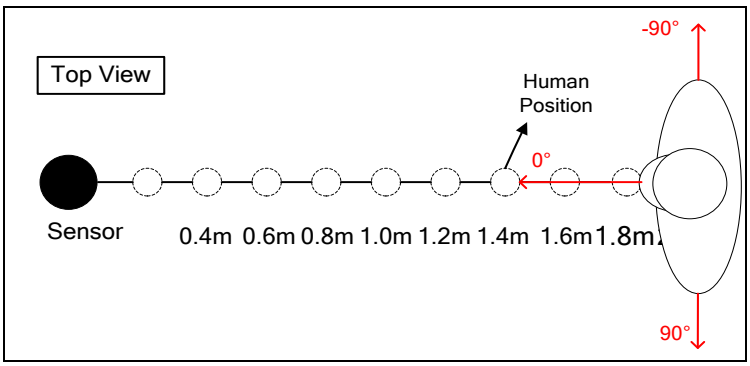


Fig. 5.18 Illustration for experiment

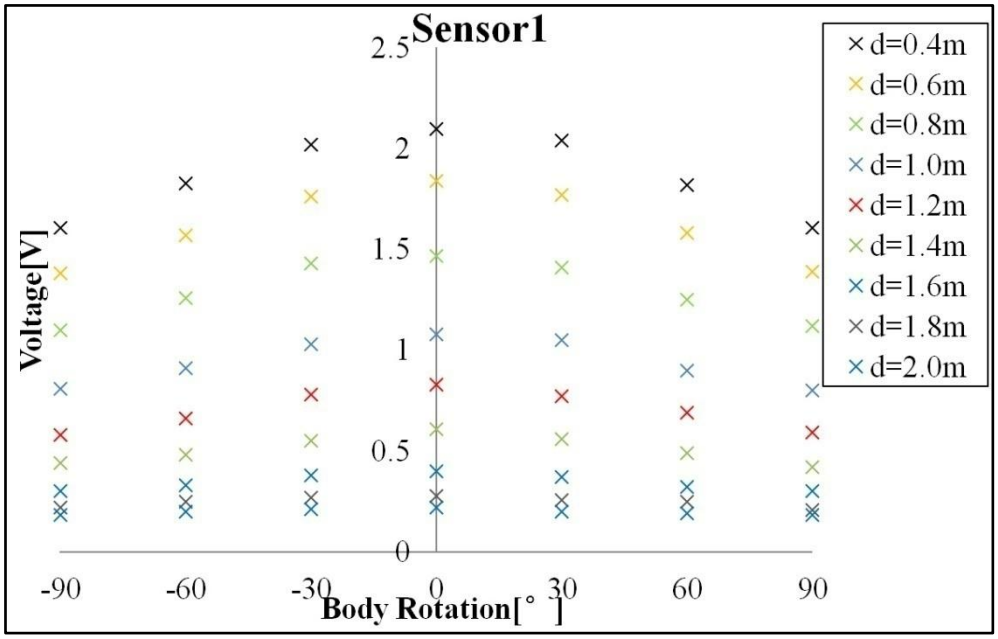


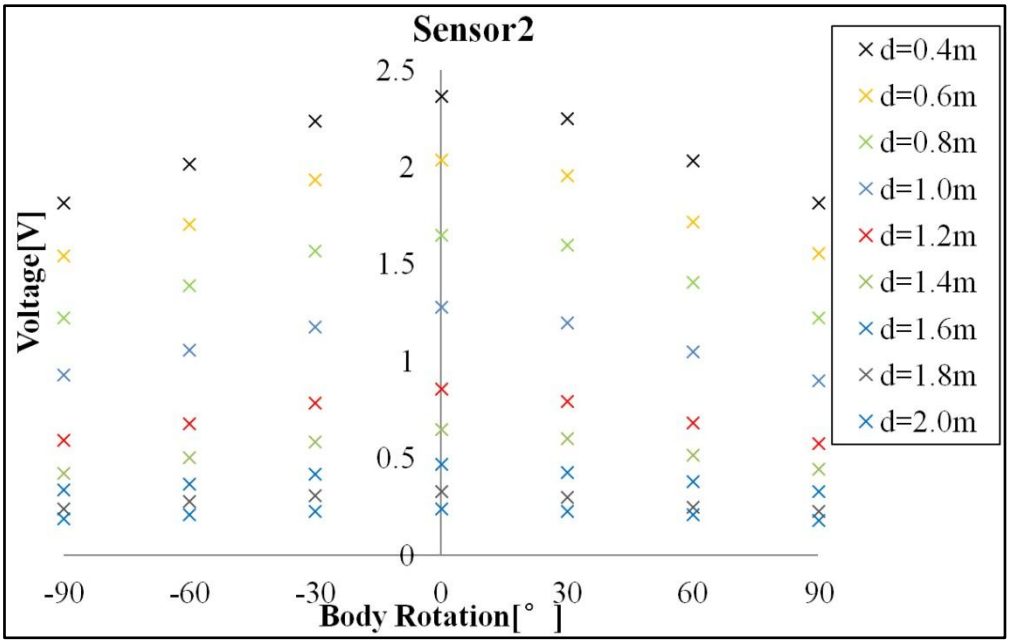


Fig. 5.19 Relationships between human rotation α and V about two sensors

After converting this graph to see the relationship between distance and sensor output, we got **Fig. 5.20,** because two sensors are very similar, only one graph is drawn below.

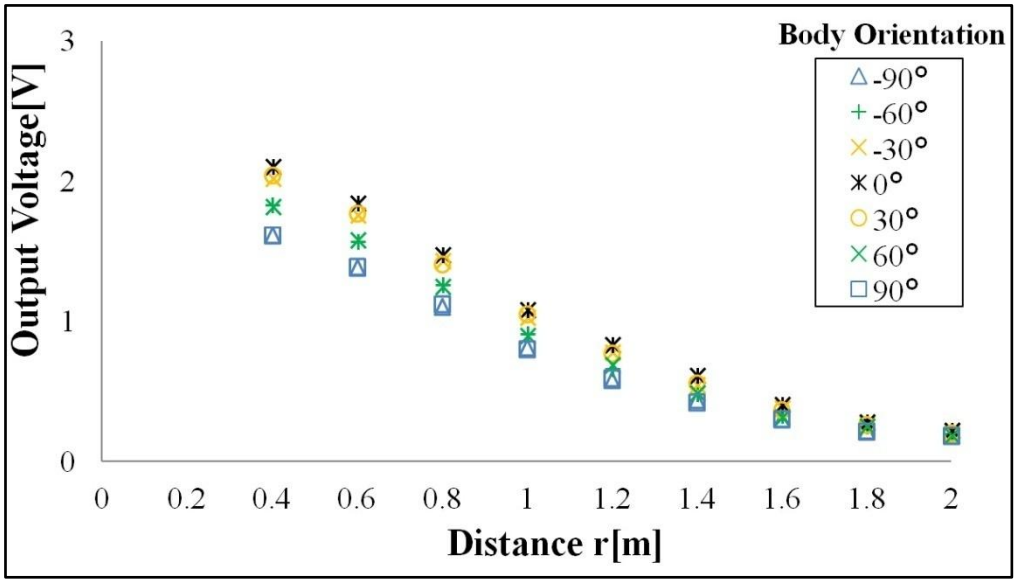


Fig. 5.20 Changes come from Fig. 5.19 expressed by r and V

Because they have a similar output curve shape, we guessed there may be a certain relationships among them, hence, first we selected the standard curve when body orientation = 0°, then other curves multiplied by a coefficient so that they can coincide with each other. Because they are symmetrical in corresponding angles, we just processed by half round, finally we got the result shows as **Fig. 5.21**.

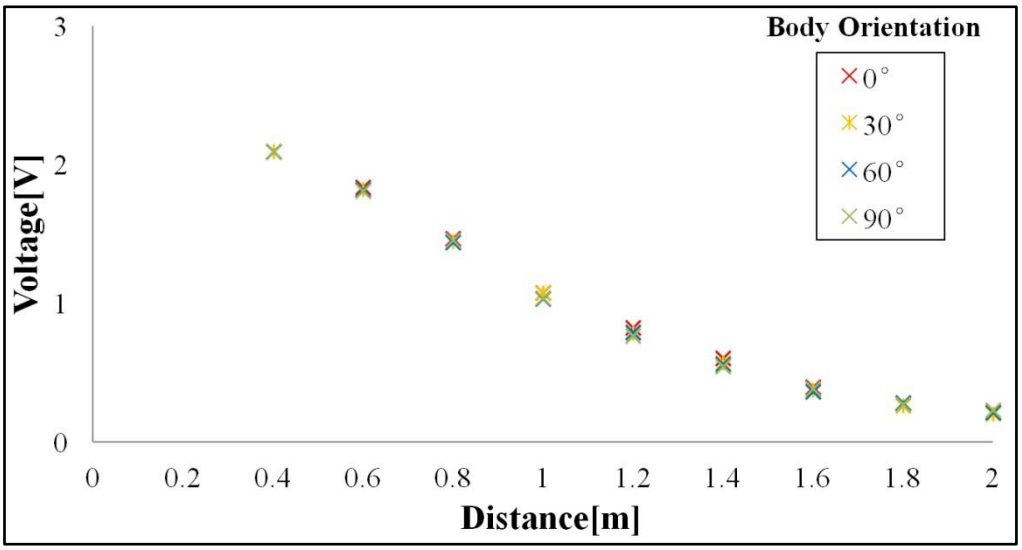


Fig. 5.21 Results after times an coefficient by each angle

**Table 5.2** shows the coefficients corresponding to each angle.

TABLE 5.2 CORRESPOINDING COEFFICIENTS

| Orientation[°] | Orientation Coefficient |
|---|---|
| 0 | 1 |
| 30 | 0.971 |
| 60 | 0.867 |
| 90 | 0.795 |

Then though curve fitting, an approximation equation will be expressed as:

$$V_\alpha(\alpha) = 1 - a_{10}\alpha^2 \quad (5.9)$$

where the parameter ($a_{10}$) in **Eq. 5.9** shows in **Table 5.3**. And result for curve fitting shows as **Fig. 5.22**.

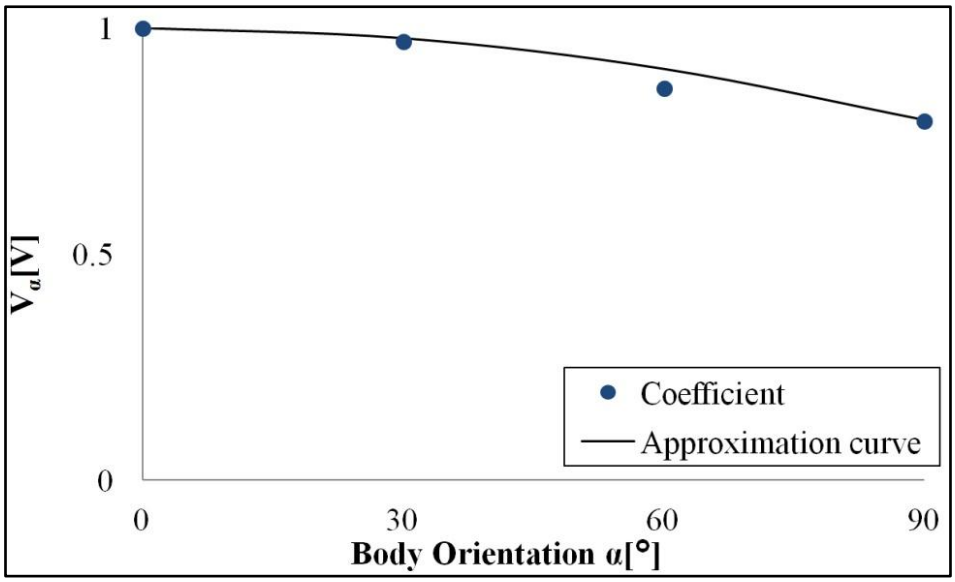


Fig. 5.22 Relationship between body orientation and coefficient

So far, we have got all of the approximation equations for expressing the sensor output. All of the specific parameter values are listed in **Table 5.3**.

TABLE 5.3 APPROXIMATED PARAMETER VALUES OF TWO SENSORS

| Parameter / Sensor | $a_1$ | $a_2$ | $a_3$ | $a_4$ | $a_5$ |
|---|---|---|---|---|---|
| Sensor1 | 0.45 | 0.071 | -0.753 | 2.82 | -4.41 |
| Sensor2 | 0.42 | -0.007 | -0.347 | 2.13 | -4.03 |
| Parameter / Sensor | $a_6$ | $a_7$ | $a_8$ | $a_9$ | $a_{10}$ |
| Sensor1 | 1.95 | 1.10 | -0.14 | 3.86 | 0.085 |
| Sensor2 | 1.93 | 1.13 | -0.094 | 3.62 | 0.097 |

## 5.2 Basic method

From **Eq. 5.1**, **Eq. 5.4**, **Eq. 5.5**, **Eq. 5.8**, **Eq. 5.9** we got in last Chapter, we can see that only distance r and orientation angle α are unknown. Therefore, if the body orientation α is given, at least two sensors are required to detect human position. Keep two sensors a certain distance at one height, the space layout is shown in **Fig. 5.23**.

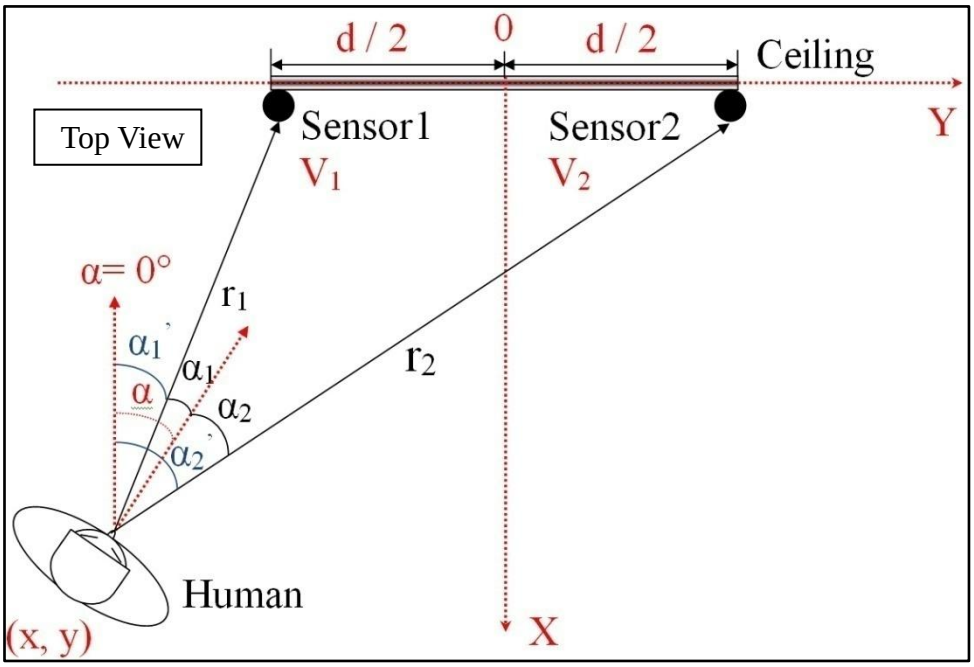


Fig. 5.23 Layout for detecting human by two thermopile sensors amounted on the ceiling

First we can clearly express the unknown r and α by 2D position (x,y) from the relationships in **Fig. 5.23**. That is,

$$r_1=\sqrt{x^2+(y-d/2)^2}, r_2=\sqrt{x^2+(y+d/2)^2} \quad (5.10)$$

$$\alpha_1 = \alpha - \alpha_1' = \alpha - \tan^{-1}((y-d/2)/2) \quad (5.11)$$

$$\alpha_2 = \alpha_2' - \alpha = \tan^{-1}((y+d/2)/2) - \alpha \quad (5.12)$$

then substituted them into the equation , and an equation set can be built by **Eq. 6.4** and **Eq. 6.5**, which is given as followings:

$$V_1 = V_T(T) \cdot V_h(h) \cdot V_r(r_1) \cdot V_\alpha(\alpha_1) \quad (5.13)$$

$$V_2 = V_T(T) \cdot V_h(h) \cdot V_r(r_2) \cdot V_\alpha(\alpha_2) \quad (5.14)$$

In other words, detecting a human-being's position becomes a problem of how to solve for *x* and *y* in the equation set formed by **Eq. 5.13** and **Eq. 5.14**.

So far, we could aware that it is still the question about how to solve a binary equation. Two proposed methods have been introduced in the chapter 4. Because it will be produce a relatively large error by using analytical method, we will not discuss about it in this Chapter. Meanwhile, steepest decent method has been introduced in detail, a brief description will be introduce in the following.

## 5.3 Steepest Descent Method

The steepest descend method is known as an optimization algorithm to find the nearest local minimum of a function. We apply this method for detecting human position stated as follows. First, we built the evaluation function like this:

$$E(x,y) = \Delta V_1^2 + \Delta V_2^2 \quad (5.15)$$

the $\Delta V_1$ and $\Delta V_2$ were respectively defined as the following form:

$$\Delta V_1 = V_1 - V_T(T) \cdot V_h(h) \cdot V_r(r_1) \cdot V_\alpha(\alpha_1) \quad (5.16)$$

$$\Delta V_2 = V_2 - V_T(T) \cdot V_h(h) \cdot V_r(r_2) \cdot V_\alpha(\alpha_2) \quad (5.17)$$

where $V_1$ and $V_2$ denote measured voltages.

We also defined that the search starts at the initial point ($x_0$, $y_0$) (e.g. $x_0$=1[m], $y_0$=0[m]), we therefore set the iterative form below:

$$x_{k+1} = x_k - C\left(\frac{\partial E}{\partial x}\right)_{\substack{x=x_k \\ y=y_k}} \quad (5.18)$$

$$y_{k+1} = y_k - C\left(\frac{\partial E}{\partial y}\right)_{\substack{x=x_k \\ y=y_k}} \quad (5.19)$$

and continue the process, by searching from ($x_k$, $y_k$) to ($x_{k+1}$, $y_{k+1}$). The most suitable point was found when function E(x,y) reaches certain accuracy (i.e., E(x,y) < 1e-5) through adjusting the value of step size C, and finally from simulation by try and error, we sought out the optimal solution C, while C =0.01, $\Delta x = 0.0001$, $\Delta y = 0.0001$.

Based on the assumed conclusion, we can further ideally understood that used the equation above to draw an image graph shown as **Fig. 5.24** below, each curve represents the same output voltage curve. Normally there should be numerous curves in some effective range, but just few curves be drawn in **Fig. 5.24**. Because many intersections are formed by many different curves, and each intersection consists of a pair of output voltage values [$V_1$, $V_2$], meanwhile it was also considered as human position. We also can see that the effective detection area is generally when x = 2m and y =2m.

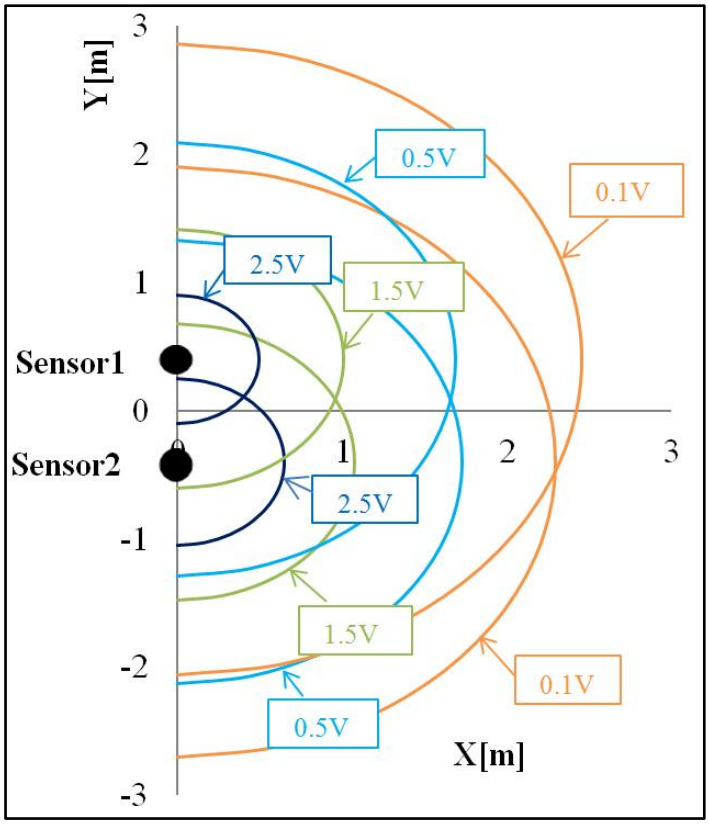


Fig. 5.24 Outline of detection by two sensors from the ceiling

## 5.4 Accuracy

If we don't consider the factor of body orientation, that is, always kept the orientation angle(α) is 0°, there will produce some errors at any detected positions. We separately

analyzed and discussed the distribution of error about detected positions at different angles in [-90°,90°] in theory, and specific approach is two steps.

Step 1: Solving position (x,y) by sensor outputs ($V_1$,$V_2$) when body orientation angle α = 0 °through simulation.

Step 2: Fixing sensor outputs ($V_1$, $V_2$) when α = 0 °, then changing the body angle by slight angle (e.g. 5°) in [-90°,90°], some new sensor outputs ($V_1$, $V_2$) corresponding to each angle will be obtained, then simulating it again, corresponding new positions (x,y) can be calculated and obtained, finally we got theoretical error results at each position shown as **Fig. 5.25**.

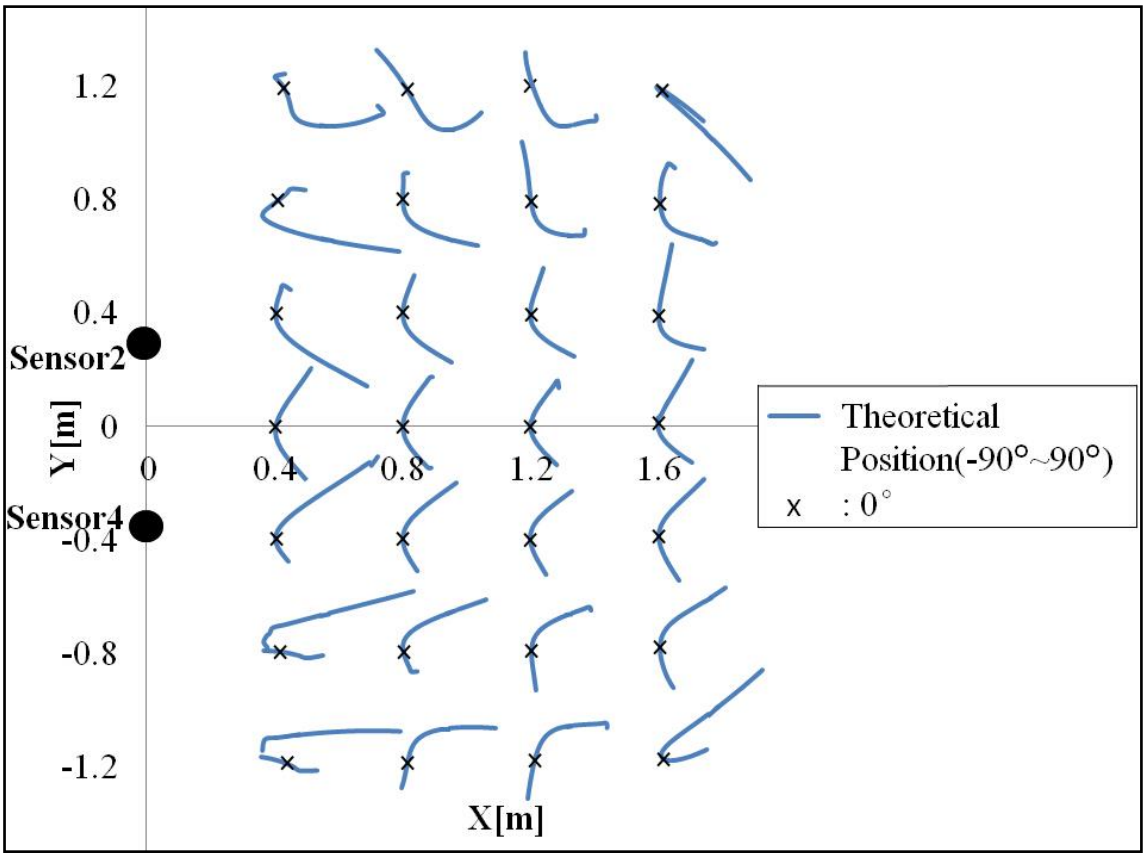


Fig. 5.25 Distribution of error and comparison result

Based on the theoretical result, we made a experiment, which separately kept body orientation is [30°,60°,90°] to verify whether the experimental positions still belong to the curve in **Fig. 5.26**. And result shows as Fig, that is, the same as we imaged, it basically proved it.

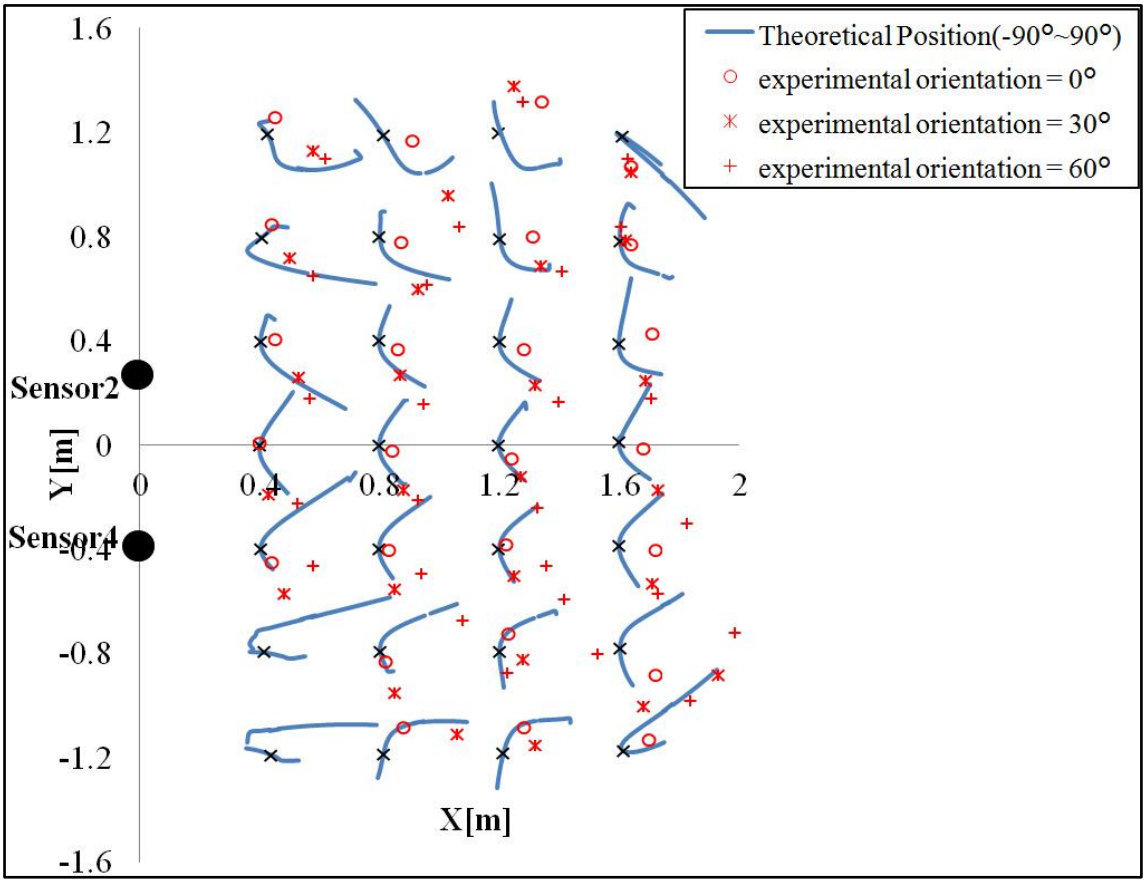


Fig. 5.26 Comparison results between theoretical and experimental

## 5.5 Method to detect human motion

The importance of detecting human motion is not inferior to detecting human position, because in the practical world, human beings are almost in walking outside, especially when somebody enter into (or get away) a building. Hence, the correct judgment from the sensor system is essential.

Let us consider the process of detecting human motion. Sensor system triggered by human detection needs to judge when human appear, when human disappear. A method will be introduced as follows.

1. Detect when human come. Sensor's output signal is almost constant in a short time which has been introduced from foregoing information, so when human instantly appears, sensor's output signal should be instantly become larger shown as **Fig. 5.27**, we can get sensor's output voltage variation by equation in differential form shown as $\Delta V/\Delta t$, when this variation value is bigger than a threshold we defined, the system starts to detect human position. Through vast experiments, we can get some results that different $\Delta t$ is corresponding to different threshold shown as **Table 6.1**.

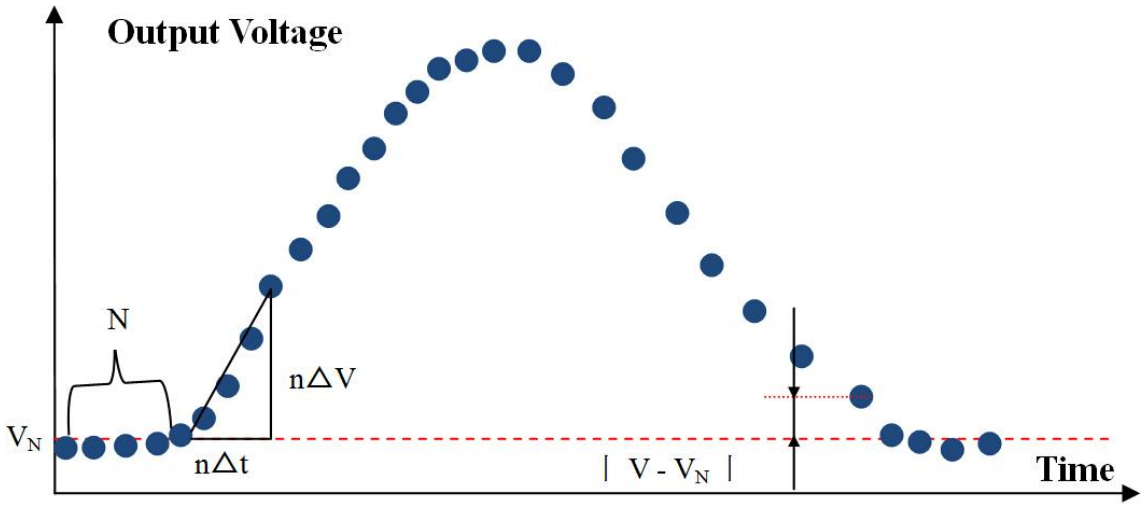


Fig. 5.27 Procedure of human motion

TABLE 5.4 COMPARISON RESULT FOR FINDING OPTIMUM Δt

| Δt[s] | Maximum without human[V] | Threshold[V/s] | Rate of change for threshold(ΔV/Δt) |
|---|---|---|---|
| 0.05 | 0.1 | 0.15 | 4 |
| 0.1 | 0.06 | 0.08 | 2 |
| 0.2 | 0.04 | 0.06 | 1 |
| 0.5 | 0.01 | 0.03 | 0.4 |
| 1 | 0 | 0.02 | 0.2 |

From the last column of **Table 5.4**, we understood when ΔV is constant, the smaller the Δt, the faster the rate of change for threshold, and the values are calculated under the premise when ΔV = 0.2.

However, if Δt is too small, which will lead a situation that even if human haven't appear, sensor system have begun to work. On the contrary, if Δt is too large, which will lead a situation that even if human have appeared, sensor system still hasn't yet begun to work. Finally, we got an optimum Δt is 0.1s and threshold is 0.08 after several repeated attempts. We can easily find which values are the most effective in **Fig. 5.28**.

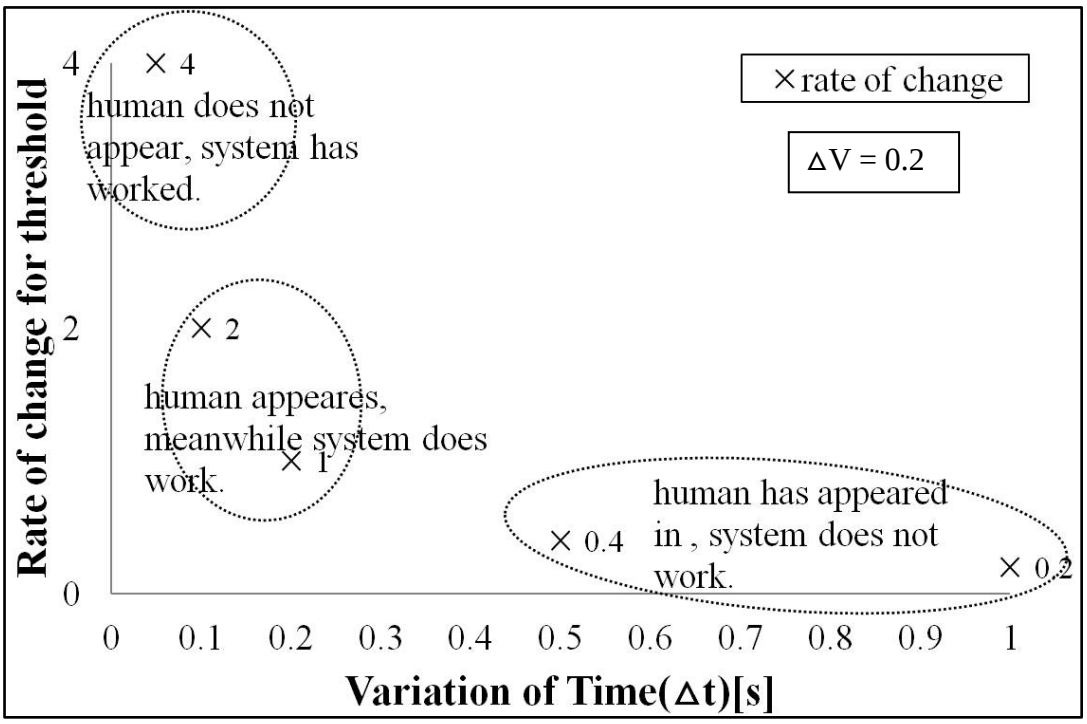


Fig. 5.28 Result for showing the most effective Δt to detect human

2. Detect when human disappears. After judging human come, meanwhile sensor system recorded the average offset value of front N points shown as **Fig. 5.27**, because as mentioned in the Chapter which introducing the sensor characteristics, we have realized the sensor has a drift, therefore, when the value of $|V - V_n|$ was smaller than threshold, sensor system considered that human is not in and stop to work, meanwhile, sensor system stores the average value for some times so that it will convenient for the next detection.

## 5.6 Detection of body orientation

When we want to solve human position by two sensors, human orientation needs to be given. How to give human orientation? We considered that human tendency in a short time should be generally represented as a direction shown like **Fig. 5.29**, and some human continuous positions can be got by sensor system in real time, in other words, the direction can be calculated by some positions. We assumed that using three positions as a group, and body orientation angle is 0°. Therefore, first estimated orientation angle can be got, then utilized estimated orientation angle which we got to calculate next group positions, and do it repeatedly.

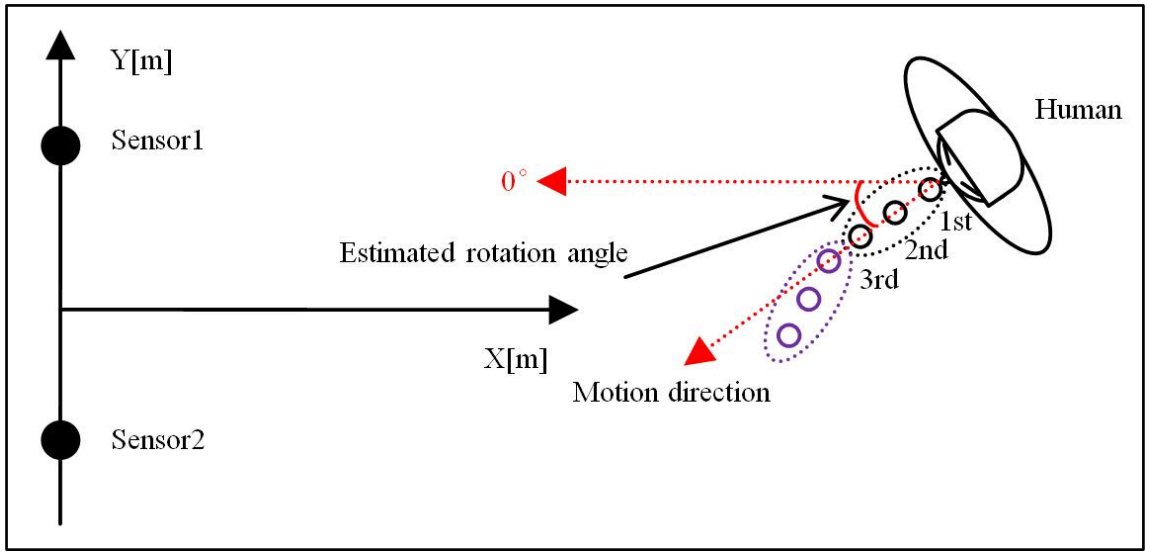


Fig. 5.29 Detection of human body orientation

We only assumed that using three positions as a group to express an estimated direction, however, we were not sure whether 3 is optimum solution or not, therefore, we did an experiment to test it. The experiment is stated as follow, that is, human moved along a direction parallel to the sensor, that is, human body orientation $\alpha = 0°$ from one side to the other side, separately making number is 2 or 3 or 4. Comparison result among them shows as **Fig. 5.30**. So we finally got that number 4 is the optimal solution when system sampling time is 0.1s through discussion.

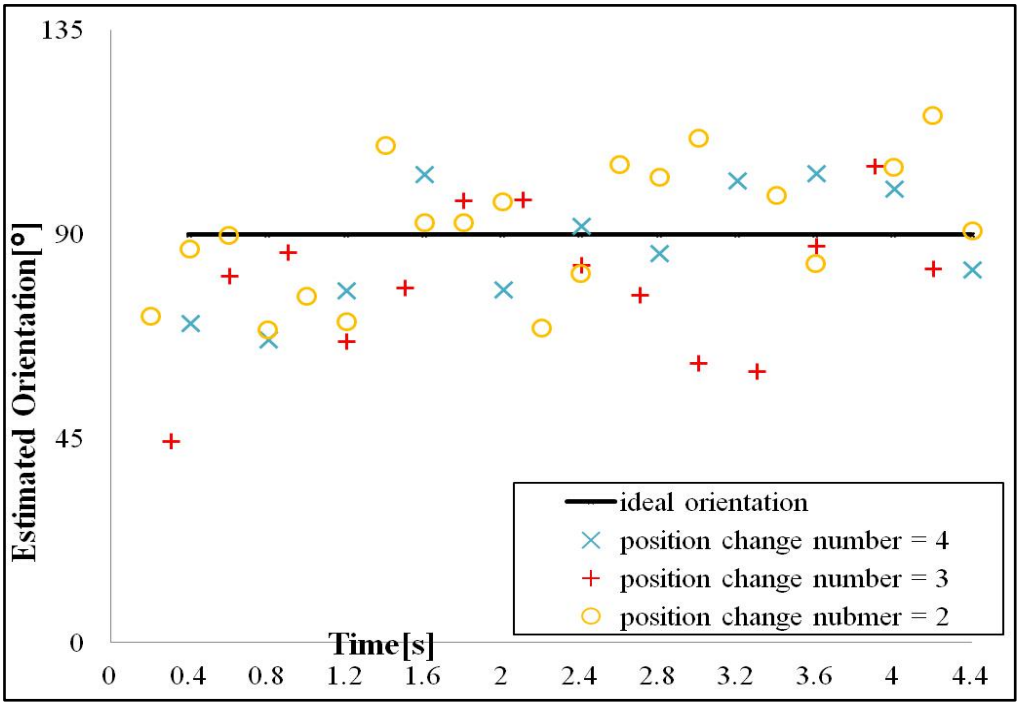


Fig. 5.30 Comparison result for finding the optimum number

Last, we summarize the entire process to get human motion by **Fig. 5.31**.

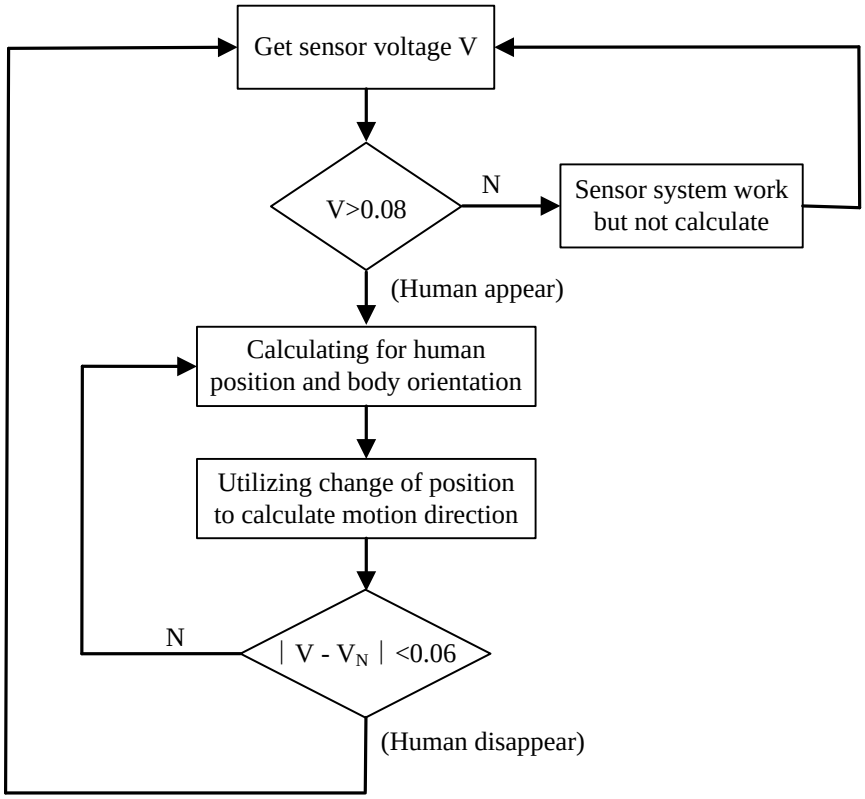


Fig. 5.31 The entire process of detecting human motion

## 5.7 Experiments

### 5.7.1 Experimental Data to Detect Human Position

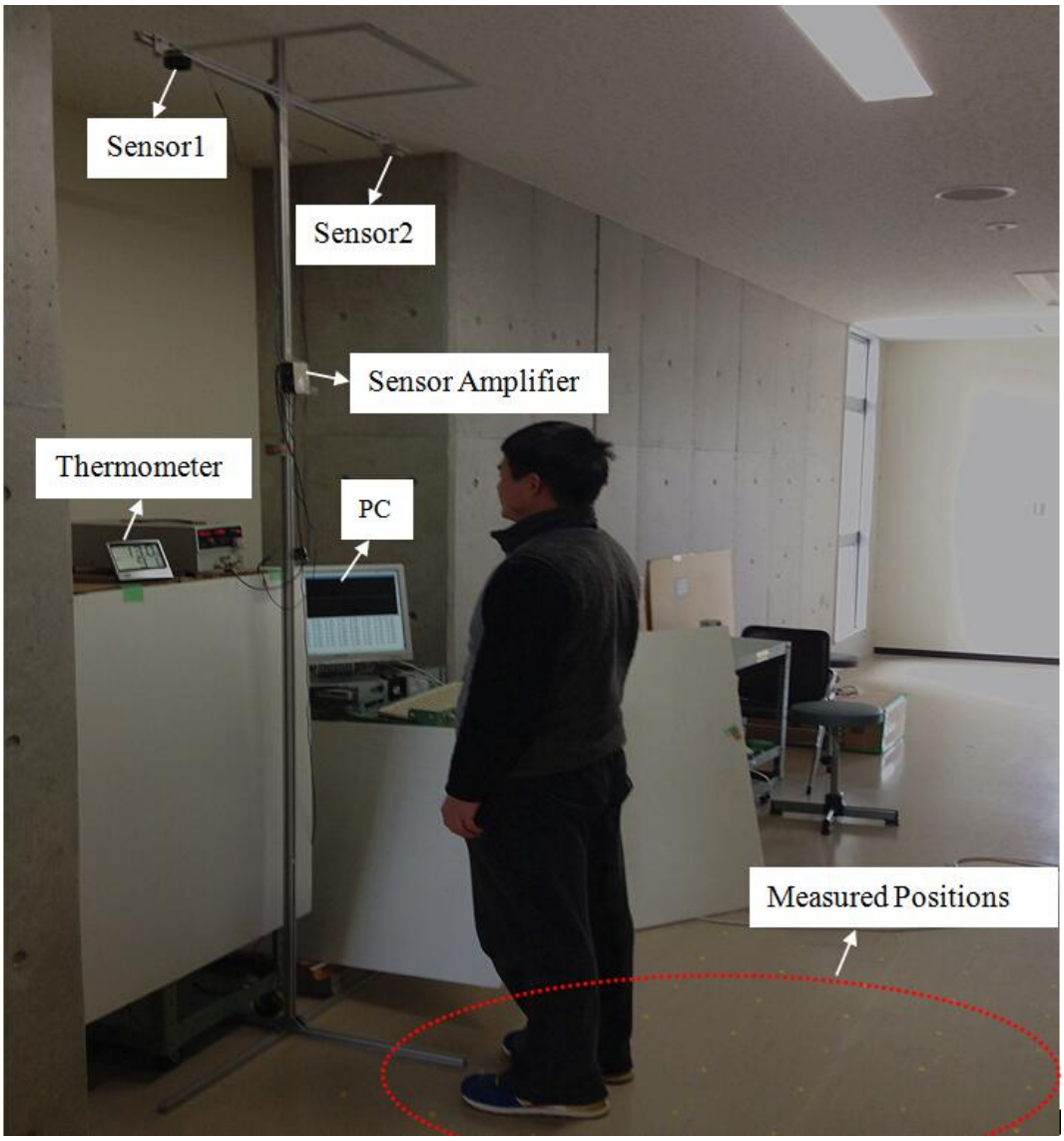


Fig. 5.32 A photo of experimental scene

**Fig. 5.32** shows the experimental scene. All the experiments were done in this scene. Two sensors were fixed on the pole at a height of 2.5m above the ground, and the distance d between them is 0.8m, the origin position, X-axis and Y-axis are defined as shown in **Fig. 5.23**, and the measured positions on the ground were marked, we designated the increment along the X-axis is 0.4m in [0.4m, 1.6m], and the increment along the Y-axis is also 0.4m in [-1.2m, 1.2m]. First, we assume body orientation α = 0°in the position calculation, then respectively did some experiments when true body

orientation angle separately is [0°, 30°, 60°, 90°]. Next, we respectively set body orientation α = [30°, 60°, 90°], then did the experiments when body orientation angle is under the corresponding angle. The results show in **Fig. 5.33**, that is, if we ignore the $V_{\alpha}(\alpha)$ in **Eq. 5.1**, the results would be similar to those in **Fig. 5.25**. On the contrary, we can get a better result.

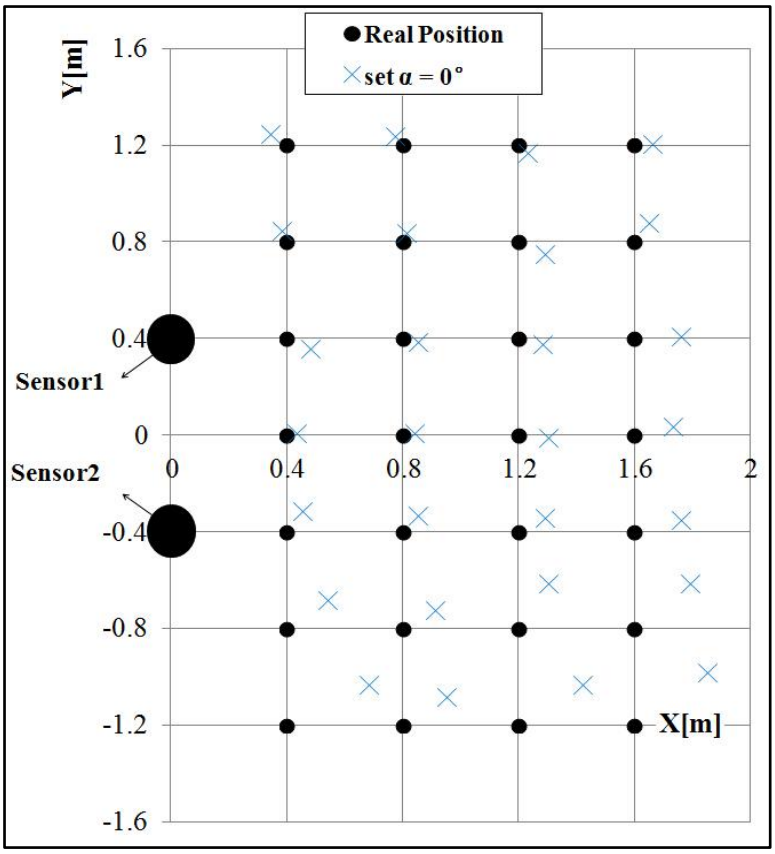

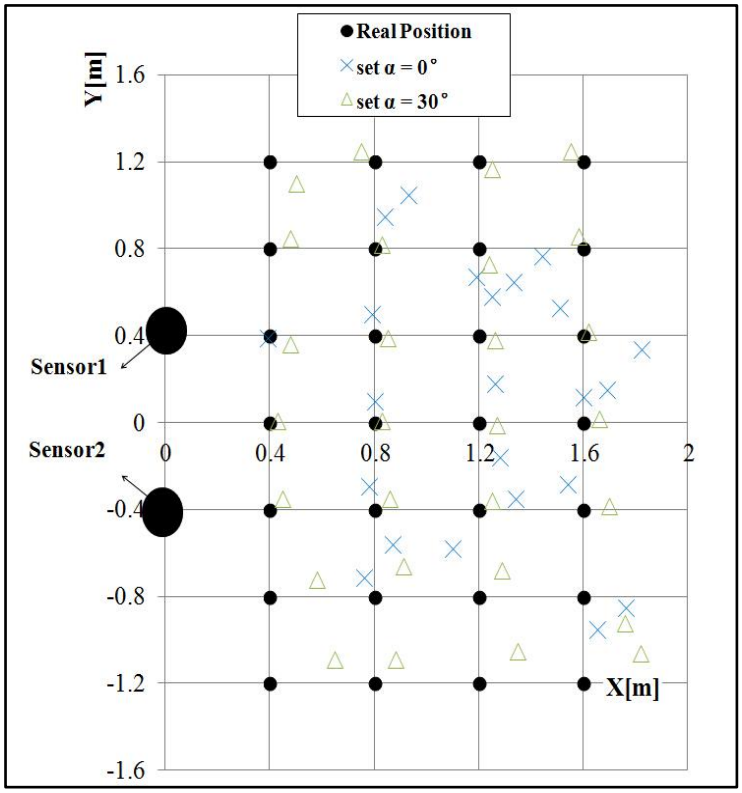
Real Position
set α = 0°
set α = 30°
Y[m]
1.6
1.2
0.8
0.4
0
-0.4
-0.8
-1.2
-1.6
Sensor1
Sensor2
0
0.4
0.8
1.2
1.6
2
X[m]

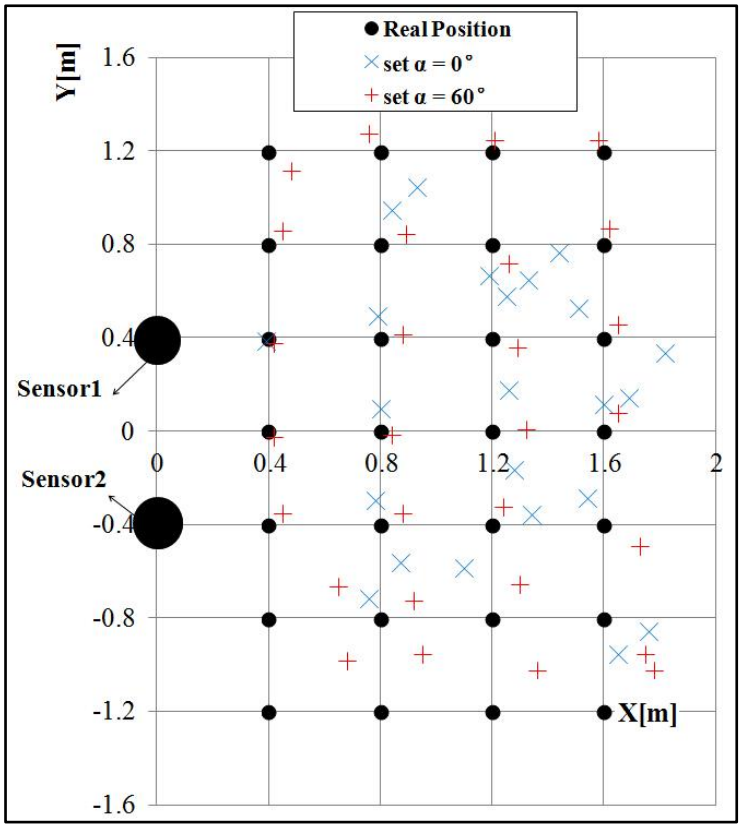
Real Position
set α = 0°
set α = 60°
Y[m]
1.6
1.2
0.8
0.4
0
-0.4
-0.8
-1.2
-1.6
Sensor1
Sensor2
0
0.4
0.8
1.2
1.6
2
X[m]

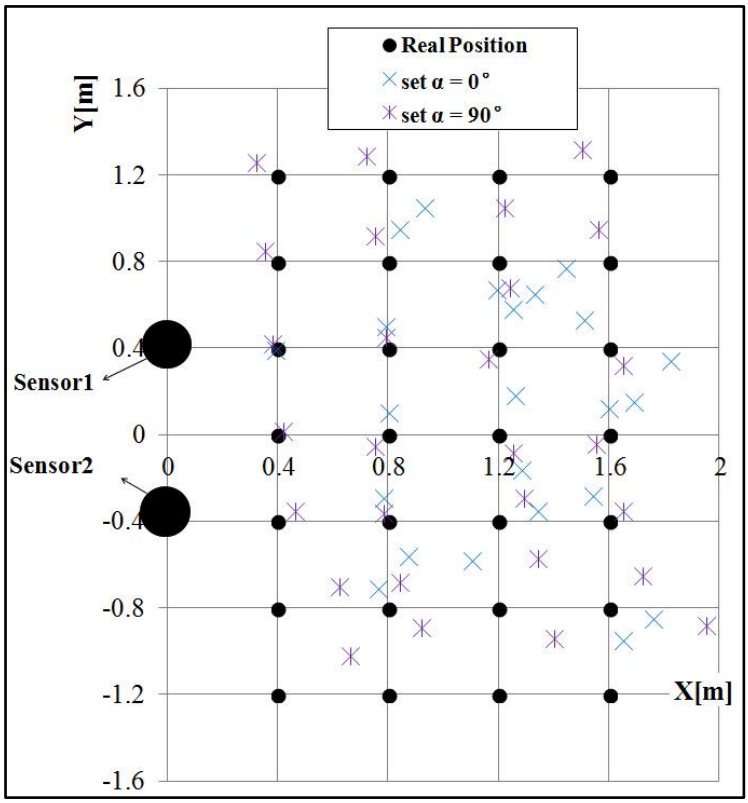


Fig. 5.33 Results for human position detection

5.7.2 Experimental Data to Detect Human motion

In order to test the sensor system can detect human position in real-time, we did an experiment for detecting human motion. That is, human walked at a speed of about 0.4m/s along a direction paralleling to the Y-axis, and always kept x = 1m. We separately did this experiment in two situations, situation1 shows that assuming body orientation angle is 0°, and situation2 shows that utilizing the estimated orientation angle to detect. **Fig. 5.34** shows the comparison result. We can obviously see that result got by situation2 is better than the result got by situation1.

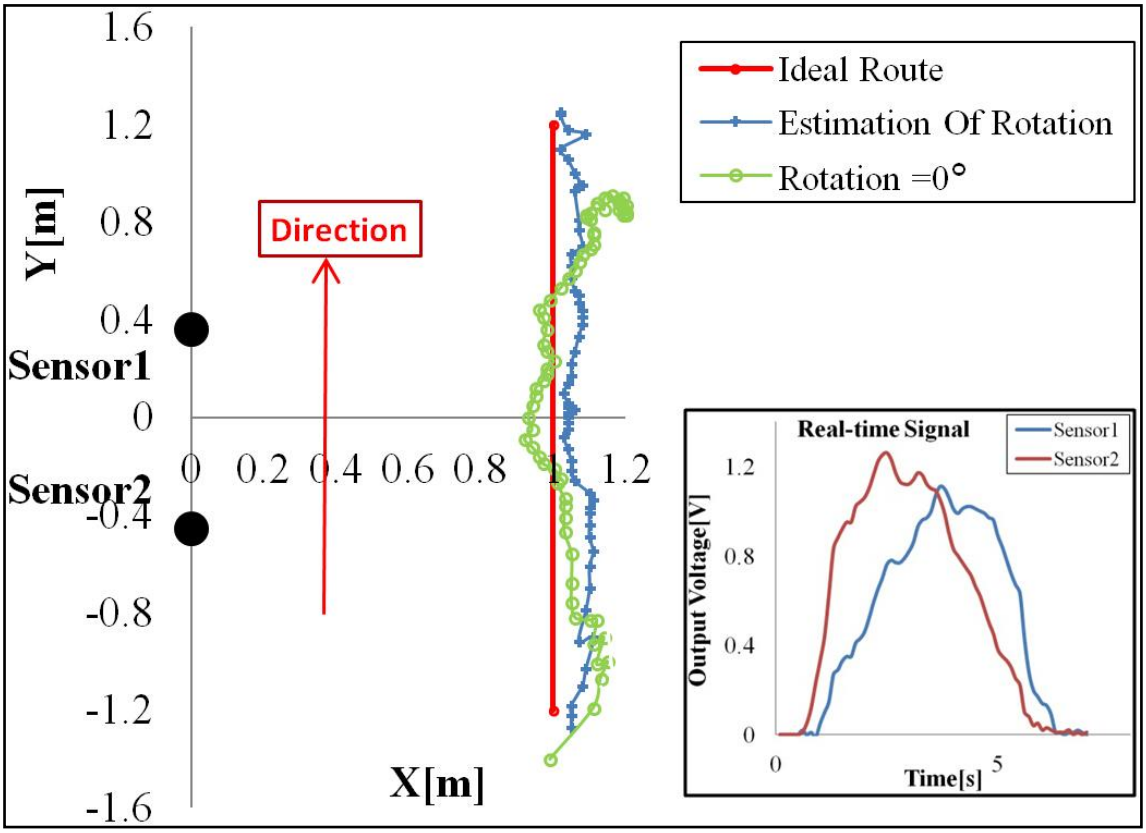


Fig. 5.34 Comparison result through using different body orientation

Meanwhile, we not only detected human walking just like simple mode to test the proposed systems, but also detected some complex routes such as circle, rectangle, zigzag and vertical direction, and results respectively show as **Fig. 5.35**, **Fig. 5.36, Fig. 5.37**, and **Fig. 5.38**. In all these figures, the red line means ideal route, and blue line means experimental route. [44]

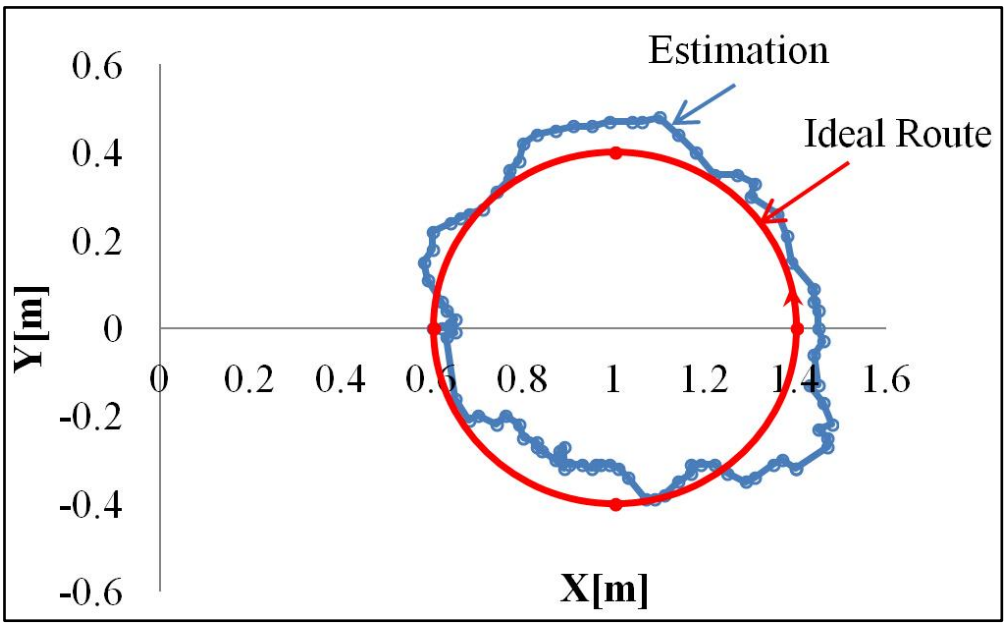


Fig. 5.35 Result when human move along a circle shape

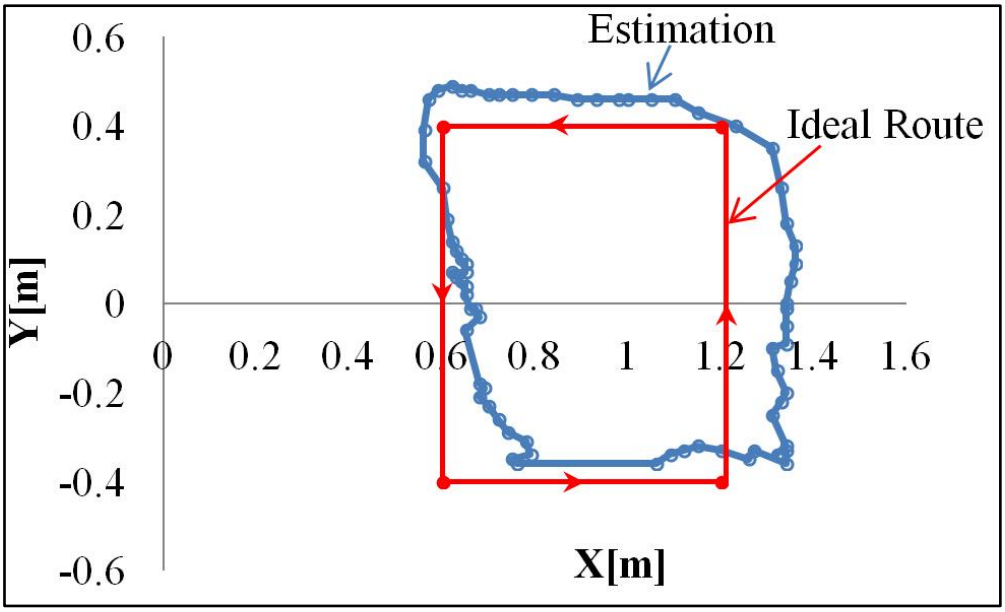


Fig. 5.36 Result when human move along a rectangle shape

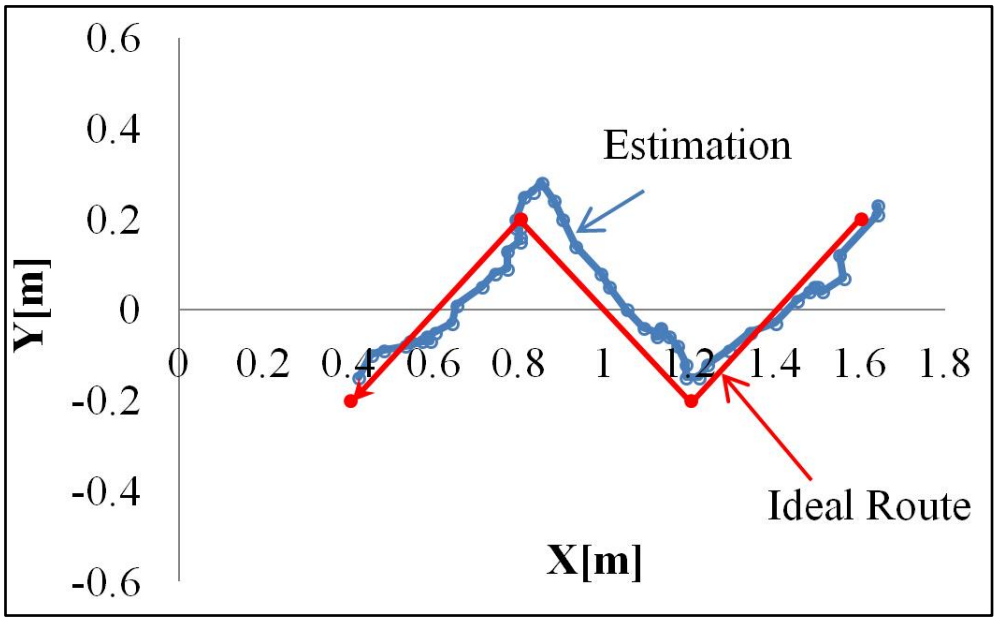


Fig. 5.37 Result when human move along a zigzag shape

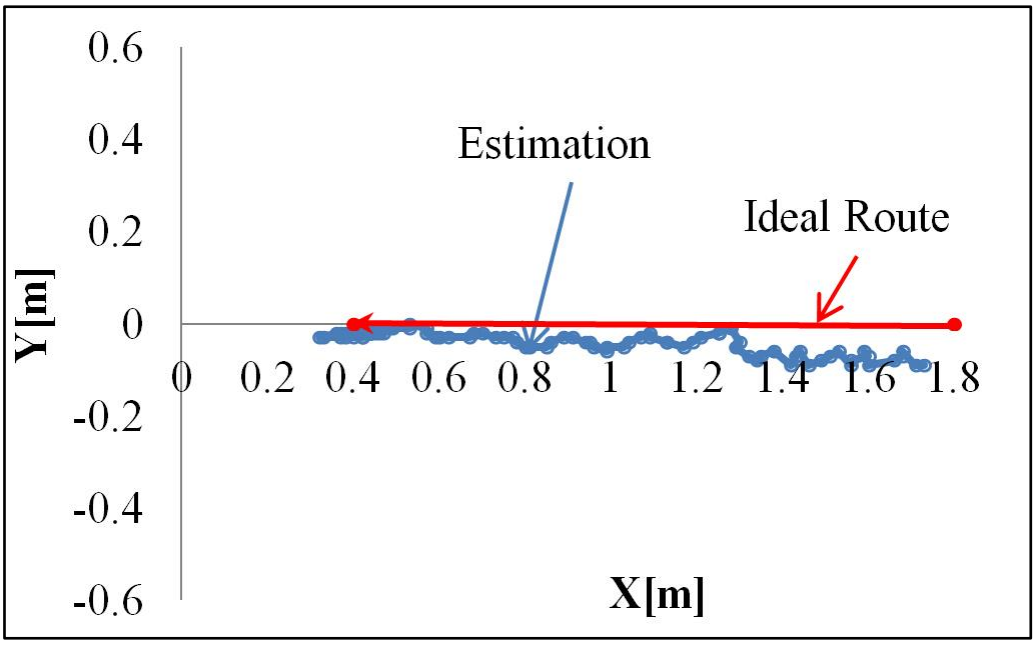


Fig. 5.38 Result when human move along a line shape

Moreover, we also have done some other experiments for testing the sensor system whether can run stable or not. For example, human turn around instantaneously, that is, body orientation from 0° to 90° , to see how it will be or some moving way just like people walking in the normal way of life. The entire measurement results show in **Fig. 5.39.**

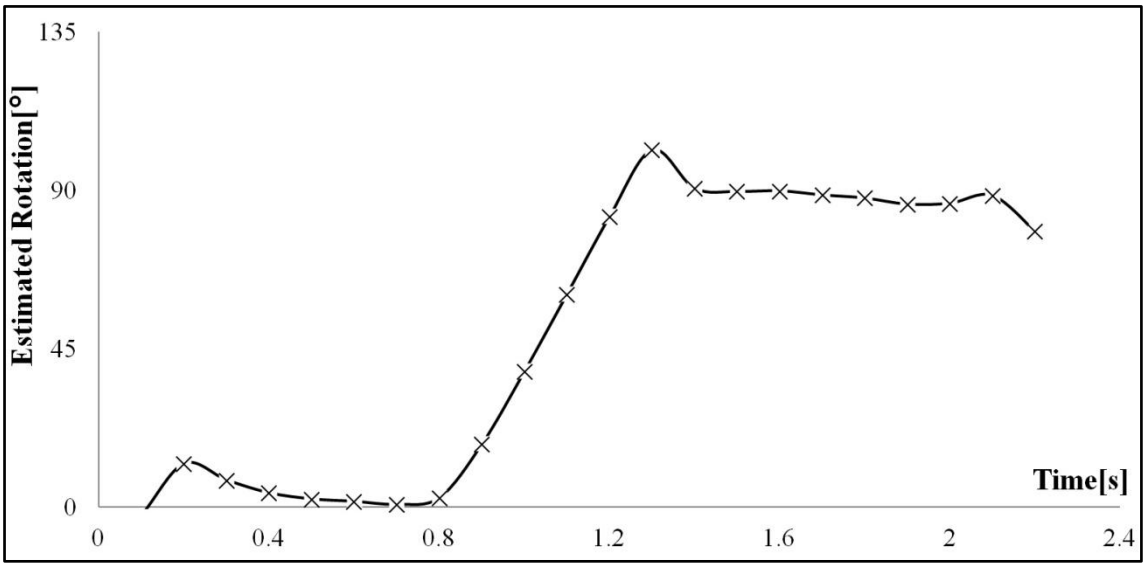


(a) human turn around suddenly

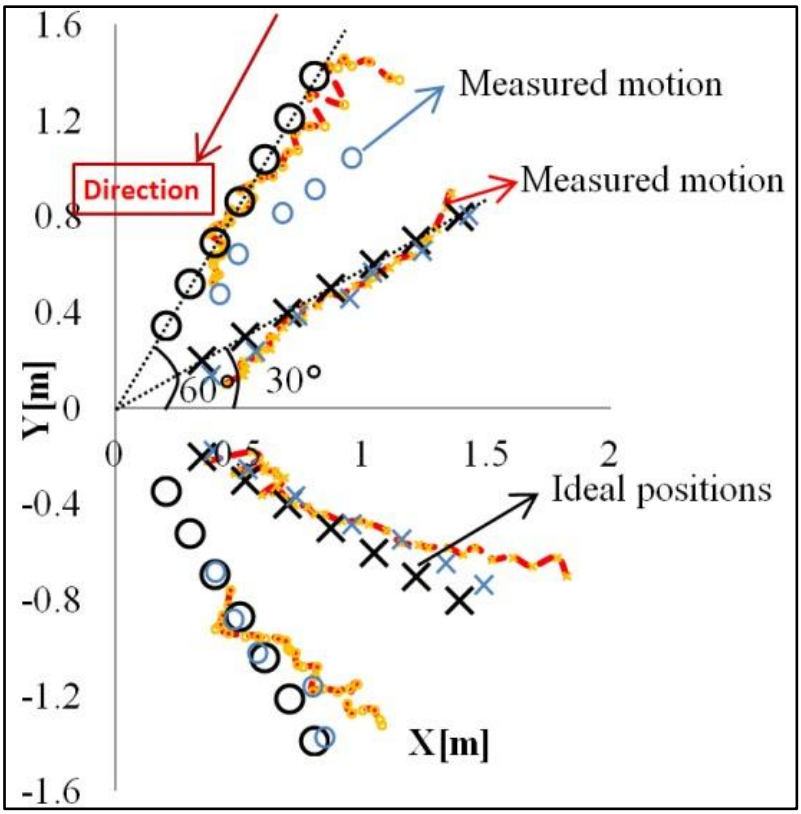


(b) human walk from far to near (diagonal)

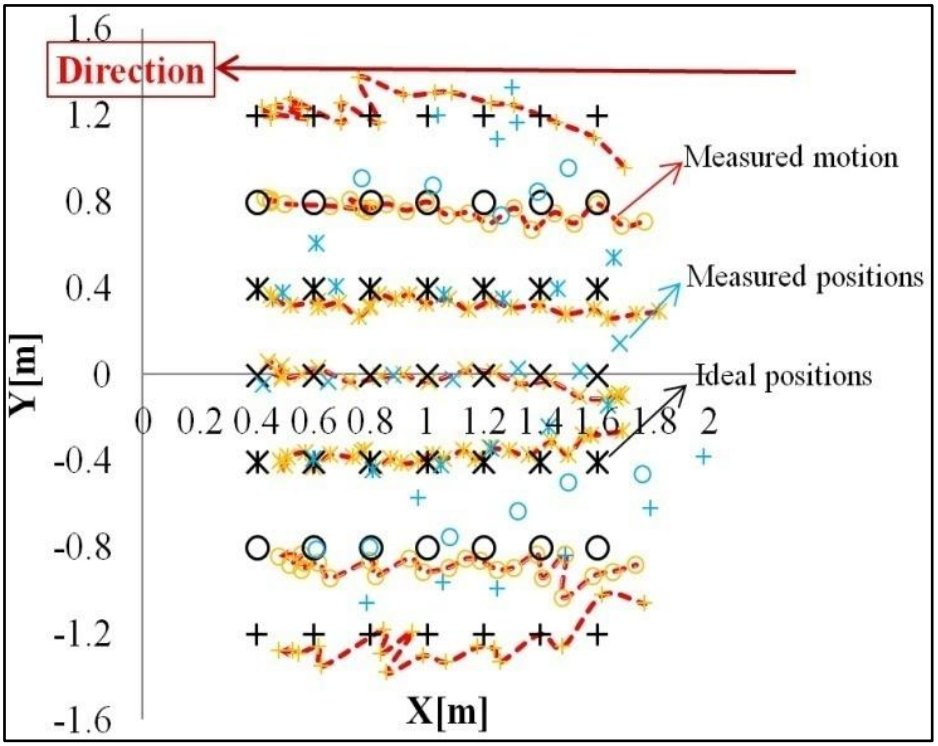


(c) human walk from far to near (straight)

Fig. 5.39 Some other measurements for testing sensor system

After various measurements, we realize that the system can detect any cases of human motion well from the comparison results.

## 5.8 Conclusion

Based on the previous chapter, which has been introduced the basic method for detecting human position by two thermopile sensors that put on the table. This chapter presented an approach for detecting human 2D position, motion and body orientation in real-time by using two thermopile infrared sensors mounted on the ceiling. Through measuring some basic characteristics of sensor itself, we built an approximate equation between sensor output voltage, height, distance and body orientation from each sensor to human, and then the entire unknown can be expressed by 2D position. Steepest descend method was briefly introduced to solve the human position and body orientation angle, which can be obtained through calculating the estimation orientation angle when human moving. Base on it, a method be introduced to detect human's situations, that is, when human appears, which direction human moves, motionless, when human disappears etc.

Through a mass of experiments, we could confirm the sensor system can work well.

However, this chapter described that detection of human by thermopile sensor amounted on the ceiling only in vertical direction, which will make the detected field restricted, in order to enlarge the detected field, we considered the case when detecting human position and motion by tilted sensor.

# CHAPTER. 6 HUMAN DETECTION BY TILTED SENSORS FROM CEILING

Based on previous studies, this paper presents an approach to detect human 2D position, body orientation and motion by using two thermopile infrared sensors which are mounted on the ceiling. Normally we want to attach sensors at corners or edges of a room, which make the detectable area narrow, hence, we attach sensors to the ceiling and detect human by making them vertically downward. In order to broaden the detectable area further, we considered to detect human by making them tilted on the ceiling.

Before starting to detect human position and motion by tilted sensors, according to previous measurement results, we have got sensor output V is expressed by following approximation equation:

$$V = V_T(T) \cdot V_h(h) \cdot V_r(r) \cdot V_\alpha(\alpha) \quad (6.1)$$

Based on it, we analyzed similarities and differences between vertical sensors and tilted sensors. That is:

Similarities:

No matter what kind of sensors be attached to the ceiling, they should have the same $V_T(T)$, $V_h(h)$ and $V_\alpha(\alpha)$.

Differences:

However, as we mentioned in the previous Chapter about characteristics of sensor, sensor has directivity itself. When sensor is vertical, that is, sensor angle is 0°, the $V_r(r)$ should consist of two parts, $V'_r(r)$ and $V_\theta(\theta)$. Here, $V'_r(r)$ denotes the real relationship between distance (r) and sensor output voltage (V). Thus,

$$V_r(r) = V'_r(r) \cdot V_\theta(\theta) \quad (6.2)$$

When sensor is tilted, the $V_\theta(\theta)$ is needed to be individually considered. Hence, we applied vector to represent θ. This Chapter will introduce how to get each approximation equation and detect human position and motion.

## 6.1 Measurement and approximation

By some measurements about height (h), ambient temperature (T) and body orientation (α), we have got their corresponding approximation equation in previous chapter 5, which separately expressed as follows:

$$V = V_T(T) \cdot V_h(h) = a_0/(h + a_1)^2 \quad (6.3)$$

$$a_0 = V_T(T) = a_8 T + a_9 \quad (6.4)$$

$$V_\alpha(\alpha) = 1 - a_{10}\alpha^2 \quad (6.5)$$

We have discussed in the introduction of this Chapter, so we will not introduce the detailed process and methods for obtaining them again here. We mainly want to introduce the measurement and approximation about the $V'_r(r)$ and $V_\theta(\theta)$. $V'_r(r)$ means the approximation equation to express the relationship between distance (r) and sensor output (V), and $V_\theta(\theta)$ means the approximation equation to express the relationship between directivity (θ) and sensor output (V). The relationships among them are shown as **Fig. 6.1**.

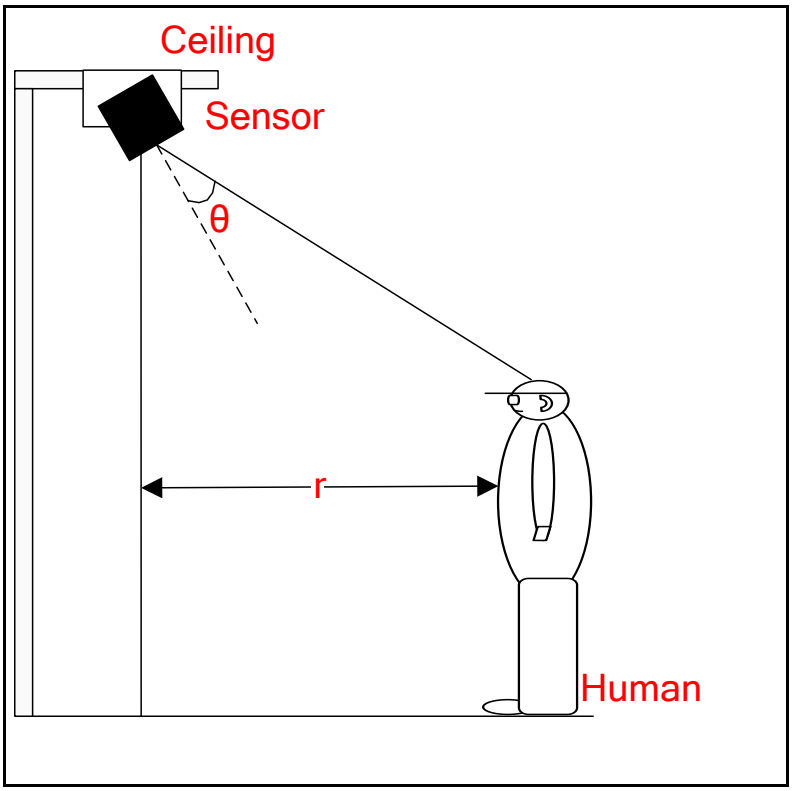


Fig. 6.1 Relationships about r, θ between human and sensor

As we thought, the total sensor output voltage should be approximately expressed like:

$$V = V_T(T) \cdot V_h(h) \cdot V'_r(r) \cdot V_\theta(\theta) \cdot V_\alpha(\alpha) \quad (6.6)$$

In this approximation equation, $V_T(T)$, $V_h(h)$, $V_\alpha(\alpha)$ are constant, but sensor directivity is depended on heat radiation, when the sensor is applied to horizontal direction, theoretically the incident radiations are always same at equidistant positions, that is to say, the center of the sensor is always corresponding to the fixed part of the body, and the case is also appropriate for detecting human on the ceiling when sensor is vertical, but which cannot applied to tilted sensor attached to the ceiling. That is because even in a situation where equidistant, the center of the sensor to the part of body is different. That will lead that we cannot directly apply $V_\theta(\theta)$. Hence, we need to capture the total sensitivity of the whole body. Hence, we considered algorithm called Rodrigues' rotation formula to calculate.

### 6.1.1 Method to calculate for total directivity

Generally, solid angle should be considered to solve the problem about calculation of total directivity, which can get a accurate result. However, to a person, there are some uncertainty factors, for example, different parts of body will produce different radiations, especially when human wear different clothes at different seasons. That will lead a large errors if we use the method of solid angle. Therefore, we discussed about other simple method-- the rodrigues formula.

The Rodrigues formula [45] is used to perform angle-axis rotation, or simply said it rotates a point in the space around a given axis by given angle. Diagonal axis of rotation is a common one might think. For example everything on Earth is rotating around the Earth's axis which is not the same as the solar system or our galaxy axis. Another example is a car. Wheel rotation around their axes from the steering wheel or the engine crankshaft axis is different.

In the theory of three-dimensional rotation, Rodrigues' rotation formula [46], named after Olinde Rodrigues, is an efficient algorithm for rotating a vector in space, given an axis and angle of rotation. By extension, this can be used to transform all three base vector calculation in a rotation matrix SO(3), all of the rotation matrix of the group, from an axis angle. In other words, the Rodrigues' formula provides an algorithm to calculate the index map from the SO(3), the Lie algebra SO(3), to SO(3) without having actually calculate the full matrix index.

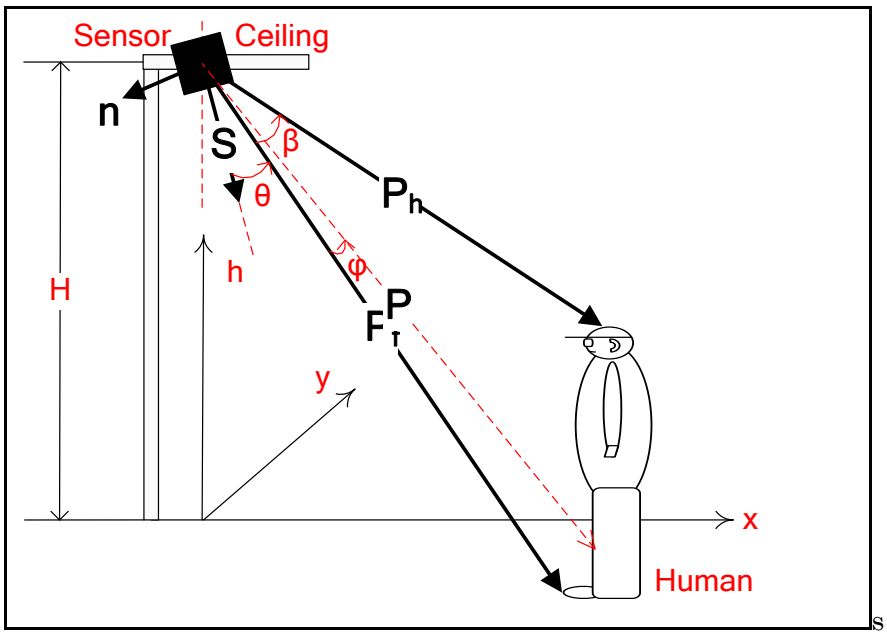


Fig. 6.2 Relationships among vectors by Rodrigues' rotation

In **Fig. 6.2**, we want to rotate the plane that is composed of vector $\mathbf{P_h}$ and vector $\mathbf{P_f}$, where $\mathbf{P_h}$ denotes the direction from sensor to human head, and $\mathbf{P_f}$ denotes the direction from sensor to human foot. β denotes the angle between two vectors, then we created a normal vector **n** perpendicular to the plane, in other words, the plane rotates around axis n. Vector **S** denotes sensor direction, and vector **P** denotes either vector in the plane which is composed of vector $\mathbf{P_h}$ and vector $\mathbf{P_f}$. Φ denotes angle between vector $\mathbf{P_f}$ and vector **P** (Φ = 0~β). θ denotes the angle between vector **S** and vector **P**.

According to the Rodrigues' rotation formula, we can write as follows:

$$\mathbf{P} = \mathbf{P_f}\cos\emptyset + \mathbf{n} \cdot (\mathbf{n} \cdot \mathbf{P_f})(1 - \cos\emptyset) - (\mathbf{P_f} \times \sin\emptyset) \tag{6.7}$$

where $\mathbf{P_f}$ = (x,y,-H), $\mathbf{P_h}$ = (x,y,-h) are known.

Then according to the relationships in **Fig. 7.2**, β can be expressed by:

$$\beta = \cos^{-1}\frac{(\mathbf{P_h} \cdot \mathbf{P_f})}{(|\mathbf{P_h}| \cdot |\mathbf{P_f}|)} \tag{6.8}$$

$$\mathbf{n} = \frac{(\mathbf{P_f} \times \mathbf{P_h})}{(|\mathbf{P_h} \times \mathbf{P_f}|)} \tag{6.9}$$

So far, we can calculate for vector **P**, and then θ can be calculated like:

$$\theta = \cos^{-1}\frac{(\mathbf{S} \cdot \mathbf{P})}{(|\mathbf{S}| \cdot |\mathbf{P}|)} \tag{6.10}$$

Hence, the total sensitivity, here we call it Vs, will be expressed as follows:

$$V_s = \int_0^{\beta} V_\theta(\theta)\, d\emptyset \qquad (6.11)$$

In the process of calculating Vs, we need to pay attention to one point, that is, the range of the angle Φ has limit. Because the FOV of sensor has limit, we have known the effective measured range (-55°~ +55°) from the basic measurement result about sensor directivity introduced in Chapter3. Hence, we did some restrictions that making Vs = 0 when Φ exceed the effective range. This can limit the opportunities to get negative Vs. Next, we made a simulation for calculating the total sensitivity of sensor by foregoing method. We separately calculated positions in equidistant but different directions shown as fig., the distance is from 0.5m to 2.5m by every 0.5m, and angle is from -90°to +90° by every 30°, which show as **Fig. 6.3**. Meanwhile, we calculated when sensor angle is different. The angle is [0°, 15°, 30°, 45°, 60°]. The calculating results for Vs at each angle are respectively shown as **Fig. 6.4**, **Fig. 6.5**, **Fig. 6.6**, **Fig. 6.7**, and **Fig. 6.8**, which show results about one sensor, because results for the other sensor are entirely same, here only one result is listed.

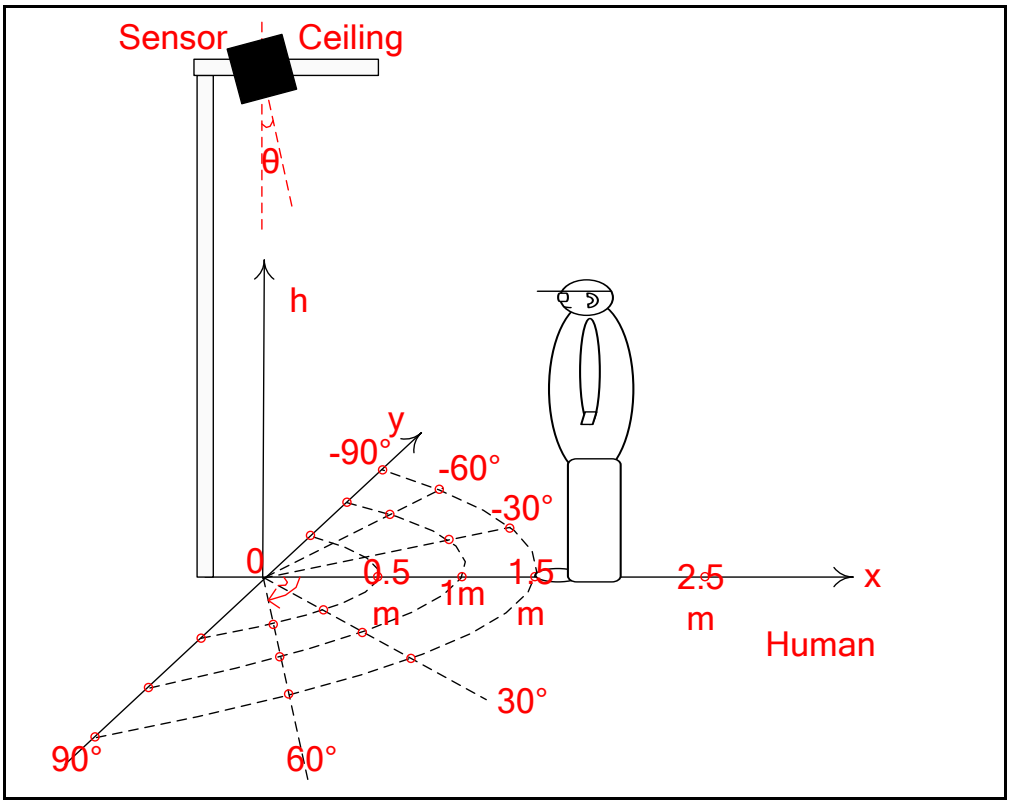


Fig. 6.3 Measurement for sensitivity of the entire body

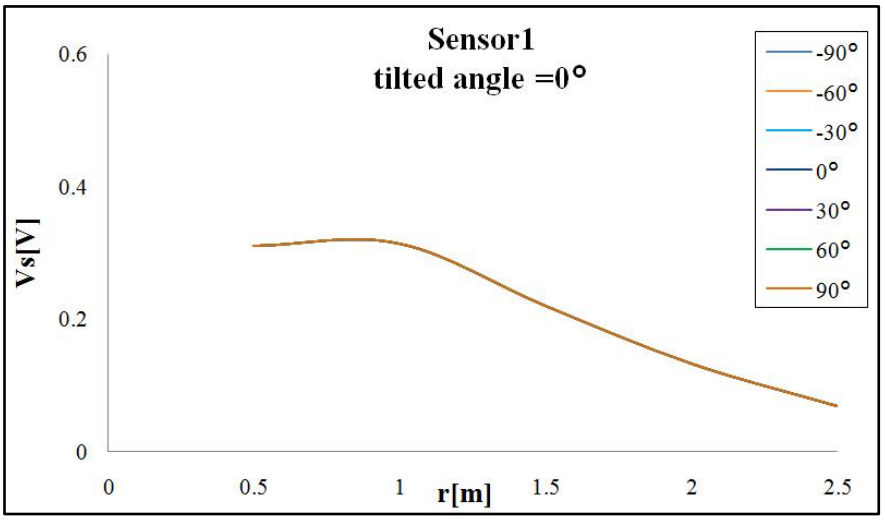


Fig. 6.4 Result for Vs calculated when titled angle is 0°

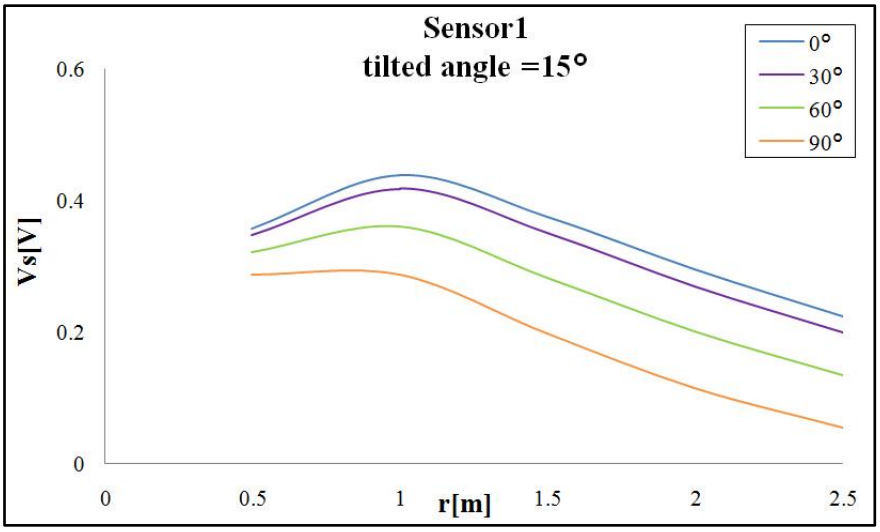


Fig. 6.5 Result for Vs calculated when titled angle is 15°

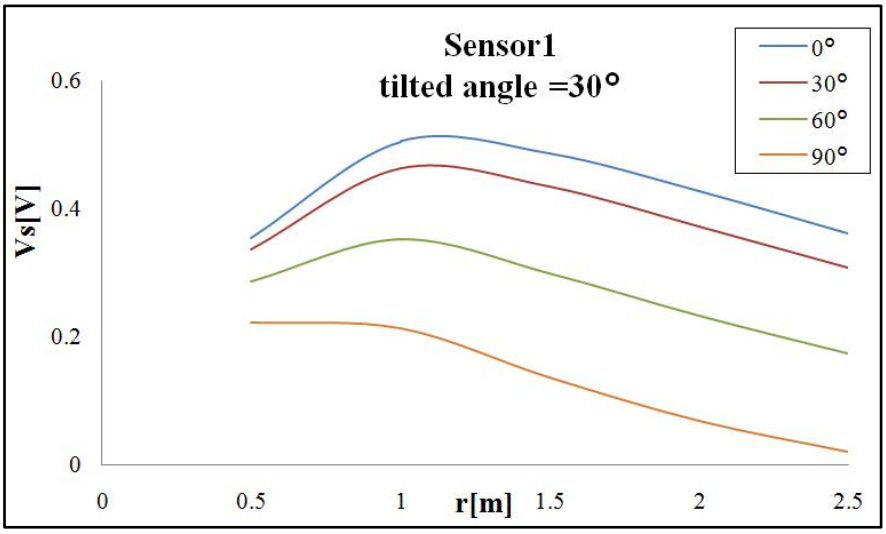


Fig. 6.6 Result for Vs calculated when titled angle is 30°

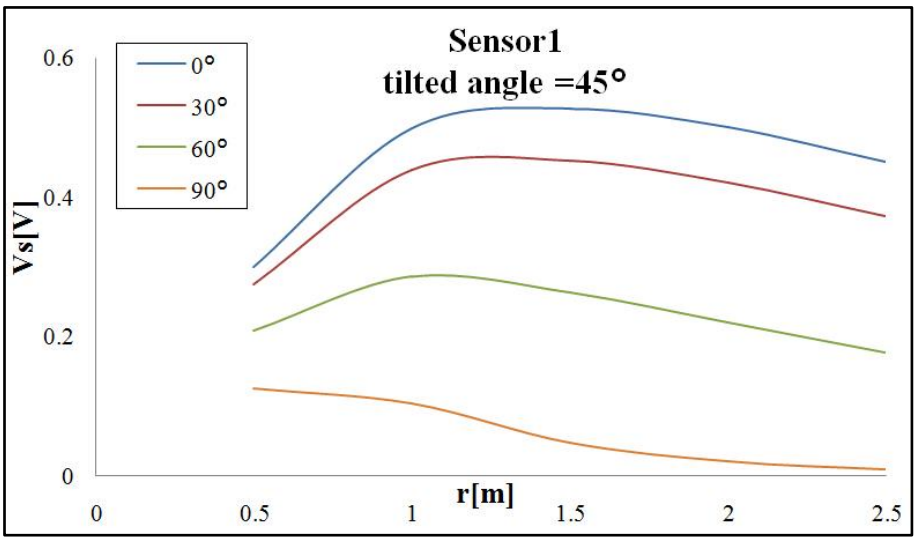


Fig. 6.7 Result for Vs calculated when titled angle is 45°

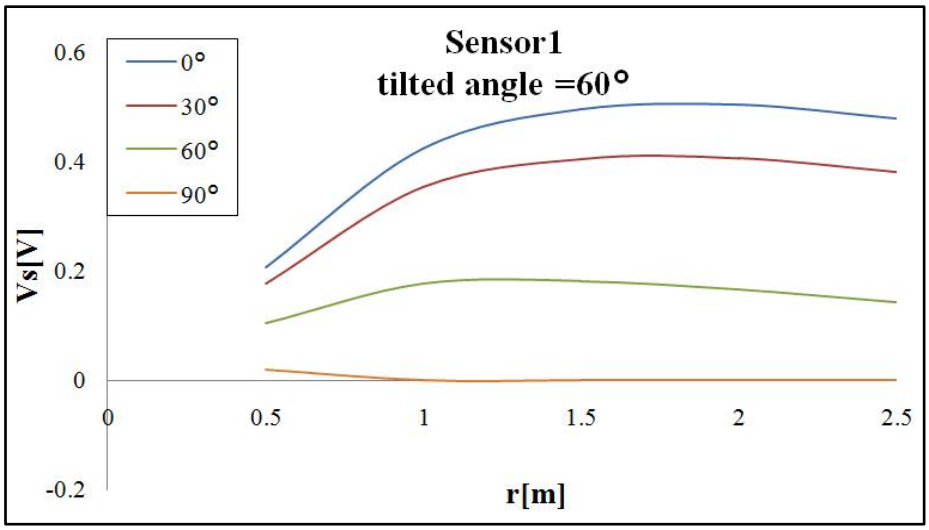


Fig. 6.8 Result for Vs calculated when titled angle is 60°

### 6.1.2 Calculation and approximation for Distance

After we got the total sensitivity of the sensor, we can further calculate for $V'_r(r)$. According to **Eq. 6.2**, the $V_\theta(\theta)$ part should be substituted by Vs, that is,

$$V_r(r) = V'_r(r) \cdot V_s \tag{6.12}$$

Moreover, by **Eq. 6.6**, we can get $V'_r(r)$ expressed as:

$$V'_r(r) = V/V_T(T) \cdot V_h(h) \cdot V_s \cdot V_\alpha(\alpha) \tag{6.13}$$

In this formula, because $\alpha = 0°$, by **Eq. 6.5**, we can know $V_\alpha(\alpha) = 1$, therefore, here we

did not need to consider it.

That is to say, **Eq. 6.13** could be written as:

$$V'_r(r) = V/V_T(T) \cdot V_h(h) \cdot V_s \quad (6.14)$$

Where the value of V is come from experiment, and all of $V_T(T)$, $V_h(h)$, Vs can be calculated by their approximation equations. Through calculating at each sensor angle, we got the results for $V'_r(r)$ separately shown as **Fig. 6.9**, **Fig. 6.10**, **Fig. 6.11**, **Fig. 6.12**, and **Fig. 6.13**.

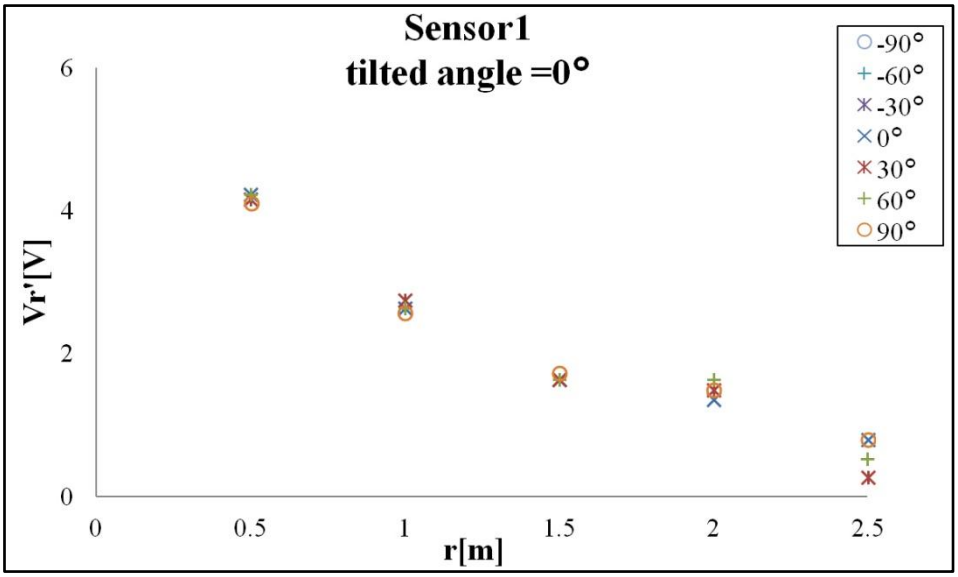


Fig. 6.9 Result for V'$_r$ when titled angle is 0°

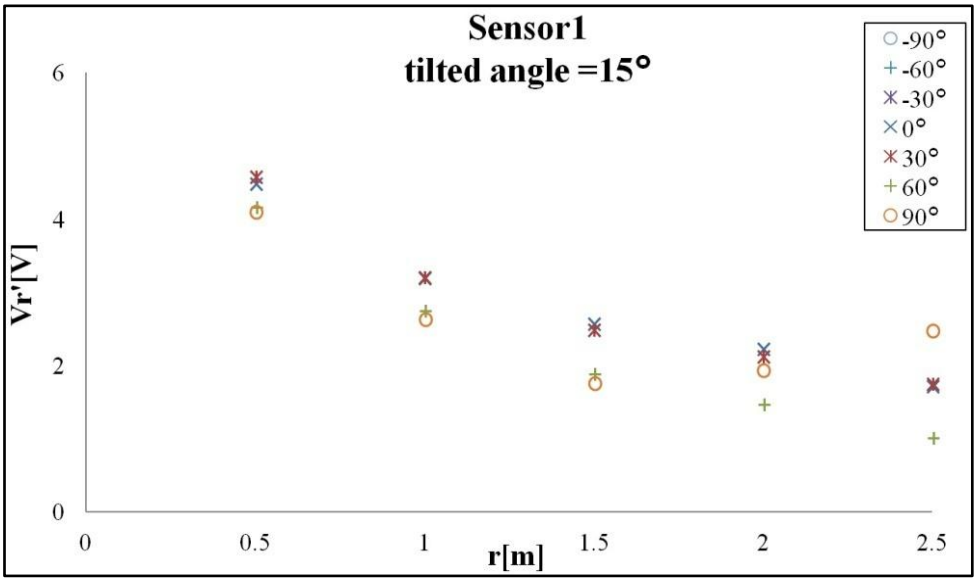


Fig. 6.10 Result for V'$_r$ when titled angle is 15°

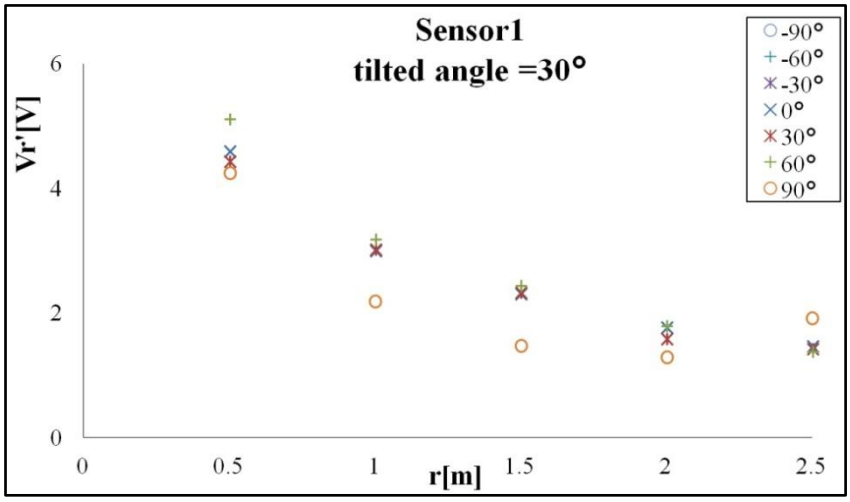


Fig. 6.11 Result for V'$_r$ when titled angle is 30°

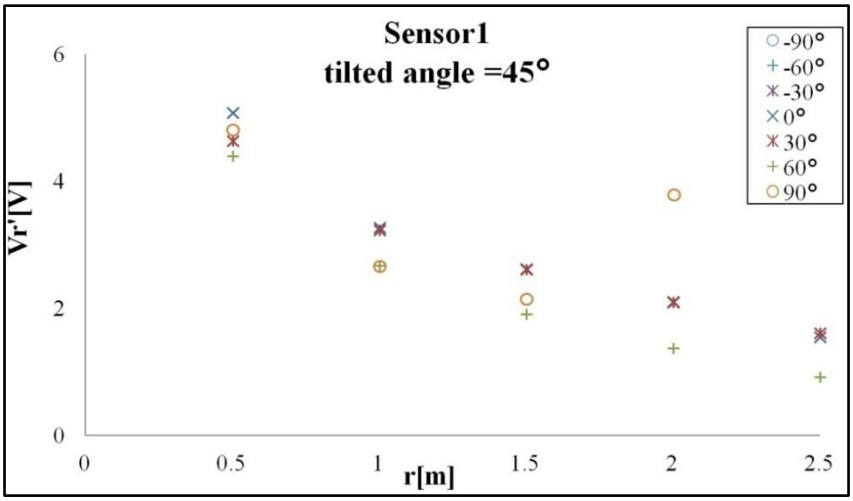


Fig. 6.12 Result for V'$_r$ when titled angle is 45°

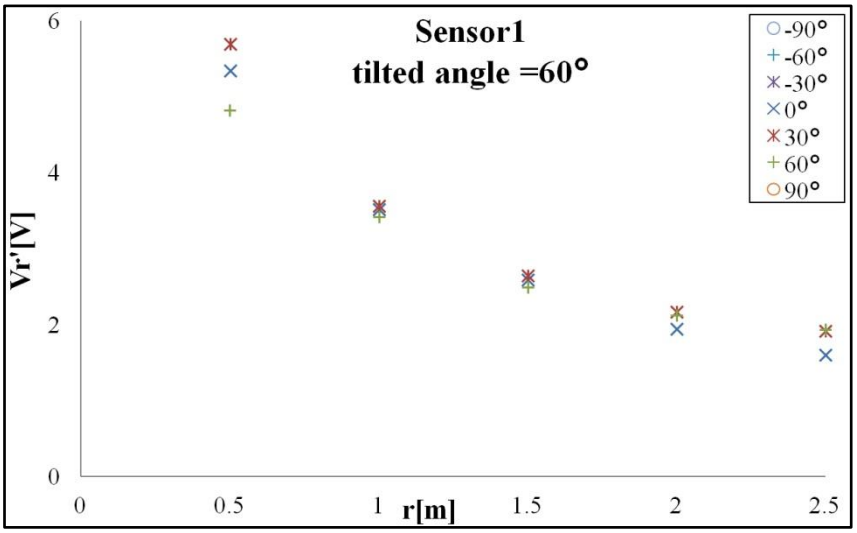


Fig. 6.13 Result for V'$_r$ when titled angle is 60°

From the results, we can see that there are almost similar output values not only at each direction angle but also at each sensor angle. Hence, we collected the entire data in **Fig. 6.14**.

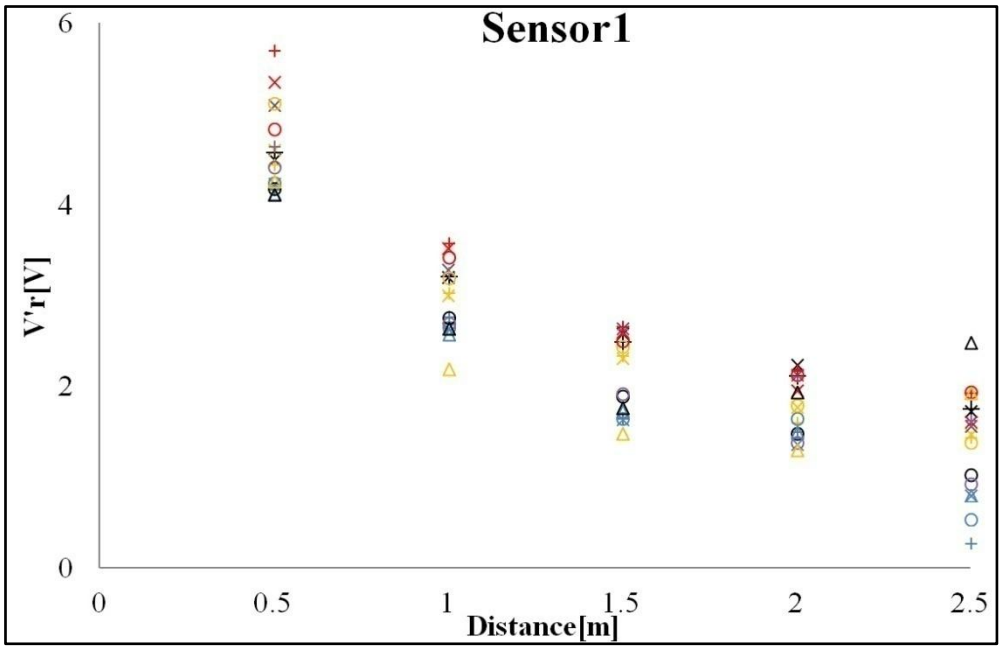


Fig. 6.14 Result for collecting all data at all angles

Then we got their average values at each positions, thus got an approximation equation by polynomial form to express V'r, and result shows in **Fig. 6.15**. Finally V'r can be expressed like **Eq. 6.15**.

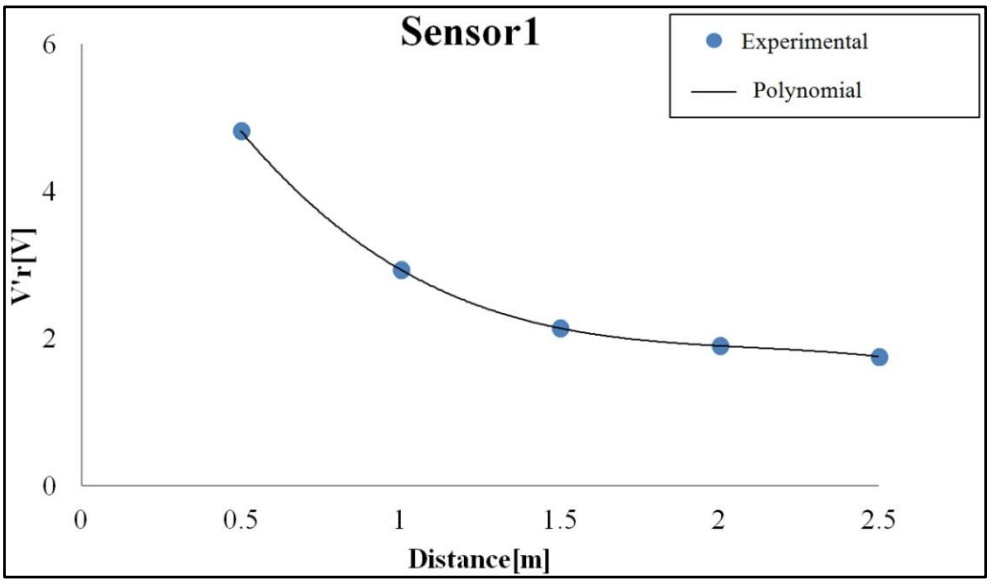


Fig. 6.15 Result about approximation for V'r

$$V'_r(r) = a_1 r^4 + a_2 r^3 + a_3 r^2 + a_4 r + a_5 \quad (6.15)$$

Where $a_1$, $a_2$, $a_3$, $a_4$, $a_5$ are constant, the values of all parameters about each sensor are shown in **Table 6.1**.

TABLE 6.1 APPROXIMATED PARAMETER VALUES OF TWO SENSORS

| Parameter Sensor | $a_1$ | $a_2$ | $a_3$ | $a_4$ | $a_5$ |
|---|---|---|---|---|---|
| Sensor1 | 0.043 | -0.917 | 4.652 | -9.218 | 8.376 |
| Sensor2 | 0.377 | -2.812 | 8.110 | -11.010 | 7.930 |

## 6.2 Basic method

From **Eq. 6.3**, **Eq. 6.4**, **Eq. 6.5**, **Eq. 6.11**, **Eq. 6.15** we got in last Chapter, we can see that only distance r and orientation angle α are unknown. Therefore, if the body orientation α is given, at least two sensors are required to detect human position. Keep two sensors a certain distance at one height, the space layout is shown in **Fig. 6.16**.

.

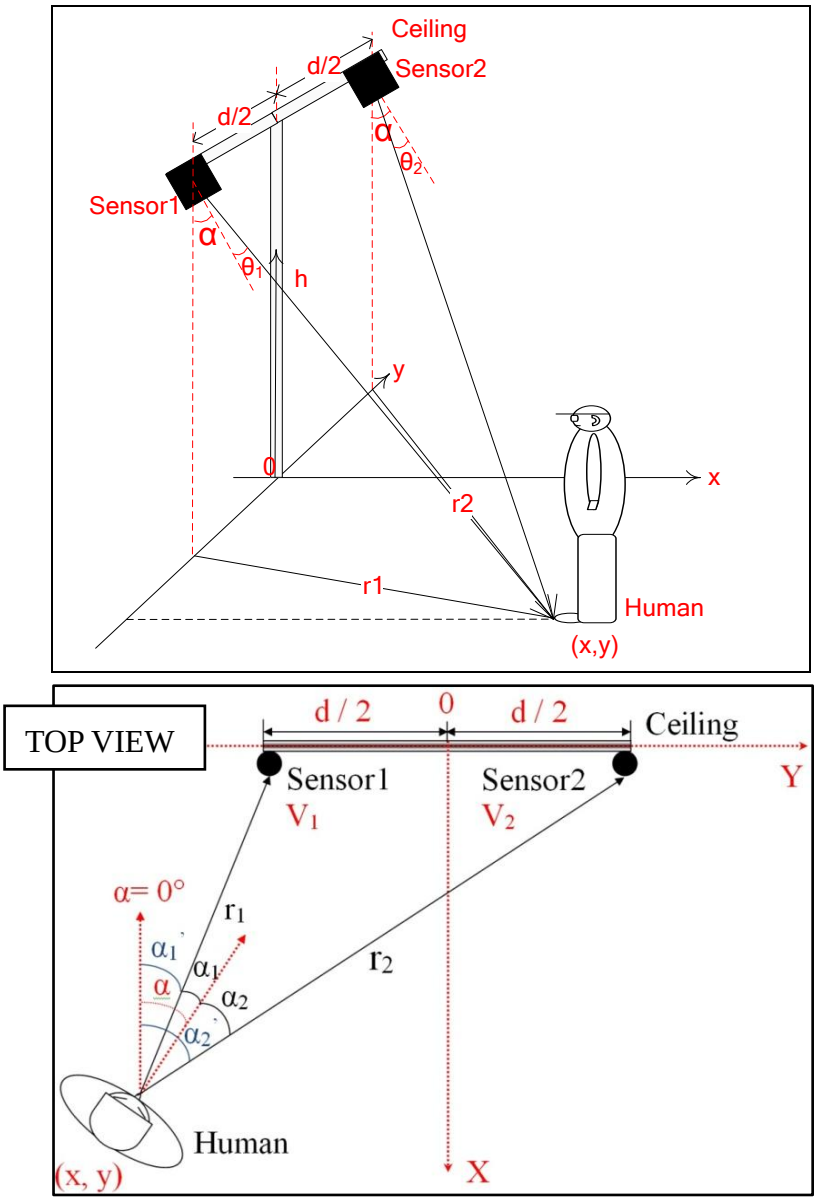


Fig. 6.16 Layout for detecting human by two thermopile sensors amounted on the ceiling

First we can clearly express the unknown r and α by 2D position (x,y) from the relationships in **Fig. 6.16**. That is,

$$r_1 = \sqrt{x^2 + (y - d/2)^2}, r_2 = \sqrt{x^2 + (y + d/2)^2} \tag{6.16}$$

$$\alpha_1 = \alpha - \alpha_1' = \alpha - \tan^{-1}((y - d/2)/2) \tag{6.17}$$

$$\alpha_2 = \alpha_2' - \alpha = \tan^{-1}((y + d/2)/2) - \alpha \tag{6.18}$$

then substituted them into the equation , and an equation set can be built by **Eq. 6.19** and **Eq. 6.20**, which is given as followings:

$$V_1 = V_T(T) \cdot V_h(h) \cdot V_{s1} \cdot V'_r(r_1) \cdot V_\alpha(\alpha_1) \tag{6.19}$$

$$V_2 = V_T(T) \cdot V_h(h) \cdot V_{s2} \cdot V'_r(r_2) \cdot V_\alpha(\alpha_2) \tag{6.20}$$

In other words, detecting a human-being's position becomes a problem of how to solve for *x* and *y* in the equation set formed by **Eq. 6.19** and **Eq. 6.20**.

So far, we could aware that it is still the question about how to solve a binary equation. Two proposed methods have been introduced in the Chapter 4. Because it will be produce a relatively large error by using analytical method, we will not discuss about it in this Chapter. Meanwhile, steepest decent method has been introduced in detail, a brief description will be introduce in the following.

## 6.3 Steepest Descent Method

The steepest descend method is known as an optimization algorithm to find the nearest local minimum of a function. We apply this method for detecting human position stated as follows. First, we built the evaluation function like this:

$$E(x,y) = \Delta V_1^2 + \Delta V_2^2 \tag{6.21}$$

the $\Delta V_1$ and $\Delta V_2$ were respectively defined as the following form:

$$\Delta V_1 = V_1 - V_T(T) \cdot V_h(h) \cdot V_{s1} \cdot V'_r(r_1) \cdot V_\alpha(\alpha_1) \tag{6.22}$$

$$\Delta V_2 = V_2 - V_T(T) \cdot V_h(h) \cdot V_{s2} \cdot V'_r(r_2) \cdot V_\alpha(\alpha_2) \tag{6.23}$$

where $V_1$ and $V_2$ denote measured voltages.

We also defined that the search starts at the initial point ($x_0$, $y_0$) (e.g. $x_0$=1.0[m], $y_0$=0.0[m]), we therefore set the iterative form below:

$$x_{k+1} = x_k - C\left(\frac{\partial E}{\partial x}\right)_{\substack{x=x_k \\ y=y_k}} \tag{6.24}$$

$$y_{k+1} = y_k - C\left(\frac{\partial E}{\partial y}\right)_{\substack{x=x_k \\ y=y_k}} \tag{6.25}$$

and continue the process, by searching from ($x_k$, $y_k$) to ($x_{k+1}$, $y_{k+1}$). The most suitable point was found when function E(x,y) reaches certain accuracy (i.e., E(x,y) < 1e-5) through adjusting the value of step size C, and finally from simulation by try and error, we sought out the optimal solution C, while C =0.1, $\Delta x = 0.0001$, $\Delta y = 0.0001$.

We discussed the detectable area separately at different tilted angles, after calculating, we draw some image graphs, which separately represent when tilted angle is

15° ,30° ,45° ,60° shown as **Fig. 6.17**, **Fig. 6.18**, **Fig. 6.19**, **Fig. 6.20** below, each curve represents the same output voltage curve. Normally there should be numerous curves in some effective range, but just few curves be drawn in these figures. Because many intersections are formed by many different curves, and each intersection consists of a pair of output voltage values [$V_1$, $V_2$], meanwhile it was also considered as human position. We also can see that the effective detection area is changed with tilted angle. The larger the tilted angle, the widen the detectable angle, but the problem is that as the tilted angle becomes larger, the area near to the sensor becomes very difficult to measure.

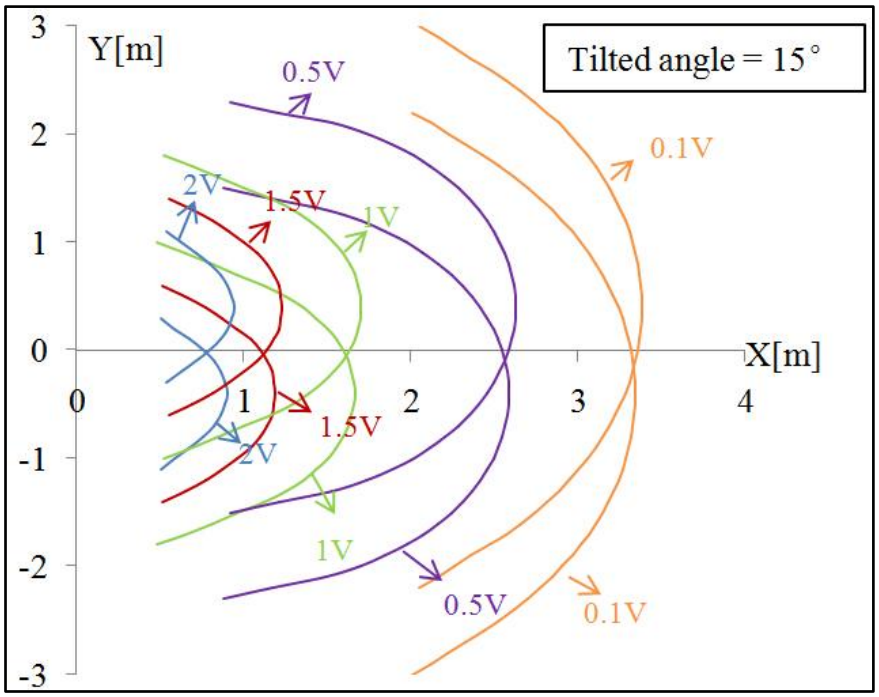


Fig. 6.17 Outline of detection by two tilted sensors from the ceiling (titled angle = 15° )

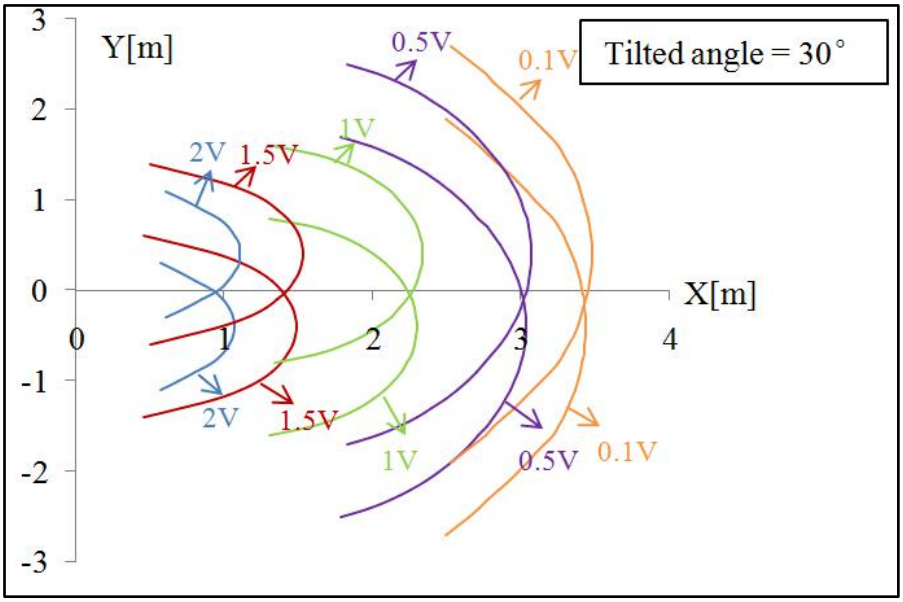


Fig. 6.18 Outline of detection by two tilted sensors from the ceiling (titled angle = 30° )

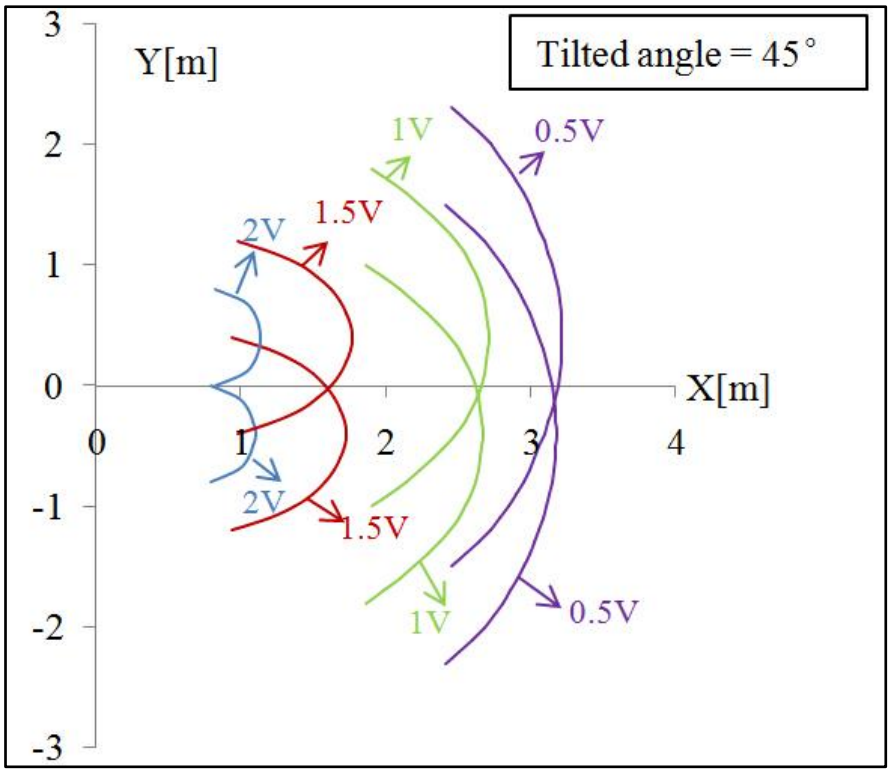


Fig. 6.19 Outline of detection by two tilted sensors from the ceiling (titled angle = 45° )

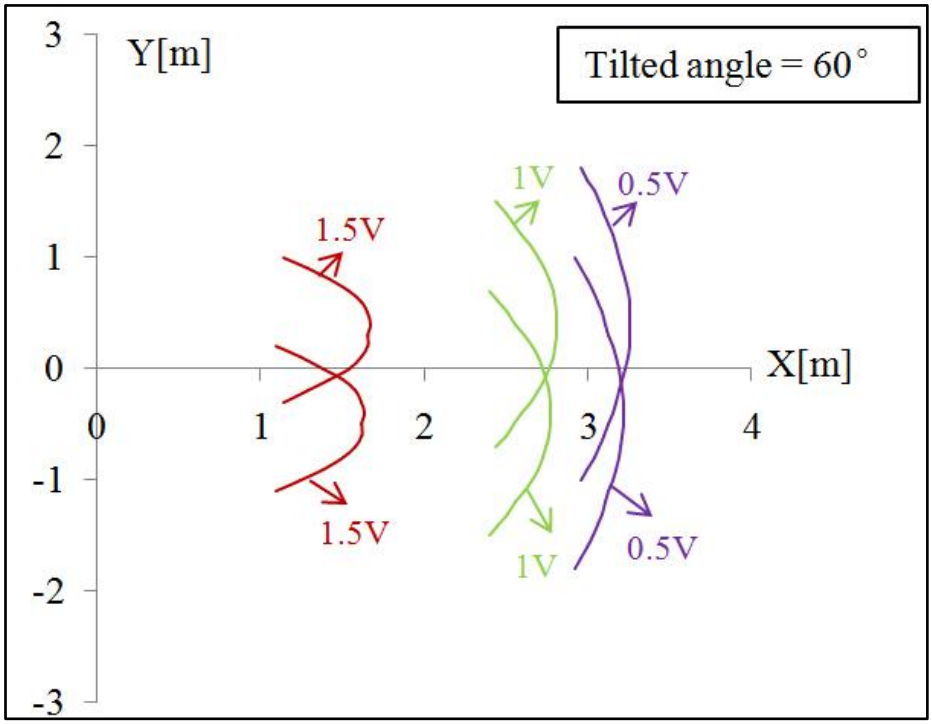


Fig. 6.20 Outline of detection by two tilted sensors from the ceiling (titled angle = 60° )

## 6.4 Accuracy

If we don't consider the factor of body orientation, that is, always kept the orientation angle(α) is 0°, there will produce some errors at any detected positions. We separately analyzed and discussed the distribution of error about detected positions at different angles in [-90°,90°] in theory, and specific approach is two steps.

Step 1: Solving position (x,y) by sensor outputs ($V_1$,$V_2$) when body orientation angle α = 0 °through simulation.

Step 2: Fixing sensor outputs ($V_1$, $V_2$) when α = 0 °, then changing the body angle by slight angle (e.g. 5°) in [-90°,90°], some new sensor outputs ($V_1$, $V_2$) corresponding to each angle will be obtained, then simulating it again, corresponding new positions (x,y) can be calculated and obtained, finally we got theoretical error results at each position shown as **Fig. 6.21**.

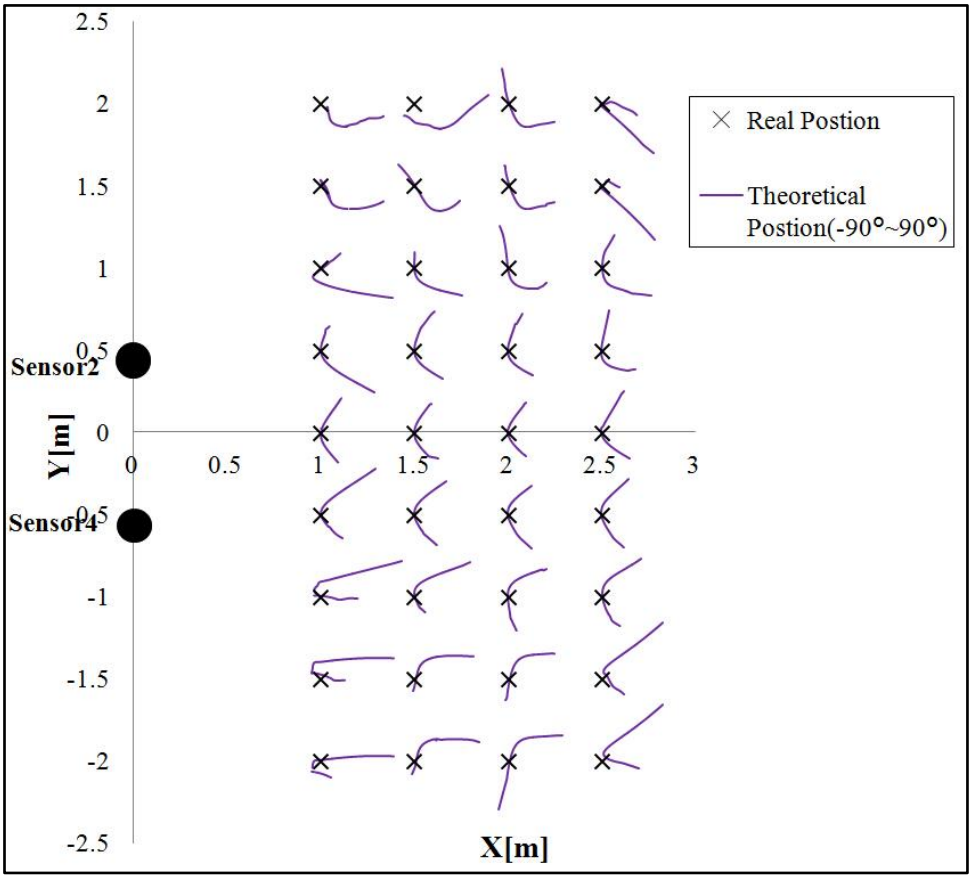


Fig. 6.21 Distribution of error and comparison result

## 6.5 Experiments

### 6.5.1 Experimental Data to Detect Human Position

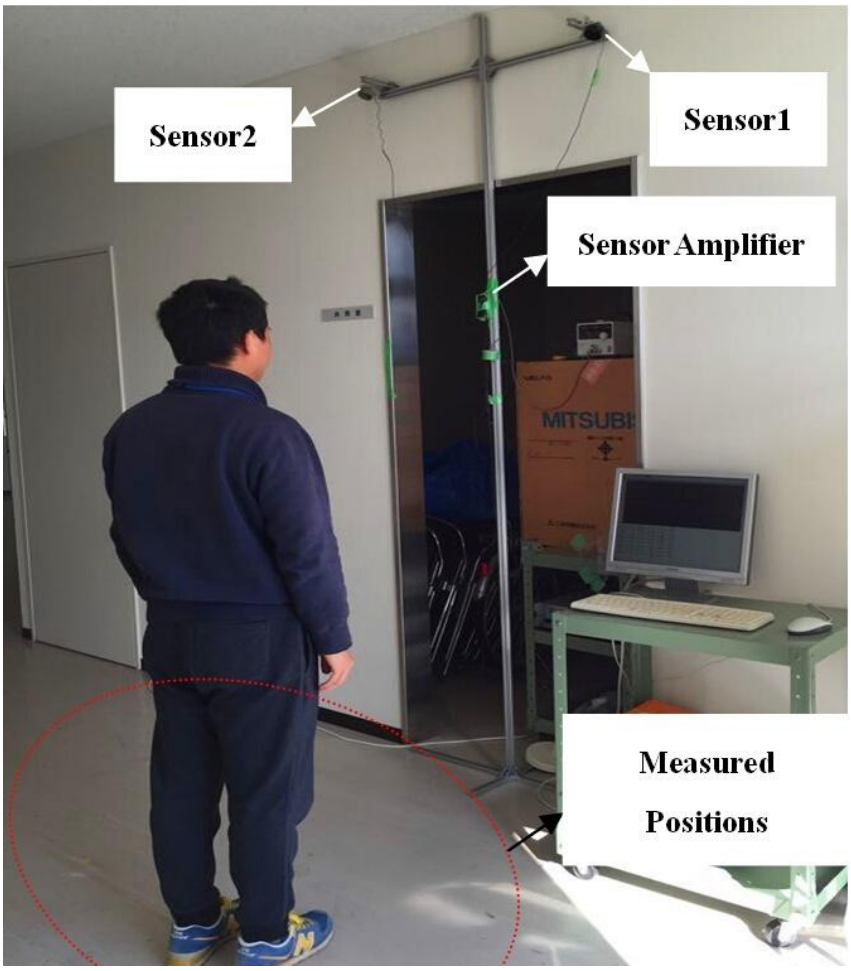


Fig. 6.22 Experimental scene by tilted sensors

**Fig. 6.22** shows the experimental scene. All the experiments were done in this scene. Two sensors were fixed on the pole at a height of 2.5m above the ground, and the distance d between them is 0.8m, the origin position, X-axis and Y-axis are defined as shown in Fig. 8.1, and the measured positions on the ground were marked, we designated the increment along the X-axis is 0.5m in [1m, 2.5m], and the increment along the Y-axis is also 0.5m in [-2m, 2m]. We separately did some experiments under the premise which sensor angle is 15°,30° or 45°.

First, we assume body orientation $\alpha = 0°$ in the position calculation, then respectively did some experiments when true body orientation angle separately is [0°, 30°, 60°, 90°]. Next, we respectively set body orientation $\alpha$ = [30°, 60°, 90°], then did the experiments

when body orientation angle is under the corresponding angle. The results show in **Fig. 6.23**, that is, if we ignore the $V_{\alpha}(\alpha)$ in **Eq. 6.19**, the results would be similar to those in **Fig. 6.21**. On the contrary, we can get a better result.

We did this measurement not only in the environment shown as **Fig. 6.22** but also in the environment shown as **Fig. 5.32**. Results separately show in upper left and upper right of **Fig. 6.23**.

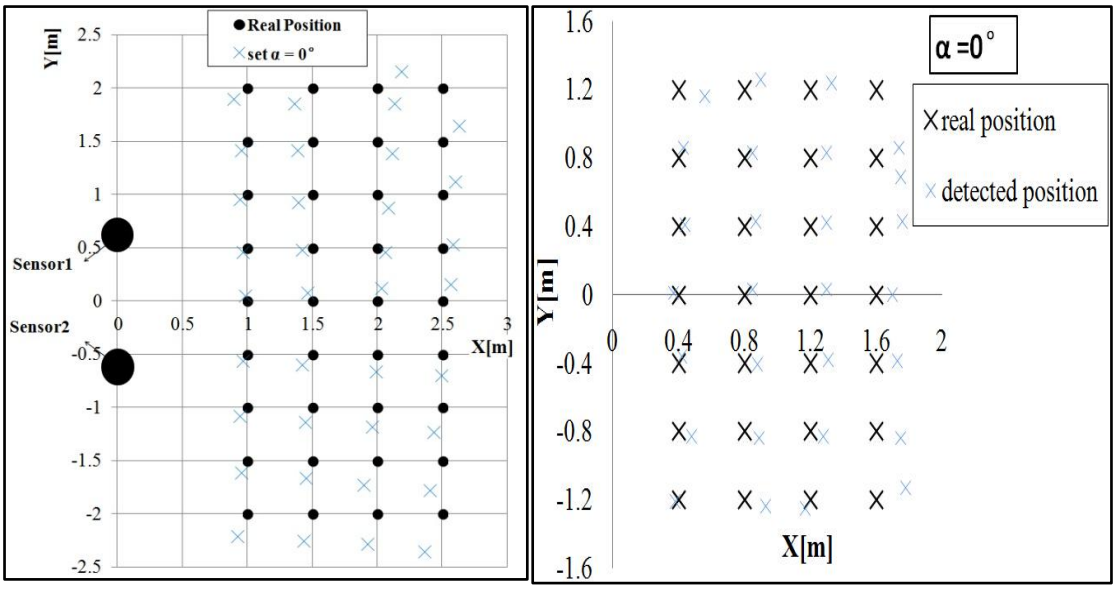

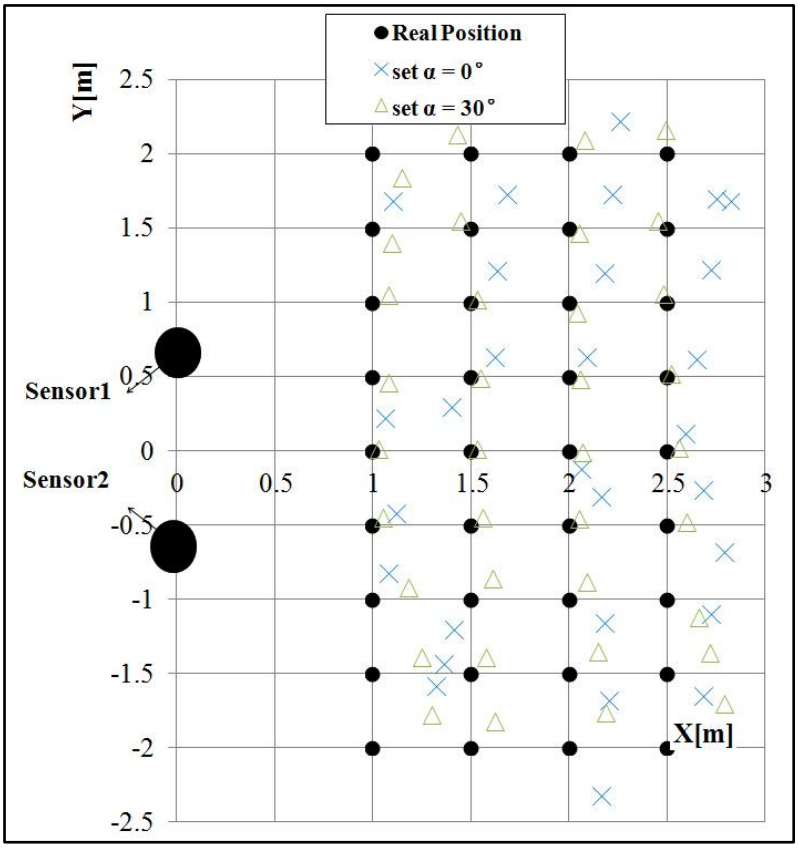
Real Position
set α = 0°
set α = 30°
Y[m]
X[m]
Sensor1
Sensor2
2.5
2
1.5
1
0.5
0
-0.5
-1
-1.5
-2
-2.5
0
0.5
1
1.5
2
2.5
3

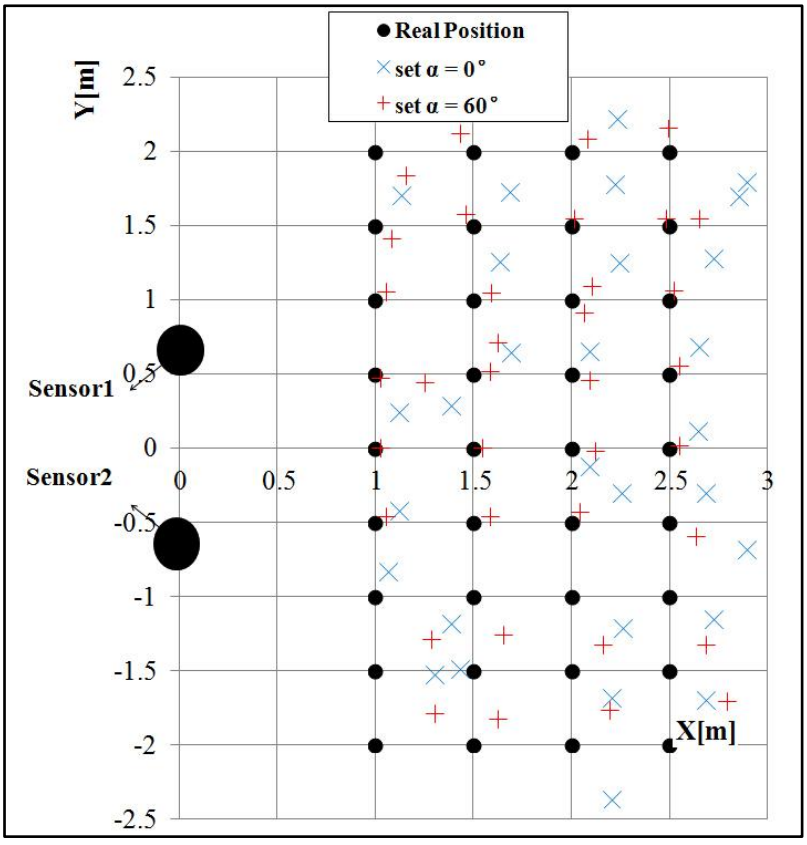
Real Position
set α = 0°
set α = 60°
Y[m]
X[m]
Sensor1
Sensor2
2.5
2
1.5
1
0.5
0
-0.5
-1
-1.5
-2
-2.5
0
0.5
1
1.5
2
2.5
3

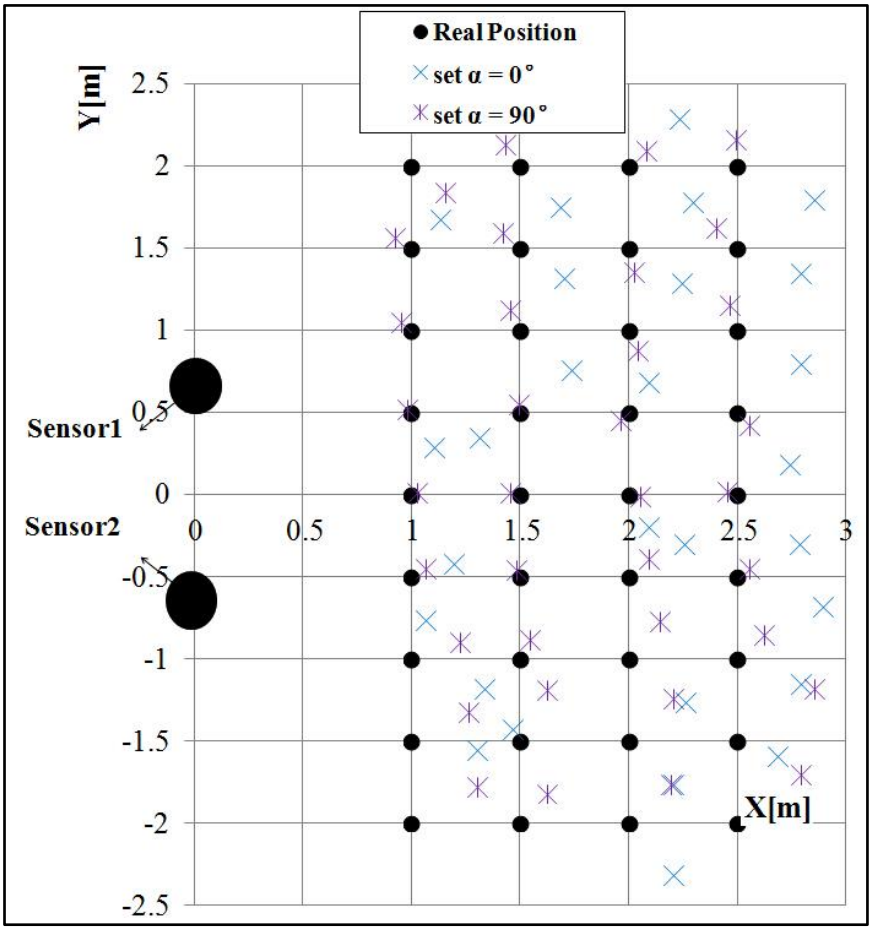


Fig. 6.23 Results for human position detection

### 6.5.2 Experimental Data to Detect Human motion

In order to test the sensor system can detect human position in real-time, we did an experiment for detecting human motion. That is, human walked at a speed of about 0.4m/s along a direction paralleling to the Y-axis, and always kept x = 1.5m. We separately did this experiment in two situations, situation1 shows that assuming body orientation angle is 0°, and situation2 shows that utilizing the estimated orientation angle to detect. **Fig. 6.24** shows the comparison result. We can obviously see that result got by situation2 is better than the result got by situation1.

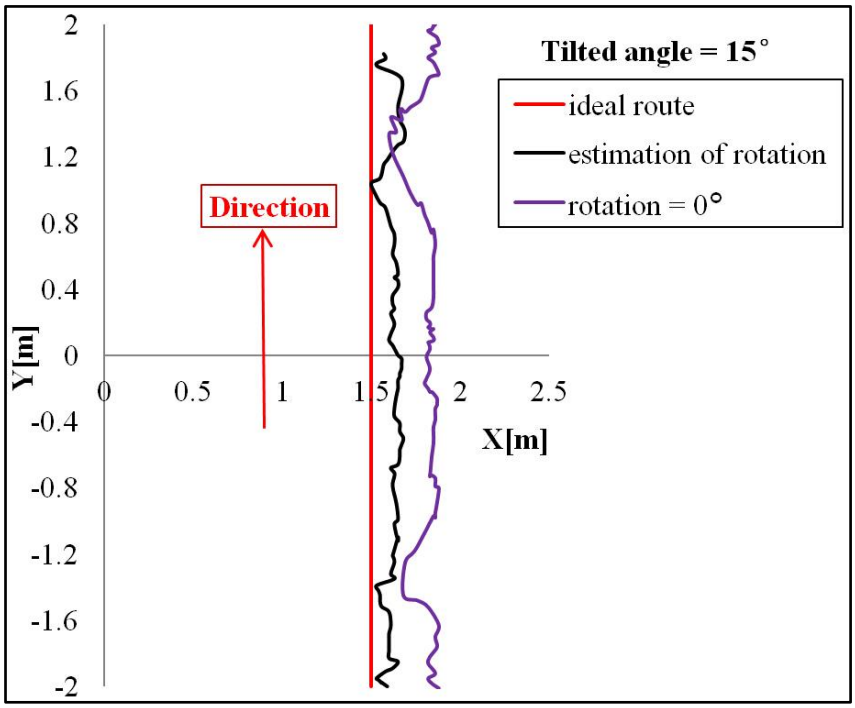


Fig. 6.24 Comparison result through using different body orientation

Meanwhile, we not only detected human walking just like simple mode to test the proposed systems, but also detected some complex routes such as circle, rectangle, zigzag and vertical direction, and results respectively show as **Fig. 6.25**, **Fig. 6.26**, **Fig. 6.27**, and **Fig. 6.28**. In all these figures, the red line means ideal route, and blue line means experimental route.

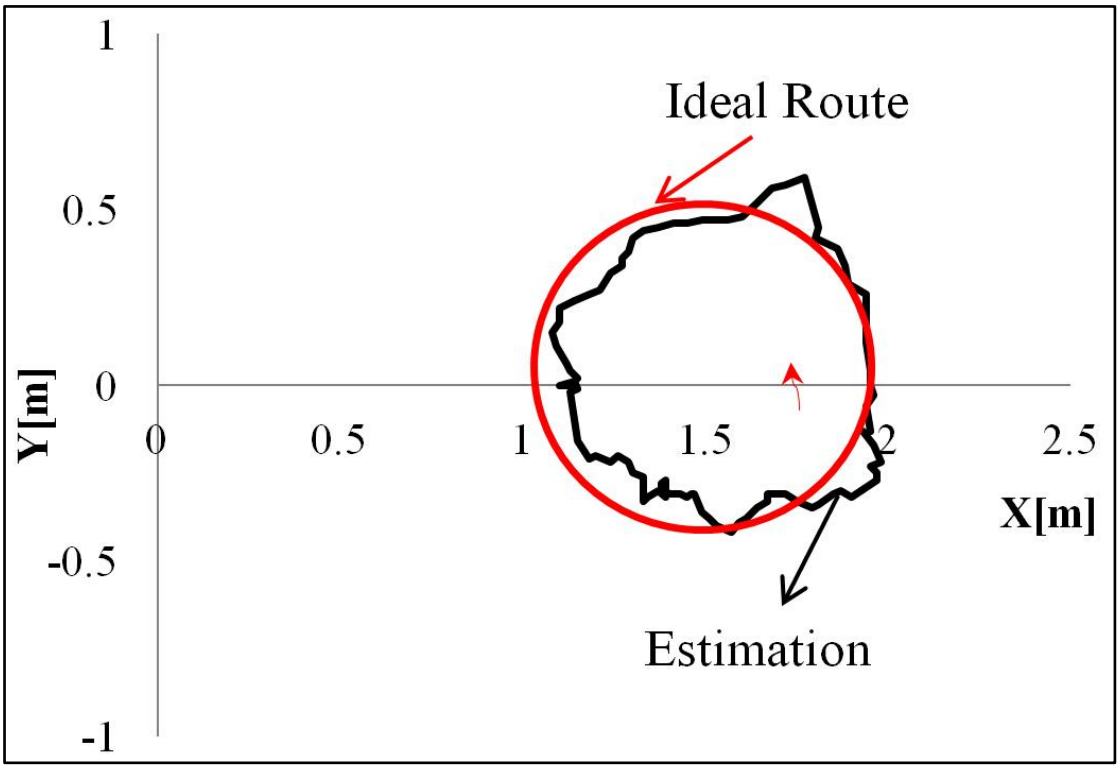


Fig. 6.25 Result when human move along a circle shape

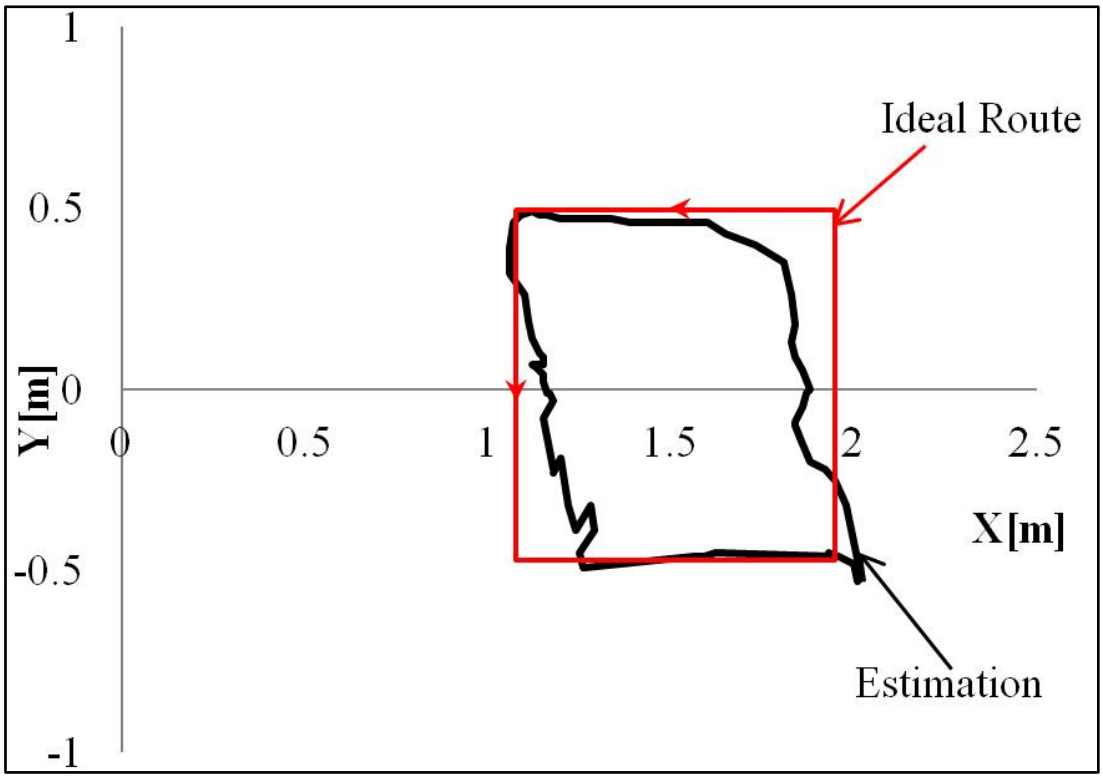


Fig. 6.26 Result when human move along a rectangle shape

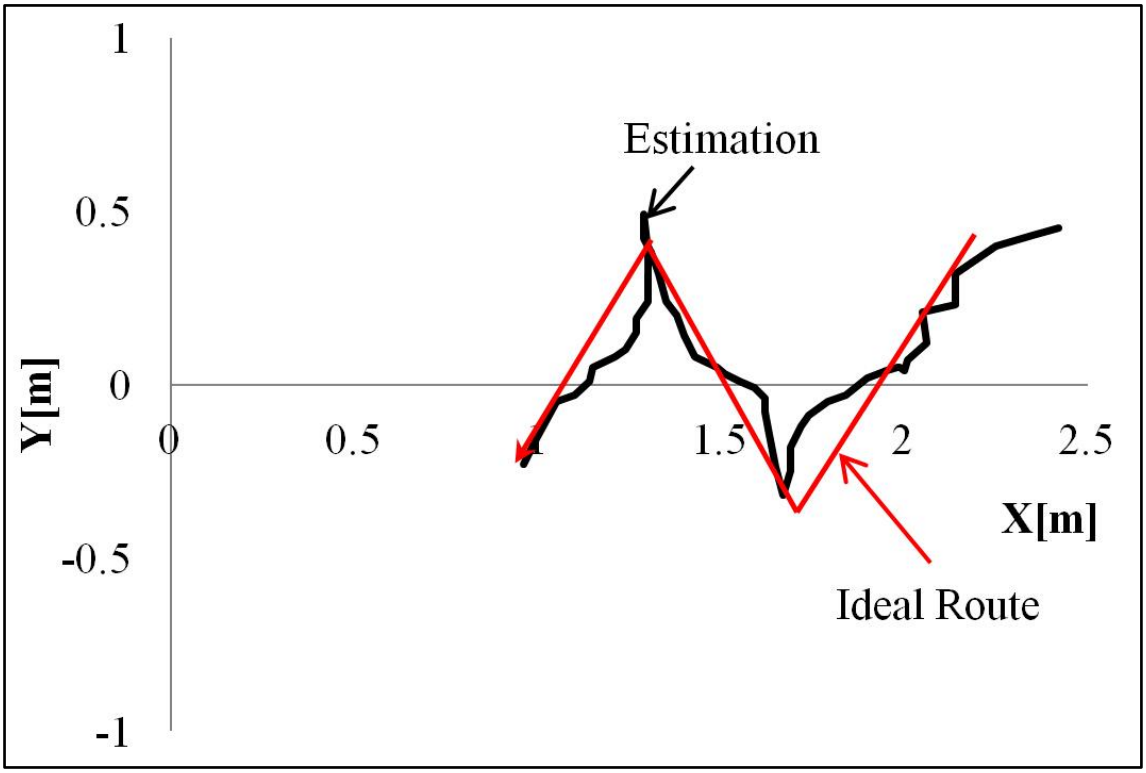


Fig. 6.27 Result when human move along a zigzag shape

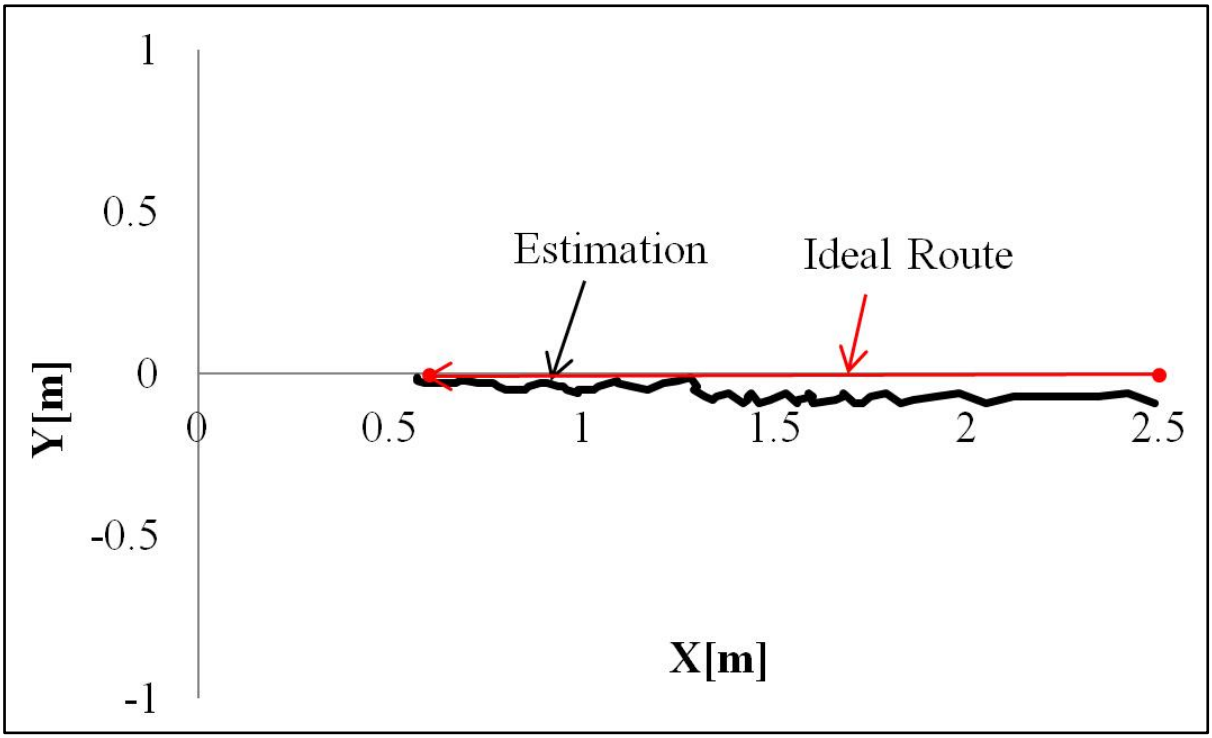


Fig. 6.28 Result when human move along a line shape

After various measurements, we realize that the system can detect any cases of human motion well from the comparison results.

## 6.6 Conclusion

Based on the previous Chapter, which has been introduced the method for detecting human position by two thermopile sensors attached on the ceiling when sensor is vertical (sensor angle $\alpha=0°$). This Chapter presented an approach for detecting human 2D position, motion and body orientation in real-time by using two thermopile infrared sensors which is kept tilted and mounted on the ceiling. Through measuring some basic characteristics of sensor itself, we built an approximate equation between sensor output voltage, height, distance, sensor total sensitivity and body orientation from each sensor to human, and then the entire unknown can be expressed by 2D position. Steepest descend method was briefly introduced to solve the human position and body orientation angle, which can be obtained though calculating the estimation orientation angle when human moving. Base on it, a method be introduced to detect human's situations, that is, when human appears, which direction human moves, motionless, when human disappears etc.

Through a mass of experiments, we could confirm the sensor system can work well.

## 6.7 Current problems and proposed solutions

Though simulation, we found that there are two solutions when a person is near to the sensor, for example, when distance $r < 0.5m$. Or, the system cannot find the final result by SDM in some positions. After check, we found the reason is that when we calculated for $V_s$ on the premise that $d\varphi$ is $1^\circ$ in **Eq. 6.11**, we just got some values of $V_s$ separately when distance is from 0.5m to 2.5m by every 0.5m, and then linked them by a smooth curve. However, the fact is that the curve is not smooth when $d\varphi$ is $1^\circ$ like **Fig. 6.29**.

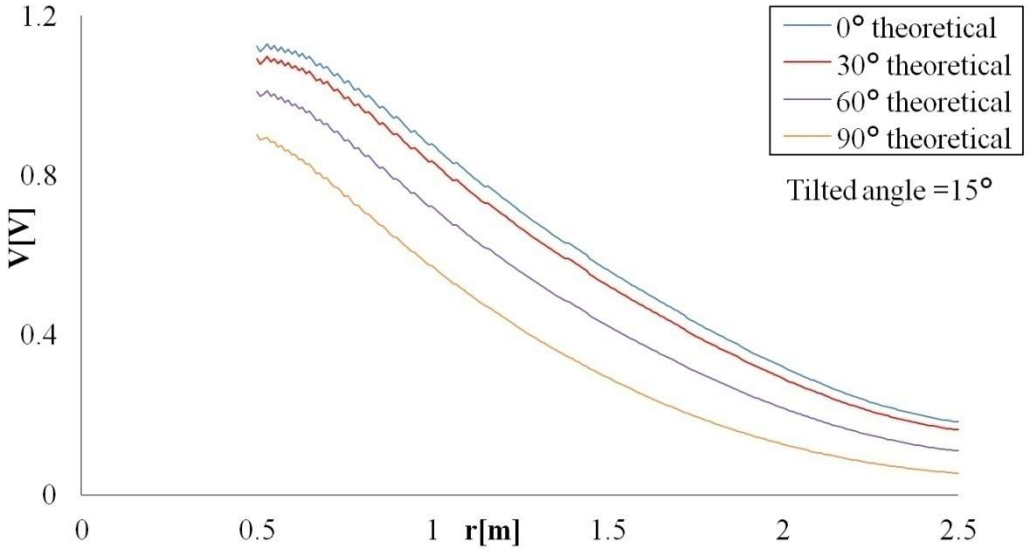


Fig. 6.29 Simulation result when dφ =1°

After adjusting and comparing some values of dφ, finally we got reasonable value that dφ =0.1°, result shows as **Fig. 6.30**.

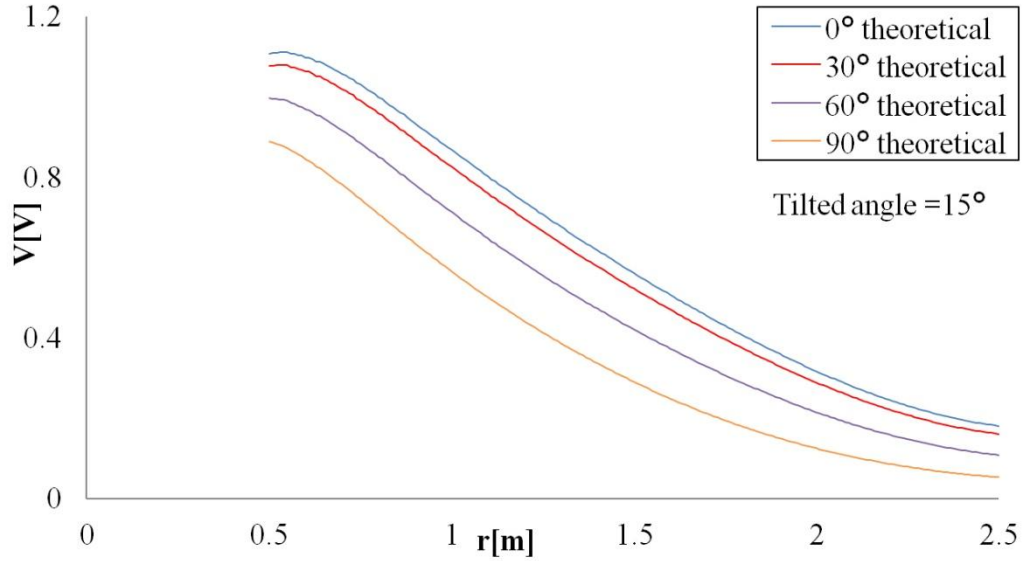


Fig. 6.30 Simulation result when dφ =0.1°

To the problem of two solutions, we checked each part of the total equation by two solutions. Finally drew a comparison result by them, shown as **Fig. 6.31**. From it, that indeed has two solutions when near to the sensors. We decided to ignore these values which resulting in two solutions. That is, we should find the maximum value of the curve.

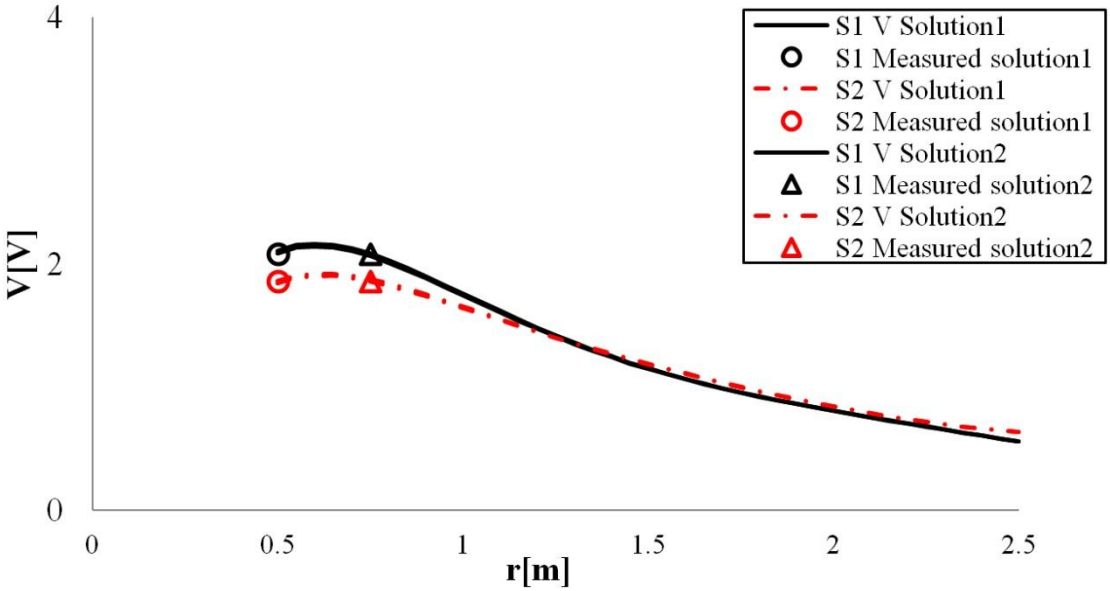


Fig. 6.31 Result after comparing two solutions

# CHAPTER 7. CONCLUSIONS AND PROJECTED PLANS

## 7.1 Conclusions

In this research, in all, three parts has been introduced about detection of human. They respectively are:

(a) Detection of human position by thermopile sensors put on the table
Through knowledge and understanding the characteristics of sensor, a basic method of finding relationships between human and sensor is presented. That is, find relationships by measurements and approximations and then build approximation equation by each sensor, and then establish equation set, solve the equation set by some methods and finally find steepest decent method as the optimal algorithm, thus obtain the human 2D position. This method has been proven to be successful through experiments.

(b) Detection of human position and motion by thermopile sensors amounted on the ceiling
Based on the basic method of human detection by thermopile sensors put on the table, we further discussed application of sensors to the ceiling and making sensor is vertical. On the basis of basic idea, how to design and analyse relationships between human and sensor is presented. That is, find relationship by each factor to the sensor, and build an approximation equation through measurements. After establishing equation set, SDM is used to solve the human position. And then a method has been introduced to detect human motion. Through vast experiments, it has been proven to be successful.

(c) Detection of human position and motion by thermopile sensors which is tilted amounted on the ceiling
Despite (b) system can measure human well, but detected area is limited, hence, we continued to consider enlarging the detected field by tilted sensors. Unlike the vertical sensor, no matter where human is, the directivity is fixed, so a method has been introduced to obtain total sensitivity of human body in any positions, then based on (b), an approximation equation is also obtained by many measurements, then SDM method is used to solving human position, and method to calculating human motion is same with (b). Finally this system has been proven to be successful after experiments.

## 7.2 Projected plans

Projected plans into this research could go into two directions.

1. This research introduces detection of human position only by two thermopile sensors, future study can include detect human position by more sensors (three or four). For example, aims at Section 9.1 (a), that is, two sensors are used to detect human position (x, y), if using three sensors, one more unknown (human body rotation) can be discussed. That is to say, how to detect human position and human body rotation in real-time by three sensors.

2. Despite this research can detect human well no matter which form in Section 9.1, however, it has drawback, that is, which can only detect one person well. Meanwhile, even though one person, because different person has different thermal radiation, how to control the affects by it. For example, through vast measurements by different persons who different heights, weights etc, we can find some laws, then select one height and weight as a standard, through installing other device, which can detect human height and weight automatically before detecting human, thus try to make the sensor system can detect anybody.

3. This research discussed about detection of human position and motion of a person by two thermopile sensors, that is to say, two sensors can calculate a group of position (x,y). Based on it, to two persons, there are two groups of positions (x,y), that is, there are four unknown parameters, we can consider to add other two sensors to calculate for redundant parameters. And by such analogy, we can image that it should be detect multiple targets by many sensors.

## REFERENCE


[1] H.K. Chan, W. Ye., T.L. Lam, Y. Ou, and Y. Xu, "Sensor system for a human-following robot", Proc. of Int. Conf. on Automation, Control, and Applications, pp.350–355, 2005.

[2] S. Grange, E. Casanova, T.W. Fong, and C. Baur, "Vision-based sensor fusion for human-computer interaction", Proc. of IEEE/RSJ Int. Conf. on Intelligent Robots and Systems, 2002.

[3] A. Ohya, Y. Nagumo, M. Takahata, "Intelligent escort robot moving together with Human-Human Following Behavior", Proc. of 12th Int. Symp. On Measurement and Control in Robotics, 2002.

[4] D. Cima, "Using Lithium Tantalate Pyroelectric Detectors in Robotics Applications", Eltecdata # 112, Eltec Instruments, Inc., 1984.

[5] H. R. Everett, "Sensors for Mobile Robots, Theory and Application", AK Peters, Ltd., 1995.

[6] F. Bu, C.Y. Chan, "Pedestrian Detection in Transit Bus Application: Sensing Technology and Safety Solutions", Proc. of IEEE Intelligent Vehicle Symp., pp.100-105, 2005.

[7] M., et al.,"Human-tracking systems using pyroelectric infrared detectors", Optical Engineering, vol. 45, no. 10, pp. 106401-1–106401-10, 2006.

[8] R. Bodor, B. Jackson, N. Papanikolopoulos, "Vision-based human tracking and activity recognition", Proc.11th Mediterranean Conf. on Control and Automation, 2003.

[9] J. M. Holland,"An army of robots that roams the night", Proc. of Int. Robot and Vision Automation Show, pp.17.1–17.12, 1993.

[10] Jianpeng Z., Jack H.," Real Time Robust Human Detection and Tracking System", Computer Vision and Pattern Recognition - Workshops, 2005. CVPR Workshops. IEEE Computer Society Conference on, pp. 149, June 2005.

[11] Fiaz, M.K. , Ijaz, B. "Vision-Based Human Tracking and Activity Recognition", Intelligent and Advanced Systems (ICIAS), 2010 International Conference on, pp. 1 – 5, June 2010.

[12] A. Ess, B. Leibe, K. Schindler, and L. Gool. A mobile vision system for robust multi-person tracking. CVPR, 2008.

[13] C. Porras-Amores., F. R.Mazarrón, I. Cañas, "Using quantitative infrared thermography to determine indoor air temperature", Energy and Buildings, Vol. 65, pp. 292-298, 2013.

[14] Alf Püttmer, "New applications for ultrasonic sensors in process industries", Ultrasonics, Vol.44, pp. 1379-e1383, 2006.

[15] Villanueva, J.M.M.; Catunda, S.Y.C.; Tanscheit, R.; Pinto, M.M.S. "Wind Speed Measurement Data Fusion of Phase Difference and Time-of-Flight Techniques Using Ultrasonic Transducers", Instrumentation and Measurement Technology Conference Proceedings, 2007. IMTC 2007. IEEE, On page(s): 1 – 6.

[16] J. Fraden, "Handbook of Modern Sensor: Physics, Designs, and Applications", 3ed ed., American Institute of Physics, 2003.

[17] Xiaomu L.,, Baihua S., Xuemei G., Guocai L., Guoli W., "Human-tracking systems using pyroelectric infrared detectors", Control and Automation, 2009. ICCA 2009. IEEE International Conference on, pp. 1716 – 1721, Dec. 2009.

[18] L., et al., “Thermopile sensor devices for the catalytic detection of hydrogen gas”, Sensors and Actuators B: Chemical, Vol. 130, Issue 1, pp. 200-206, 2008.
[ 19 ] PerkinElmer Corp., “Product Note--Thermopile sensor”, http://www.optelectrncs.perknelmer.com.
[20] L., et al., “Thermopile sensor devices for the catalytic detection of hydrogen gas”, Journal of Network and Computer Applications, Vol. 36, Issue 1, pp. 25-41, 2013.
[21] P., et al., “Thermal measurements using ultrasonic acoustical pyrometry”, Ultrasonics, in press, Uncorrected proof, Available online, 2013.
[ 22 ] Seebeck, T. J. Magnetische Polarisation der Metalle und Erze durch Temperatur-Differenz. Abh. Deutsch. Akad. Wiss. Berlin, 1822, 265–373.
[23] A., et al., ” Integrated Thermopile Sensors”, Sensors and Actuators, A21-A23 (1989) 621-630 621.
[24] L. W. Da Silva, M. Kaviany, A. DeHennis and J. S. Dyck: Proc. 22nd Int. Conf. on Thermoelectrics, (International Society of Thermoelectrics, (2003) pp. 665–668.
[25] Schettino, E. A new instrument for infrared radiation measurements: the thermopile of Macedonio Melloni. Ann. Sci., 1989, 46, 511–517.
[26] B. J. Huang, “A Precise Measurement of Temperature Difference Using Thermopiles”, Experimental Thermal and Fluid Science 1990; 3:265-271.
[27] A. G, M. A and G.G, Proc. Estonian Acad. Sci. Eng., 2007, 13, 4, 338–353.
[28] M. Kim, T. Oh, “Thermoelectric Characteristics of the Thermopile Sensors with Variations of the Width and the Thickness of the Electrodeposited Bismuth-Telluride and Antimony-Telluride Thin Films”, Materials Transactions, Vol. 51, No. 10 (2010) pp. 1909 to 1913.
[29] J. Kemper and H. Linde, Challenges of passive infrared indoor localization, in 5th Workshop on Positioning, Navigation and Communication, 2008. WPNC 2008., march 2008, pp. 63-70.
[30] Kemper and D. Hauschildt, Passive infrared localization with a Probability Hypothesis Density filter, in 7th Workshop on Positioning Navigation and Communication. IEEE, 2010.
[31] D. Hauschildt and N. Kirchhof, Improving indoor position estimation by combining active TDOA ultrasound and passive thermal infrared localization, in 8th Workshop on Positioning Navigation and Communication (WPNC), 2011, April 2011, pp. 94-99.
[32] D. Hauschildt and N. Kirchhof, Advances in thermal infrared localization: Challenges and solutions, in International Conference Indoor Positioning and Indoor Navigation. IEEE, 2010.
[ 33 ] Honorato, J.L. , Spiniak, I. , Torres-Torriti, Human Detection Using Thermopiles, M.Robotic Symposium, 2008. LARS '08. IEEE Latin American, pp. 151 – 157.
[34] L.I. Lopera Gonzalez, M. Troost and O. Amft. (2013) Using a thermopile matrix sensor to recognize energy-related activities in offices. SEIT 2013: Proceedings of the 3rd International Conference on Sustainable Energy Information Technology, Elsevier, volume 19, pp. 678-685.
[35] T. J. Seebeck, T.J., “Magnetische Polarisation der Metalle und Erze durch Temperatur-Differenz”, Abh. D. pp. 265–373, 1822.
[36] FUJI & CO.(Piezo Science) website at: http://www.fuji-piezo.com/.

[37] SSC Company Website at: http://www.ssc-inc.jp/products.
[38] I. Montvay, E. Pietarinen, “The Stefan-Boltzmann law at high temperature for the gluon gas”, Physics Letters B, Vol. 110, issue 2, pp. 148-154, 1982.
[39] T. Dekker, "Finding a zero by successive linear interpolation" B. Dejon (ed.) P. Henrici (ed.) , Constructive aspects of the fundamental theorem of algebra , Wiley (1969) pp. 37–48.
[40] B.P. Demidovich, I.A. Maron, "Foundations of computational mathematics", Moscow (1966) (In Russian).
[41] L.M. G. Drummond, B.F. Svaiter, “A steepest descent method for vector optimization”, Journal of Computational and Applied Mathematics, Vol. 175, issue 2, pp. 395-414, 2005.
[42] M. Gerard , B.D. Schutter, M. Verhaege, “A hybrid steepest descent method for constrained convex optimization”, Journal of Computational and Applied Mathematics, Volume 175, Issue 2, March 2005, Pages 395–414.
[43] X. Zhang, H. Seki, Y. Kamiya, M. Hikizu, "Detection of Human Position by Thermopile Infrared Sensors", Proceedings of the 15th International Conference on Precision Engineering, pp.436-441, 2014.7.
[44] X. Zhang, H. Seki, M. Hikizu, "Detection of Human Position and Motion by Thermopile Infrared Sensor", International Journal of Automation Technology, Vol.9, No.5, pp.580-587, 2015.9.
[45] J. S. Dai, " Euler–Rodrigues formula variations, quaternion conjugation and intrinsic connections", Mechanism and Machine Theory, Volume 92, October 2015, Pages 144–152.
[46] https://en.wikipedia.org/wiki/Rodrigues%27_rotation_formula.

## ACKNOWLEDGEMENTS

Foremost, I would like to express my sincerest gratitude to Associate Professor Hiroaki Seki for his expert guidance, caring, patience, kind and that helped me in all the time of research and writing of this thesis. I could not have imagined having a better advisor and mentor for my Ph.D study. Thank you from my bottom of my heart.

Besides, I would like to thank Professor Dr. Yoshitsugu Kamiya and Mr. Masatoshi Hikizu for their beneficial advices throughout my stay in Kanazawa University.

Special thanks to Professor Adachi, Tachiya, Asakawa, Tokutake, for their dedicated advises and also precious time spent in helping me completing this thesis.

My sincere thanks also go to my friends Yu xiaoming, Wang Ning, Sun Han, Li Ruyue, Yang Jingyi, Fan Ruikang, for offering me many help whether life or study.

I thank my fellow lab mates in for the stimulating discussions and for all the fun we have had in the last four years, they are Leong, Mikami, Ono, Kato, Katayama, Hayashi, Kashiwa. I would like to thank you partially you gave me helps when my Japanese was poor.

Last but not the least, I would like to thank my family: my parents Xingjian Zhang and Yueling Pan, for giving birth to me at the first place and supporting me spiritually throughout my life. I would like to thank my wife Shuai Zhu for providing me various assistance and always give me strong support in daily life. My life becomes colorful and enriched because of you.